Fall 2010

CFD study on effect of branch sizes in human coronary artery

Liza Shrestha
University of Iowa

CFD STUDY ON EFFECT OF BRANCH SIZES IN HUMAN CORONARY ARTERY

by

Liza Shrestha

A thesis submitted in partial fulfillment
of the requirements for the Master of
Science degree in Biomedical Engineering
in the Graduate College of
The University of Iowa

December 2010

Thesis Supervisor: Assistant Professor S. C. Vigmostad

Graduate College
The University of Iowa
Iowa City, Iowa

CERTIFICATE OF APPROVAL

_____

MASTER‟S THESIS

_____

This is to certify that the Master‟s thesis of

Liza Shrestha

has been approved by the Examining Committee for the thesis requirement for the Master of Science degree in Biomedical Engineering at the December 2010 graduation.

Thesis Committee: _____

Sarah Celeste Vigmostad, Thesis Supervisor

_____

K.B. Chandran

_____

Uday Kumar H.S.

_____

Justin Garvin

_____

Andreas Wahle

To my parents who made me the person I am, to my brother who stood by me at every single step I took, and to my angels who guided me through my toughest times

ACKNOWLEGDEMENTS

I am grateful to my advisor Assistant Professor Sarah C. Vigmostad for her encouragement and guidance throughout the period of my Master‟s degree course. Guidance and help from Justin Garvin has been invaluable to me, mostly during the last few months of my research. My sincere gratitude to him.

My special thanks to Professor Uday Kumar for his support and kindness throughout this period.

I would like to convey my gratitude to Professor Nicole Grosland and her students Nicole Kallemeyn, Kiran Shivanna for kindness during my interaction with Surgical Suite.

I want to express my sincere gratitude to Justin Hannon for guiding me through Pointwise in the most crucial times during my thesis.

I am greatly appreciative to all my colleagues the entire IIHR family for creating a warm and pleasant research environment.

I am also thankful to all my labmates specially John Mousel and Anil Kapahi for helping me during my course works, research and for their sincere suggestions and friendship throughout this period of my studies.

Finally, I can‟t stay without acknowledging Hari for his sincere help and comments on my research.

ABSTRACT

To improve our understanding of Coronary Artery Disease, much research is focused on understanding wall shear stress and other hemodynamic indices associated with plaque development. Computational fluid dynamics (CFD) is an important tool for quantifying hemodynamics, but often, many assumptions are made when these simulations are performed. For example, most coronary artery models neglect (Steinman, 2001, Wentzel et al. (2003), Wahle et al. 2006) branching when performing CFD analysis. The goal of this study is to determine the threshold size of the branches in the coronary arteries that should be incorporated in geometric reconstruction for the simulation of blood flow. This is performed using patient-specific human coronary arteries, and hemodynamics are computed using a new algorithm that minimizes user intervention for CFD analysis Patient-specific human coronary artery geometry is obtained via a fusion of IVUS and bi-plane angiography images, in which a surface mesh is then generated for CFD analysis using in-house, level-set-based CFD software. Research has suggested that blood flow patterns are highly affected by branch flows, and branching is one of the leading locations of plaque accumulation. In this study, we have examined the role that various branch dimensions play on downstream blood flow in the main branch, to determine what branches could be reasonably neglected, and which must be included for reasonable hemodynamic studies. Secondary flow patterns and wall shear stress were examined at numerous distal locations for differences in blood flow due to branching. Results from this study suggested that presence of branches caused low local axial wall shear stress (TWSS) and reverse flows in the vicinity of branching in both upstream as well as downstream region. The region of impact however depended on the size of the cross section of the artery and of the branch; larger the cross section higher the impact.

TABLE OF CONTENTS

LIST OF TABLES

LIST OF FIGURES

CHAPTER 1 INTRODUCTION

Atherosclerosis is the one of the leading cause of death in developed countries. For instance, in America alone, about every 25 seconds, someone will suffer a coronary event, an about every minute someone will die from one (Heart disease and stroke statistics, 2010). Coronary artery disease (CAD) is responsible for half the mortality in Europe alone (Andrew, 2010). Similarly, estimates of National Vital Statistics Report 2009 suggest that every one of six deaths in US is caused by this.

1.1 Atherosclerosis

Atherosclerosis is a term coined to describe a state in which arterial wall thickens due to the accumulation of fatty materials like cholesterol. Calcifications too develop in this process. Though not completely understood, it is believed to occur due to the accumulation of macrophage white blood cells and promoted by low density lipoprotein (Krams et al., 2010). Increase in accumulation of plaque, also known as stenosis (narrowing of arterial cross sectional area), leads to enlargement of arteries as arterial wall tries to remodel itself. But eventually the plaque ruptures, letting out its inner content to blood stream. The ruptured plaque clots and heals and shrinks down as well but leaves behind multilayered complex lesions (Chandran, 2006). Plaques can be stable as well as vulnerable. In the case of stable plaques, depending on the degree of stenosis blood supply from the artery to its respective organ could decrease and even get blocked completely. On the other hand, vulnerable plaques have a tendency to rupture due to the presence of calcium streaks. Frequently, as the vulnerable plaques rupture, thrombus formed as such could block that vessel or could also flow through bloodstream towards smaller vessels and block them, leading to a sudden death of tissues fed by that vessel. If the plaques do not rupture and artery gets enlarged to a great extent then it results in an aneurysm (Berne and Levy,

2009). Such blockage of coronary arteries in heart can lead to myocardial infarction – heart attack, in carotid arteries in brain can lead to what is called a stroke, in peripheral arteries in legs can lead to ulcers, gangrene (death of tissue) and hence loss of leg, in renal arteries can lead to kidney malfunction (Chandran, 2006). The most disturbing fact about atherosclerosis is the inability to detect the disease in preliminary stages. As stated by Miller (2001), most of the times coronary artery disease (CAD) gets diagnosed only after 50-75 percent occlusion of arteries.

1.2 Factors Affecting Atherosclerosis

Numerous diseases like diabetes, hypercholesterolemia, hypertension, have been linked to thickening of intimal layer of arteries. Studies have suggested that some particular arterial sites are more prominent to lesion development than others. And these sites generally have lower wall shear stress (WSS) and oscillatory WSS (Gibson, 1993, Krams et al., 2010). Flow of blood in a vessel generates a frictional force opposing its motion in the intimal lining of the vessel which is termed as Wall Shear Stress (WSS). Studies have always shown a high correlation in between the progression of lesion and WSS (Krams et al., 2010). Initially it was believed that progression of such lesions were due to the occurrence of high WSS (Lutz, 1977). However, recent and more advanced studies have clearly indicated the existence of accumulation of lesion in the regions of low WSS, flow separation, and in the regions where there is departure from axially aligned unidirectional flow (C. Zarins, 1983, White and Frangos, 2007). Similar results have been advocated in the case of carotid arteries (Ku, 1985), in abdominal aorta (Yutani, 1988), and also in coronary arteries (Kirpalini, 1999). Though the ultimate mechanisms relating low WSS and lesion accumulation are not clear, Caro et al. (1971) have suggested that because of low shear rate there occurs a significant retardation in the transportation of circulating materials away from wall, resulting in what is called the accumulation of lipids in the intimal linings of vessel.

Factors known to influence hemodynamics can be broadly classified into following five categories; vessel geometry, vessel movement and compliance, flow waveform shape, the shape of the inlet ostium or velocity profile, and branch flows (Mayers et al., 2000). Several studies have been conducted to correlate the above variables with atherosclerosis. According to recent studies done in static anatomically realistic RCA models, inlet velocity profile were observed to impart minor effect in WSS and hemodynamics (Mayers et al., 2000) where as vessel geometry were observed to impart major effect (Wentzel, 2000, Krams, 1997). Santamarina (1998) reported a high significance of modeling vessel geometry and movement as they played key role in determining the locations of low and oscillating WSS. Qui (2000) reported the same for compliance.

The carotid artery and abdominal aorta are other prominent sites of atherosclerosis along with coronary arteries. The role of branching in hemodynamics of larger arteries like aorta and carotid arteries has already been studied. Previous in vivo study by Zarins (1983) showed that the regions with relatively low wall shear stress, flow separation and departure from axially aligned unidirectional flow in Carotid bifurcation were the most prominent regions for intimal thickening. Similar study has been conducted by Pederson (1999) in abdominal aorta. These findings have been validated time and again in more recent studies as in the study by White and Frangos in 2007.

1.3 Atherosclerosis Diagnosis and Treatment

Coronary artery bypass grafting (CABG) and angioplasty introduced in late 1970ʺs can be considered as one of the primary physical treatment for occluded arteries that may include stents to provide support and retain the vessel lumen after they have been expanded. Balloon angioplasty, an invasive interventional procedure involves inserting of a balloon-tipped catheter into groin or arm and then advancing it to the occluded point in the diseased artery. The balloon is then inflated such that the occlusion is pushed away from the center of the lumen and towards

the arterial wall. This removal of occlusion reinstates flow in the vessel. (Berne and Levy, 2009). However, balloon angioplasty cannot be taken as an ultimate solution for occlusion because there have been 40-50% cases of restenosis at the same point. With the view of alleviating restenosis, stents were introduced along with balloon-tipped catheter to the point of occlusion. Stents are wire-like mechanical devices that act as a scaffold and hold back the lesions causing occlusion. Implanting of stents has reduced the probability of restenosis by 70 -80% (Wentzel et al., 2000), however it does introduce other potential complications including stent migration (Chandran, 2006) compliance mismatch, failure, and risk of restenosis (Chandran, 2006), though reduced, still exists.

1.4 Angiography

Angiography, a medical imaging technique that is used to visualize the lumen of blood vessels and organs, may be used to diagnose atherosclerosis. In a standard X-ray based invasive angiography, a contrast agent is injected into vessel with a catheter and guide wires system. The injected contrast dye creates an X-ray shadow image of lumen only. It fails to picture different layers. It simply gives back a side view of artery. Depending upon the angle of view, occlusion may or may not get visualized correctly. Though angiography strictly refers to imaging based on projection radiography, with the development of newer imaging techniques there are different methods of angiography available today such as CT angiography (CTA), MR angiography (MRA. In CTA, X-ray contrast material is injected in to the region of interest and X-ray beams is passed through patients‟ body from different angles so as to reproduce an image. It gives much precise anatomical detail for overall vessel course than others along with the disadvantages of exposure to large amount of ionizing radiation. MRA is non invasive method and there is no exposure to ionizing radiation, the contrasting dye used is far less toxic than in the case of other angiography. Though it is quite popular for imaging large arteries (e.g., the aorta), MRA hasn‟t found much success when it comes to coronary arteries. IVUS uses echocardiography where a

very high frequency sound wave-ultrasound is emitted from a transducer. These waves impinge on targeted tissue and echo forms which is recorded and decoded to form an image of the tissue. Transducers as such are miniaturized and are placed on the tip of a catheter which is made to slip into coronary arteries. For coronary arteries, frequencies in the range of 20-45 Mhz are usually employed. If balloon or stent is being imparted, same guide wire can be used to position this transducer. It generates a unique point of view picture in real time. IVUS is particularly popular when it comes to coronary angiography.

1.5 Motivation and Objective

Branching sites have always been an area of interest to physicians because of high probability of accumulation of plaque in these regions. These sites hold special significance to fluid analysts as well because of the generation of low wall shear stress (Gijsen et al., 2008, Wahle et al., 2006, Gibson et al., 1993), oscillatory wall shear stress and recirculation (Shabban and Duerinckx, 2000, Gibson et al. 1993, Krams et al., 2010) brought about by sudden change in geometry and division of flow. Arterial remodeling from imaging data and preservation of geometrical properties is a pre-requisite for an accurate prediction of wall shear stress.

Simulation of blood flow in arteries targets to understand the fluid dynamic properties in the region of occlusion and build up relationship between them. Research have suggested that blood flow patterns are highly affected by vessel geometry, branch flows, vessel movement and compliance, flow waveform shape, and shape of the inlet ostium. Numerous studies have been conducted to determine the nature and degree of affect caused by each of above. However, regarding the effect of branches researchers have mainly focused on the affect of bifurcation angle and position of bifurcation. Very less emphasis has been given to the size of the branching arteries. In these studies, the most common assumption done by researchers to simplify the model creation has been to completely neglect the existence (and hence effect) of any branches in the main artery (Steinman, 2001, Wentzel et al. 2003, Wahle et al. 2006). Limited studies

performed have focused on small branches only; suggest that the effect of branch flow exists only in a short length of 3mm downstream. However, these studies were very limited in scope, and have not examined the threshold size of branches that can be reasonably neglected while still providing confidence in results and conclusions drawn.

Recent progress in medical imaging has equipped researchers with the capability of imaging smaller and smaller arterial vessels, but the reconstruction of these additional branches for flow simulation remains a challenge due to the cost involved in meshing and solving the flow. However, since coronary arteries are highly branched, and branching regions are frequent sites of plaque accumulation (Wentzel et al., 2003), it is essential to better understand the impact of neglecting branches in geometric reconstruction of coronary arteries, and when this is a reasonable approach.

This study is hence aimed to examine how the size of coronary artery branches impacts the flow in the main vessel, and determine whether a threshold exists for reasonably neglecting branches based on their size and impact on downstream flow.

CHAPTER 2 LITERATURE REVIEW

2.1 Previous Studies in Coronary Arteries

2.1.1 Overview of Coronary Physiology

Arteries that supply blood to myocardium are termed as coronary arteries. They are highly curved and have a unique feature of tethering into heart. Coronary arteries can be divided into two, left and right coronary arteries according to the left and right cusp of the aortic valve from where they arise. Left coronary artery further divides into two branches namely, the left anterior descending (LAD) branch and the left circumflex branch (LCx).

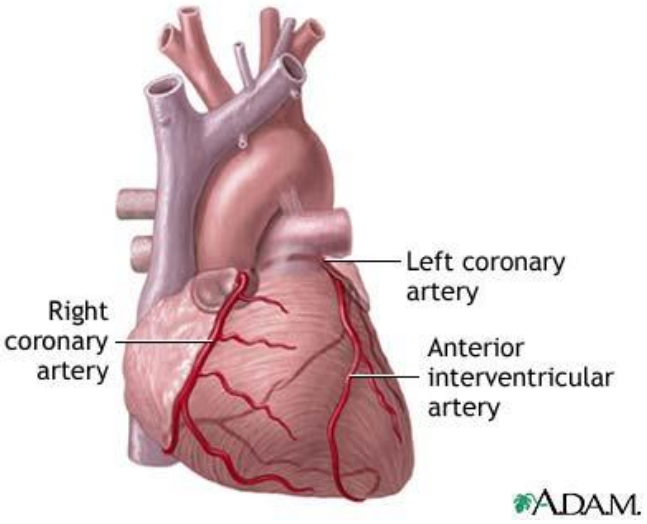

Figure 2-1 Diagram showing coronary arteries and their location on the heart

Source: clarian.org , "Atherosclerosis", 2010

It is the pressure generated by the contraction of the heart muscles that give driving force for coronary circulation. In the systolic phase, the muscles of heart contract creating high pressure in the left ventricle and cause the aortic valve to open allowing the flow of blood into aorta and through coronary arteries. As the systolic phase ends, pressure decreases in aorta and so does the coronary blood flow. Similarly, in the diastole phase the muscles of heart relax and increasing coronary flow. Blood flow is comparatively higher in left coronary artery in diastole phase.

2.1.2 The Coronary Artery as a Curved Tube

The fact that the coronary arteries have large curvatures in comparison to other arteries, led to early simulation studies that modeled them as curved tubes. Two major findings on coronary simulations included shift of axial velocity towards the outer wall of curved tube (Williams, 1902) and the presence of secondary flow (Berger, Talbot and Yao, 1983). Dean was first to observe the existence of secondary flow in uniformly curved tubes with small curvature in the form of a pair of vortices. Depending upon the ratio of pipe radius to the radius of curvature in tubes, a new parameter- Dean Number was coined (1927, 1928). These secondary flows were examined by Greenspan in 1972, using a finite difference scheme by varying Reynolds number. He numerically proved that the flow in curved tubes were more stable than in straight tubes, because of which flow remains laminar in curved tubes despite of higher values of Reynolds number. So after a gap of about half a century Greenspan numerically justified researches by Eustice (1911) and Taylor (1929).

Reynolds number (Re) is a ratio of inertial force to viscous force. According to Murata, Miyake and Inaba, in the cases of low Re when viscous forces were dominant, flow was found to be directed towards the inner wall of the curved tube and reverse in the cases of high Re - inertia dominant flow. Along with the increase in fluid flow, Reynolds number increases; because of

this dominance of inertial force, centrifugal force increases and hence secondary flow comes into picture (Murata, 1976).

The phenomenon of formation of secondary flows in curved tubes may be briefly explained as follows. When flow enters the site of curvature, fluid gets forced to change its direction in order to follow the bend. This causes the development of radial pressure gradient between the inner and the outer walls of the curvature. Fluid as such is also subjected to centrifugal force proportional to the square of axial velocity. In the case of inviscid fluids the axial velocity profile gets skewed towards the inner wall of the curvature because the two forces- radial velocity gradient and the centrifugal force, balance out each other. Hence a secondary flow does not develop in an inviscid case. In the case of viscous fluids, it is the imbalance of these two forces that result in a secondary flow giving rise to two vortices referred as "Dean"s vortices." The axial velocity profile in viscous fluids through curved tubes hence becomes skewed towards the outer wall.

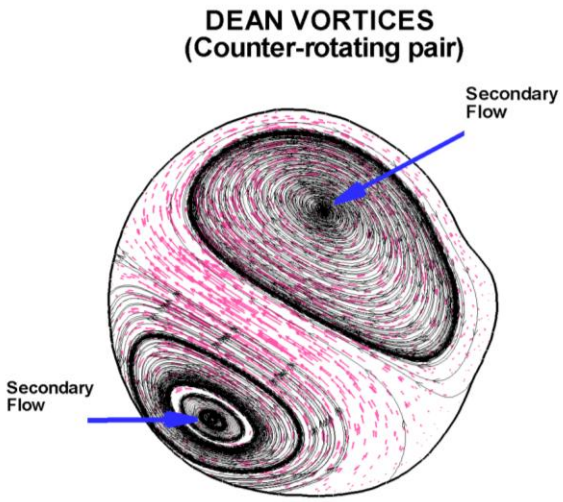

Figure 2-2 Schematic of secondary flow motion: Dean vortices

Studies related to unsteady flow in curved tubes were also carried in previous research. Lyne in 1970, solved the case of unsteady, sinusoidal flow (with zero mean value) in a curved tube and found that the maximum axial velocity was located closer to the inner wall for both the cases of lower as well as higher Re. Later in 1979 an experiment was conducted by Chandran, Yearwood, and Wieting where they examined pulsatile flow in a curved tube using a physiological flow profile. According to their results, flow reversals occurred at the inner walls of the curved tube during diastole. Though maximum flow occurred at the inner wall initially, the apex moved towards the outer wall as flow went downstream (1979). More recently, with advent of imaging technologies, more realistic reconstruction of arteries are being used. These studies will be reviewed in the subsequent sections.

2.1.3 Implementing Realistic Artery Geometry for Hemodynamic Studies

Early hemodynamic investigations started with larger arteries like aorta and theories linking WSS and plaque accumulation were developed. Aorta is the largest artery in human body originating from left ventricle of the heart and extending down to abdomen. Aorta has significant curved geometry and sites of branching similar to coronary arteries hence studies on aorta proved to be stepping stones towards the study of smaller and more curved coronary arteries. Hence, later these theories were implemented on coronary arteries. Caro et al claimed the first relationship in between low WSS and atherosclerosis in arteries. They examined the casts of human aorta and dogs. Sabbah et al. (1984) examined blood velocity in human coronary arteries with the aid of angiographic images. They observed the rate of clearance of injected contrast-dye in the RCA of 30 patients. Their results showed that the rate of movement of contrast dye was much faster along the outer wall than along the inner wall. This finding led to the interpretation that the wall shear stress was comparatively lower in inner wall. In the same year another histological study was done by Sabbah in RCAs from 17 human cadavers who died from non

cardiac disease. The study suggested that the plaques were accumulated in significant amount in the inner walls of coronary arteries. This study further supported the low WSS assumption.

Friedman et al. (1983) who examined hemodynamics in human aortic bifurcations showed that arterial geometry played significant role in fluid parameters like WSS. According to their observation, variation in the bifurcation, curvature of aorta, curvatures of daughter branches and asymmetrical branching from aorta were the key factors that governed the fluid parameters.

Later Asakura and Karino in 1990 treated cadavers of coronary arteries such that they could be transparent and inner fluid flow could be observed. They observed that lesion accumulation occurred at two places – first being the outer wall of bifurcation and second inner wall along the curvature. Further studies showed that these locations were the most prominent sites for secondary flow, flow reversals and low WSS. Mayers et al. in 2000 studied the effects of several factors like vessel geometry, branching, compliance and movement of vessels applying both the steady as well as pulsatile flow in RCA. They found that secondary flow produced large variations in wall shear stress along blood vessel. They further added that geometric effects were the determining factors on RCA hemodynamics.

Right coronary artery functions as a distributing vessel, that distributes blood to a specific region of myocardium, and not a delivering vessel (that delivers blood from that region to different parts of myocardium). This is why right coronary arteries lack a lot of branching; they have relatively same trunk diameter and small branches in their periphery. On this basis researchers found it safe to neglect branches in RCA proximal to the posterior descending artery (PDA), and considered other factors such as curvature, pulsatility, oscillation etc as the main causes behind lesion accumulation. (Bruschke, 1981)

2.2 Previous Studies Related to Branching

To examine the effect of branching, previous researchers have examined flow through the carotid artery (technically a bifurcation), the aorta, and the coronary arteries. However, most of

those studies have focused on the angle of bifurcation or branching, rather than the role that the size of the branch plays on the hemodynamics in the vessel. Below, each of these studies has been discussed, explaining the findings of the significance of the branch-related feature.

In a paper by Zhao et al. (1999), CFD based study of pulsatile blood flow was done in an average human carotid bifurcation model with and without the superior thyroid artery (STA), and also by changing the position of the STA after bifurcation. Variations in flow pattern, shear stress have been studied in detail. Study was conducted by keeping STA at three different distances of 5mm, 10mm and 20mm from bifurcation apex. Another model was also studied by completely omitting the presence of STA. This study suggested that the presence of small artery did not have much impact on the flow velocity or wall shear stress distribution in the Common Internal side branch. If the ratio of flow division between STA and external plus superior thyroid arteries was small, the effect on the maximum reversed flow velocity would also be less. The flow ratios taken for the simulation were 5%, 10% and 20%. In case the amount of blood flowing through the STA is added up to the external carotid artery and the former was completely neglected from the arterial geometry, it would cause negligible change in flow within the carotid sinus. However, removal of STA does have significant impact in the common external branch side. And these findings were found true for all the three placements of the STA from the bifurcation apex. This study touches the essence of the objective of my research. However, since this is a specialized research on Superior Thyroid artery of particular diameter of 1.9mm the findings on coronary artery could be much different because of high tortuousness and different boundary conditions. Though the researchers have analyzed the significance of blood flow with respect of ratio of flow division as 5%, 10% and 20%, they have not clearly specified the threshold ratio that can or cannot be neglected.

In the same year Zhou Y. et al (1999) in their study mentioned that the coronary circulation had a design constraint. According to this, length of the sub-tree from a segment determined the diameter of an arterial segment. It could be said that variations in inter-individual branch diameter as well as flow rate would be in accordance with the variations in patterns of

myocardial perfusion. Coronary trees were found to obey self-similarity patterns (Bassingthwaighte et al. 1990). Studies conducted afterwards by Y. Zhou (1999) showed the existence of power law relationship between the diameter of a stem and length of the subtree‟s crown, but it doesn‟t take into account the vessel tapering and hence is considered as a comparatively weaker measurement.

$$d_N = l_N^{\frac{4-3\varepsilon}{4(3-\varepsilon)}} \ldots\ldots (1)$$

Where, d_N = stem‟s nomalized diameter

l_N = total length of artery distal of the bifurcation

$\boldsymbol{\varepsilon}$ = empirical constant to be determined from a least squares fit of the anatomical data

Similarly, relationship between stem‟s nomalized diameter and normalized flow was determined to be:

$$q_N = d_N^{\frac{4(3-\varepsilon)}{4-3\varepsilon}} \ldots\ldots (2)$$

Where, q_N = normalized flow

Later in 2001 Steinman D.A. reported that in most cases the small side branches which were arising from targeted vessels were ignored. It was mainly because of the technical difficulties involved in in-vivo imaging. It was particularly difficult when dealing with branches oriented parallel to the imaging slice plane. But few studies during that time showed that such small branches only had small effect in overall blood flow. Image based CFD models could get advanced and it might be possible to include such small branches. But it would be difficult to measure flow rates and assign boundary conditions to these branches. Hence in compare to the method of incorporating individual branches, the models based on vascular resistance would get more popular.

Richter et al. in 2004 reported several in vivo studies as well as parametric comparison of the relation between main branch and side branch. Because the arterial bifurcations differed in shape and size (lumen size), a study for the effects due to the variation in these geometric parameters was done. In order to investigate the effect of the diameter ratio of main branch to side branch

three different models were built possessing following main to side branch diameter ratio: 2:1, 4:3, 1:1. Parametric comparison between the models with 1:1 and 2:1 main to side branch diameter ratio suggested that variations in diameter size did not alter the nature of flow separation in the main branch. This led to the conclusion that the effects on the main branch were governed by the total flow in the side branch and not by the diameter size of side branch. However, the nature of flow separation was observed to be different.

More recently, Gijsen et al. (2008) studied patient specific main branch of Lower Anterior Descending (LAD) artery by imaging in vivo and reconstructed the geometry in 3D using ultrasound and biplane angiography. On the other hand, they reconstructed the side branch using biplane angiography. In studies before this, whenever shear stress distribution was accounted in interrogated coronary artery with ANGUS (an approach for 3D reconstruction of coronary arteries by combined use of IVUS and angiography; discussed in detail in Chapter 3) imaging method branches had been neglected. This limitation in geometrical imaging was due to the limited penetration depth of IVUS (max=5-6mm depth) which depends on the catheter frequency (For example, a 20 MHz catheter has a better penetration than a 40MHz catheter, but less spatial resolution). After reconstruction of geometry using Gambit and CFD analysis through Fluent Inc. they found that geometrical and flow parameters dictated the flow phenomenon in the second diagonal of LAD; the main geometrical factors being angle between the branches and surface ratio of the two daughter branches. They did not create models for different angles or surface ratios of the branch. However, they concluded that larger the angle and the ratio, more impact the branch was expected to have. The length of the analyzed LAD (distal) was 5.5mm with average diameter of 2.0+-0.2mm, while the proximal region had length of 7.5mm and average diameter of 2.3+-0.1mm. When comparing the two models with and without the second branch, variation of 12% was observed in Wall Shear Stress in both divider and non divider wall walls of LAD. Small bifurcation angle between LAD and Left Circumflex (LCX) artery was considered for study because the lumen of LCX would more readily disappear from the IVUS imaging if larger angles were taken. For Reynolds number taken as 60 and a small bifurcation angle, despite of a

relatively large lumen area, the second diagonal did not influence the flow pattern in LAD after 3mm downstream. This result was found to be in agreement with that of (Richter et al., 2004). Hence, the paper concludes with a remark that instead of merging the branches in the main geometry, it would be more appropriate to add elliptical contours derived from the reconstruction of 3D angiography to account for the presence of side branches in the shear stress distribution of the main branch. This paper does not clarify the angle considered between the branches in their geometry nor the surface ratio was altered for studying the impact and simply states that greater the angle more will be the impact.

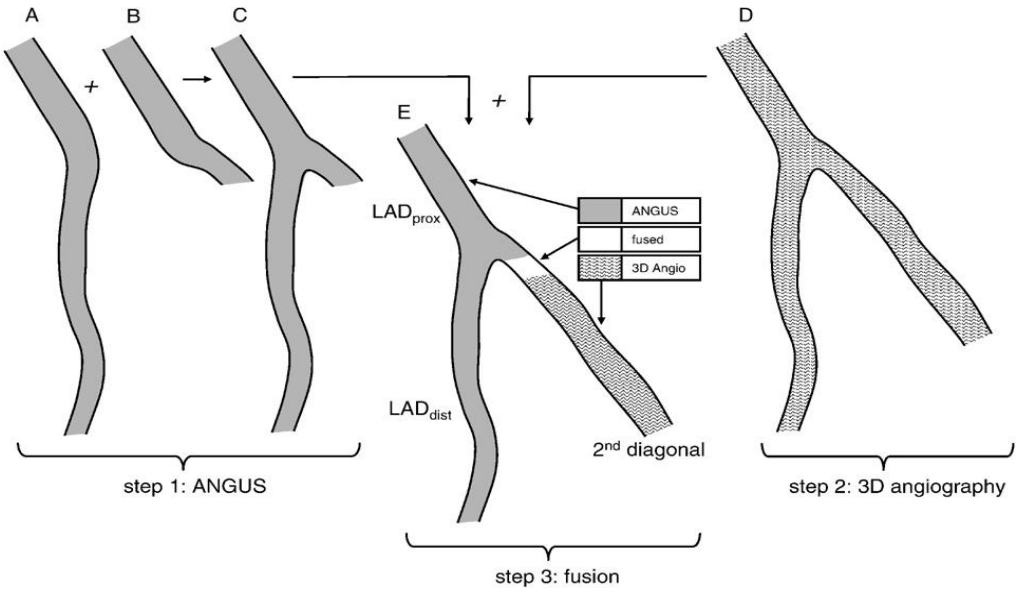

Figure 2-3 Final reconstructed bifurcation and its different parts.

The LAD and bifurcation region are reconstructed using ANGUS (panels A–C). The lumen of the distal part of the 2nd diagonal is derived from 3-D angiography (panel D) and the proximal part of the second diagonal is generated by fusing data from the ANGUS procedure and 3-D angiography (panel E).

Source: Gijsen F.J.H., Wentzel J.J., Thury A., Lamers B., Schuurbiers J.C.H., Serruys P.W., Steen A.F. "A new imaging technique to study 3-D plaque and shear stress distribution in human coronary artery bifurcations in vivo". Journal of Biomechanics 40 (2007) 2349–2357

2.3 Boundary Conditions at Outlet

In addition to the challenges associated with the coronary artery reconstruction, simulating blood flow in a branched or bifurcated geometry introduces an additional complication due to the presence of multiple outlets in addition to the local and global curvatures. Arterial geometries affect the local hemodynamics including secondary flow, recirculation, etc but the inlet and outlet boundary conditions affect the large scale features of the flow such as the flow ratio in the site of branching and pressure distribution (Grinberg. et al., 2008). Hence, physiologically accurate boundary conditions that are robust as well as simple to implement are necessary for confidence in the computational solution. Ideally, patient- specific boundary conditions should be implemented in simulations. However, this is not always feasible, and hence reasonable assumptions must otherwise be made.

Flow and pressure waves emanate from the heart and travel through arteries to finally get damped, dispersed and even reflected. This happens because of fluctuation in vessel caliber, tissue properties and branching of geometry. Hence in large arteries, solutions to the governing equations of blood flow are highly dependent on the outflow boundary conditions that are imposed to represent the vascular bed downstream of the modeled domain. It has always been an area of great interest to designate most physiologic boundary conditions for simulations. The most commonly used outflow boundary conditions while simulating blood flow in arteries are constant pressure or traction and prescribed velocity profiles According to Vignon-Clementel (2006), if an explicit relationship between pressure as a function of flow rate or velocities at the coupling interfaces could be determined then it is possible to derive outflow boundary conditions for that downstream domain. In this study, out of several approach that have been developed to accurate represent outflow boundary conditions, Impedance boundary condition, a model based on the concept of impedance in electricity, was concluded to be the most appropriate approach for addressing natural sites of wave reflection in downstream region (Vignon-Clementel et al., 2006)

Another popular method of deriving boundary condition is Resistance /Windkessel boundary condition. It envelops the general concept of resistance to define a relationship between mean pressure and flow rate, consistent with Poiseuille flow where the flow is fully developed (gradients in the axial direction is zero). Here, an assumption of constant pressure in the downstream domain over the cross sectional area of the inlet boundary is made. (Vignon-Clementel et al., 2006, Grinberg and Karniadakis, 2008)

Another approach widely described in the literature is to assign mass flow ratios to different outlet branches. For example, a study carried out to compare the impact of geometrical differences obtained from Computed Tomography (CT) , Magnetic Resonance Imaging (MRI), and optically digitized post mortem vessel cast was done by Goubertrigz. In this study, a 50/45/5 flow rate relation was assumed between the three outlet vessels of the LCA (Left Coronary Artery) bifurcation. The flow rate relation was estimated based on the cross section areas of the three outlet vessels measured proximal to the bifurcation (Goubergrits, 2008).

The boundary conditions hence used purely depend on the physiological information available to the researchers. As discussed earlier, generally such information is not always available and thus researchers need to make reasonable assumptions when needed.

2.4 Application: Anastomosis

The study of flow splitting at branches of different sizes could have a direct and interesting application in some surgical treatment procedures for stenosis. One of the popular means of treating stenosed arteries is to provide an alternative path, or a bypass for the blood (Chandran K.B., 2006). This will enable blood to circumvent the obstruction and reach the end-organ. Arterial bypasses can readily be created by implanting a vascular graft around the diseased area. The arterial stenosis are focal in nature. This leaves neighboring segments of the artery relatively unaffected once the graft is placed. In these surgical procedures, the affected vessel is exposed and the bypass graft is placed alongside it and sewn to arterial sites well

upstream and downstream of the stenosis. The junction between the artery and the graft is called anastomosis (Chandran K.B., 2006) and is generally constructed in an end-to-side fashion. Once the graft is in place, blood flow is then re-instituted in the diseased area often with some residual flow still being carried through the native artery through the stenosis. It is beneficial to know beforehand the size and flow characteristics of the blood flow in such a setting. Hence fluid dynamic simulations will prove as a useful tool to provide the necessary inputs for effective design and modeling of the graft. The current study investigates the effects of different branch sizes attached to a main artery on the upstream and the resulting downstream flows. Hence the physical insights gained from this study will provide the necessary inputs for the case described above.

Figure 2-4 Cartoon of an anastomosis showing a graft connecting two arterial structures

Source: clarian.org, "Anastomosis", 2010

CHAPTER 3 METHODOLOGY

In order to understand the effect of branch size on flow in the coronary vessel, this study will employ computational fluid dynamics (CFD) to simulate blood flow. CFD requires information about the geometry to be simulated, which in the current case will be obtained from human coronary arteries.

3.1 3-D Reconstruction of Coronary Arteries

In an intravascular ultrasound, an ultrasound tipped catheter is inserted into a blood vessel and is extended to the point of diseased cross section. It allows the physician to visualize the cross-section of the artery at the particular location of the transducer in current time. In a relatively straight blood vessel like a carotid or femoral artery, IVUS is sufficient to generate complete vessel geometry. In this case, vessel geometry is just a compilation of subsequent cross sectional geometries. However, when it comes to coronary arteries, this approach is not sufficient because of the highly curvy nature of its geometry of the same. Cross sections obtained from IVUS lack information about the tortuous path travelled by catheter. Hence, it fails to give the true geometry of coronary arteries. In order to incorporate curvature and hence generate the coronary geometry, angiographic images can be used in assistance to the IVUS imaging (Wahle et al., 1999a).

An angiogram provides one image/plane of an artery from one angle. By acquiring and combining two orthogonal planes, it is possible to create a 3D image of tortuous coronary and hence retrieve the path information that IVUS lacks. Combination of these two methods allows the possibility of relating cross sections to their correct geometric location (i.e. Angio-IVUS fusion) and hence an accurate representation of coronary arteries may be achieved.

Figure 3-1 shows a typical IVUS image of coronary artery, showing traced borders. The yellow border denotes the lumen-plaque interface, and red border is the location of the media-adventia interface.

Figure 3-2 shows an angiogram image in a one-plane view of the coronary artery. The red arrow points to the catheter tip. The catheter can be seen throughout the vessel.

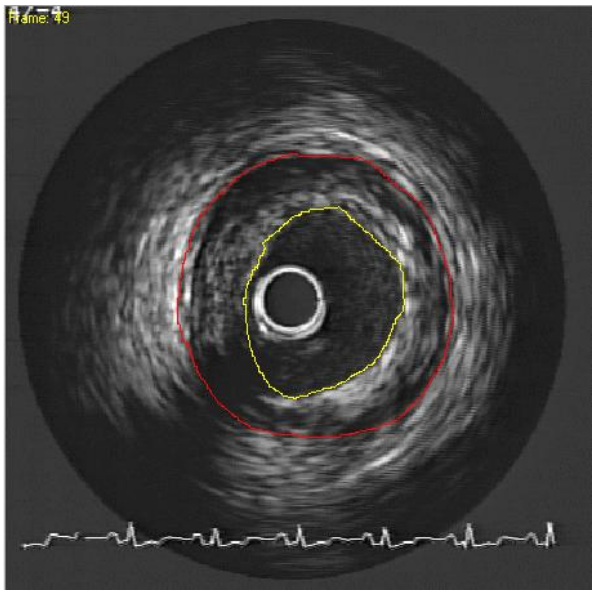

Figure 3-1 A typical IVUS image, demonstrating traced borders

Yellow denotes the lumen-plaque interface, and red is the location of the media-adventitia interface.

Source: Vigmostad S.C., "Hemodynamics and Wall Thickness in Relation to Localized Geometric Changes in Human Coronary Arteries", Masters Dissertation, The University of Iowa, Iowa City, Iowa, 2003.

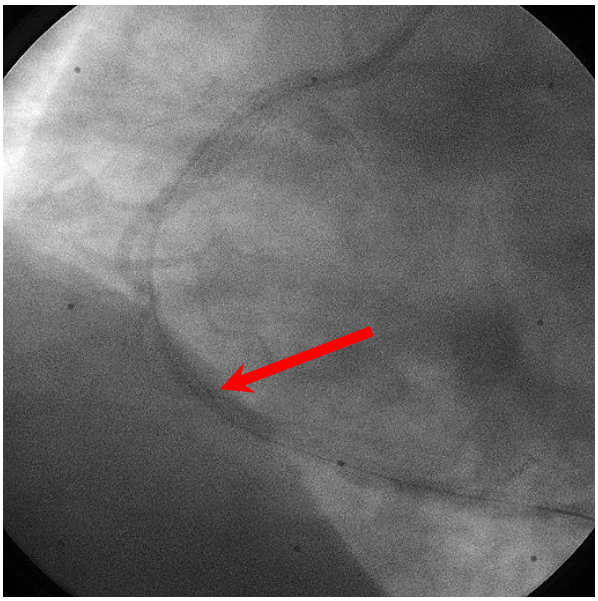

Figure 3-2 An angiogram image showing a one-plane view of the coronary artery

The red arrow points to the catheter tip, and the catheter can be seen throughout the vessel.

Source: Vigmostad S.C., "Hemodynamics and Wall Thickness in Relation to Localized Geometric Changes in Human Coronary Arteries", Masters Dissertation, The University of Iowa, Iowa City, Iowa, 2003.

3. 2 Volume and Mesh Generation in Pointwise 64 Bit Version16.03R1

In this study, to reconstruct the patient specific coronary arteries, combined data from intra vascular ultrasound (IVUS) and biplane angiography were utilized. In order to conduct a computational fluid dynamic (CFD) analysis a volumetric mesh is required that truly represents the geometrical properties of the body being analyzed. Since the coronary arteries have highly torturous features and complex geometry an unstructured mesh comprising of tetrahedral elements was chosen which could preserve the geometrical properties. The unstructured mesh as such was generated using Pointwise 64bit Version 16.03R1.

This study dealt with investigating the role of different ostium sizes of branches in the main vessel, hence reconstruction of branches were an integral part of it. In addition to the main vessel geometry, it was necessary to extend the arteries by 10 diameters in the inlet and 5

diameters at the outlet so as to have a fully developed flow at the inlet and to cancel the entrance and exit effects. The generation of volume, extensions, volumetric mesh and the extrusion of branches are discussed below in detail.

3.2.1 Without Branch Case

Surface meshes of arteries were obtained in the format of stereolithography (STL) files. These files were generated from the 3d reconstruction via fusion of angiography and IVUS. Files as such were imported as grid points in Pointwise 64bit Version 16.03R1. Unstructured domains were created by specifying the connectors and then these domains were assembled into a block. These blocks were then initialized to obtain an unstructured tetrahedral volumetric mesh. The length of the artery was extended in the inlet by about ten times the inlet diameter and at outlet by 5 times of the outlet diameter by extruding the faces in their normal direction.

Boundary conditions were then specified at different faces of the block. Inlet was specified as mass flow inlet and outlet was specified as mass outflow. The artery wall and extended surfaces were defined as wall. These files were exported as case files for FLUENT.

3.2.2 With Branch Case

All of the above mentioned steps were similarly followed while creating a volume with a branch, but with a few additional steps. In order to create a branched geometry a hollow cylinder of required diameter (see below) and orientation was created and intersected with the vessel geometry representing the artery. The intersection curve obtained as such was extruded in the direction of branch away from the artery. An offset distance of 10^{-9} m was maintained in between the artery and the branch as required by FLUENT to solve unconventional meshes. The reader is referred to FLUENT Manual, (Chapter 7) on using a non-conformal mesh for further details. The branch geometry was then assembled as domains and block and initialized to obtain a volumetric mesh. Branch outlets were also defined as „Outflow boundary condition“ and their

surfaces were defined as „Wall". While solving flow using this interface approach, very large local shear stress was observed only in a localized region of intersection or interface purely due to the presence of this offset distance. Since these values were localized only in the interface region and not in the downstream or upstream region of branching, the data extracted remained unaffected.

3.3 Mesh

The volumetric mesh generated as described above had unstructured tetrahedral mesh in the region that defined the main artery as well as in the extruded extensions at the inlet, outlet and the extruded branch outlet.

3.4 Solving Flow in FLUENT 12.0.16 (ANSYS 12.0)

The case files exported from Pointwise 64bit Version 16.03R1 were read in FLUENT 12.0.16. Blood was selected as the working fluid in a viscous laminar model. Blood flow was considered laminar, incompressible and approximated as Newtonian. The density of blood was taken to be 1050 kg/m^3, and viscosity was taken to be 0.00402 kg/m-s. Since patient-specific information on coronary artery flow rate was not available, a value of mass flow at the inlet was assumed to be 0.00167kg/s (100ml/min) in the direction normal to the boundary (Vigmostad, 2004). Solution scheme was set to SIMPLE. Residuals were set at 10^{-4} for accuracy of results. Solver was chosen to be steady and pressure based. The calculations were iterated until a steady state convergence was achieved within prescribed tolerances. In all studies considered, Reynolds number is defined with respect to the main artery inlet diameter and the prescribed velocity (that can be computed from the specified mass flow rate) as $Re=\rho UD/\mu$ where ρ is the density of blood, V is the velocity, D is the diameter and μ is the dynamic viscosity.

As discussed in CHAPTER 2, ideally patient specific boundary conditions should be used for hemodynamic simulations. However, obtaining such patient-specific pressure and flow conditions as boundary conditions is not always feasible due to the complications involved in obtaining them. In current study, we could not obtain such patient specific physiologic information. Hence, an acceptable assumption of mass outflow boundary condition was made, as done by Goubergrits(2007) and Hassan(2004). The cross sectional areas of the two daughter vessels at the point of branching were calculated. The ratio that the individual cross sectional area made with the sum of both the outlets were taken as the values for mass flow split. For example, if the sum of the cross sectional areas of the daughter vessel and main outlet were considered as one, and ratio of cross-sectional areas of the main to daughter vessel was .7 to .3, then the mass split in those two vessels would also be 70% and 30% of the total inflow.

3.5 Validation

3.5.1 Grid Independency Study

From a CFD point of view, it is very important that the solution from the grid being used be independent of the number of nodes used and hence the size of the element used in the mesh. A representative artery was chosen for the grid independency study, and for simplification, branches were neglected in this initial study.

When volumetric mesh was created in a representative vessel without any manipulation, the surface mesh resulted in a volumetric mesh with 44388 nodes. This surface mesh has been shown in figure 3-4. This mesh appeared coarser with concern to obtaining the accurate flow results in a complicated geometry of coronary arteries. The number of nodes was hence increased in Pointwise V16.03R1 by decreasing the average element size. Since the mesh was unstructured it was not possible to get all the elements of the equal sizes. Further it was also not possible to aim for a specific number of nodes in the volumetric mesh, a typical characteristic of unstructured meshes.

	Finest (avg dx=0.08 mm)	Fine (avg dx=0.1mm)	Coarse (avg dx=0.2 mm)
No of Mix cells	8843736	2058243	515145
No of Nodes	1563967	393704	100936

Table 3-1 The number of nodes present in a representative vessel for the three cases of refinement done for grid independent study.

Three cases were chosen (see table 3-1) each having roughly four times the number of nodes than the coarser one; these meshes were termed as coarse, fine and the finest cases with each of them having 100936, 393704, and 1563967 nodes respectively. The surface meshes of these three degree of refinements used have been shown below in Figure 3-5 at a particular region of the artery. As the goal was to analyze the flow properties in main vessel and not in the extensions or in the branches, care was given on increasing the number of nodes in the main vessel. Flow was analyzed in FLUENT for all these three cases of refinement.

As this entire study in subsequent chapters are based on analysis of wall shear stress as a key variable for detection of secondary flow structure, this variables was chosen when performing the mesh dependency study. The wall shear stress was plotted along the circumference of the main artery for all three cases of refinement as shown in Figures 3-8 and 3-9. Two representative slices were selected having the largest and the smallest cross sectional areas in the vessel under study. These slices can be seen below in Figure 3-7. It could be seen that the wall shear stress measurement in the fine case was almost identical to that in the finest case. On the other hand, although the coarse case showed a trend comparable to the finest case, the percentage error (Table 3-2 and 3-3) calculated was significantly larger compared to the fine mesh case. In comparison to the finest case, the coarse mesh had percentage error ranging from 0.93-2.16%; while the percentage error for finer case ranged from 0.43- 1.31%. Hence fine mesh

case was chosen to carry out this study from an economical point of view. The final chosen mesh in a region of the artery has been shown in Figure 3-10.

3.5.2 Study of Effect of "Sharpness" of Flow Divider on Hemodynamics

Artery bifurcation and branching is an area of interest for fluid analysts because of the sudden transition in the geometry for blood flow. Figure 3-3 shows a schematic of an arterial bifurcation where the flow from the main branch splits from the parent to the daughter branches. The portion or region of the main artery closer to the branch is usually referred to as the divider wall. The region of the main artery wall away from or distal to the branch is simply the outer wall. The region of the branch may also be referred as the flow divider at the site of bifurcation. The take-off angle is the angle between axis of the main artery and the axis of the branch. As the flow splits at the location of the branch, a thin boundary layer is generated in that transition region with high axial velocity outside the boundary layer. The velocity profiles in the region downstream to the bifurcation are skewed towards the divider wall. This subsequently gives rise to low wall shear stress in the outer walls of bifurcation and hence causes flow to separate (Chandran, 2006). If the corners of the outer walls are sharp then there is more possibility of flow separation like in the case of lateral iliac artery. The regions of low WSS (Wahle et al., 2006) and flow separation are again interesting from a physiologic point of view as they are one of the most prominent regions of artery occlusion.

Bifurcation regions of arteries do not have sharp interfaces, they are naturally curved or filleted with finite radius of curvature. Such natural curvature in the branch region provides smooth transition for the motion of blood. It was not possible to imitate such smooth filleted transition in a model of artery-branched geometry in the software used for this study. Hence in order to account for possible error in results that could occur while using sharp cornered artery-branch interface, a study is conducted on few simple filleted and unfilleted models in two- and three-dimensions that could be constructed easily.

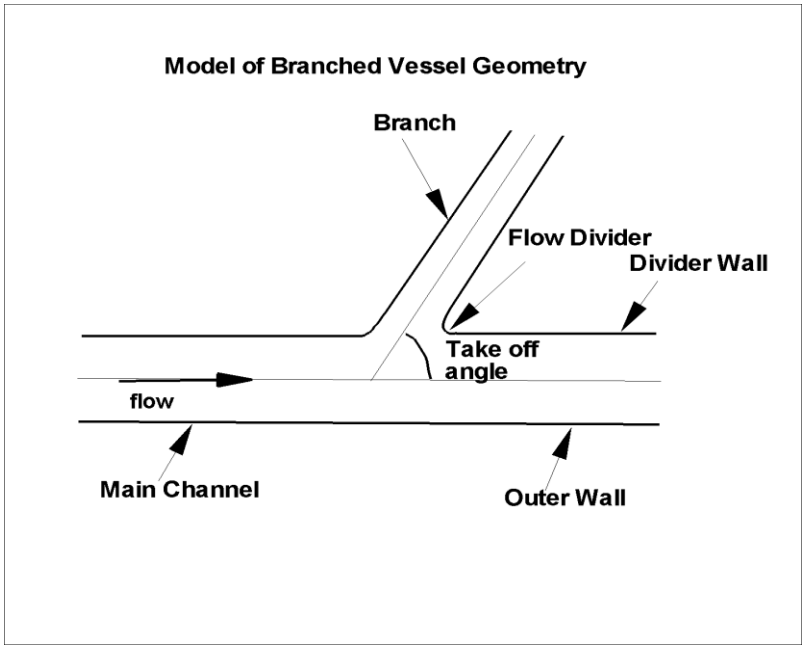

Figure 3-3 Schematic of branched vessel geometry indicating different components

A hollow cylinder was modeled as an artery to study the effect of sharp and filleted branch interface region on the nature of flow downstream. The diameter of the cylinder was 1.6mm; and length was 30mm. A branch radius was modeled to be one third of the radius of the main cylinder.

Three pairs of geometrical models were compared for this purpose out of which two were two-dimensional and the third was 3-dimensional. The first one was a 2-dimensional 90 degree case. In this geometry, a two dimensional branch channel was attached to the main channel at a take-off angle of ninety degrees from the axis of the main channel. In the second case, a 2-dimensional branch was added to the main channel carrying the flow at an angle of 65 degrees to the axis of the duct. Finally, a 3-dimensional 90 degree case was considered. The geometry of this three-dimensional model was same as the 2-dimensional 90-degree model considered above. Physiologically wide discrepancy in take off angle of branches are seen in general, with many of

these being large and even approaching 90 degrees (Chandran, 2006), the take off angles of the branches selected for this study can be justified. For each of these three cases described above, a filleted geometry was also considered. For further analysis, in the two-dimensional setting with fillets, two additional cases were explored. Two degrees of fillets were considered for the 90-degree bifurcation geometry. The first one which will be referred to as „lightly-filleted" has an approximate fillet radius of 0.015 mm. The second variation which will be referred as „highly-filleted" has as approximate fillet radius of 0.5 mm. Nonetheless, the „highly-filleted" case was considered for academic purposes and it will be seen later that some interesting differences were observed because of this geometrical modification of the fillet radius. Also, the Reynolds number regime based on the flow conditions through-out this study fell in the intermediate Re-regime. It could be speculated that for much lower Re (~ Re<10), the presence of the fillet radius may not play a major role in modifying the flow structure to noticeable levels. But, for higher Re, as in cases considered here, the inertia of the flow was significant. Particularly, how the inertia of the flow interacted with the bifurcation nature of the arterial geometry in the presence or absence of the corner fillet was not clear. Hence, this motivated the comparison of lightly-filleted and highly-filleted cases.

Blood was taken as the fluid under study with a density of 1050 kg/m^3, and dynamic viscosity of 0.00402kg/m-s. The inlet velocity was specified as 0.791m/s (100ml/s) (Vigmostad, 2003) for simulation such that the Reynolds number of the flow was 330. The length of the main-flow carrying channel or duct upstream and downstream of the branch in all the models were designed to be more than ten times the diameter at inlet and five times the diameter at outlet respectively to cancel the end effects (Vigmostad, 2003). Highly refined meshes necessary to tap the flow behavior were created in Gambit. Figure 3-11, 3-12 and 3-13 show the models of the cases described above.

Once the model and mesh were created, the mesh (Figure 3-14) was imported into Fluent. As described later in Chapter 4, FLUENT, a finite volume based fluid solver was used. The model was supplemented with appropriate boundary conditions at the inlet and outlet. The

solution was iterated to a steady-state convergence. Below, the flow results of the different cases described above have been presented. Flow results have been presented and analyzed using streamline plots, and contours of velocity and wall shear stress. Each of the subsections below describes these results.

3.5.2.1 2D 90-Degree Case

Figures 3-15 to 3-18 show results for the two-dimensional 90-degree bifurcation case. Fig. 3-15 shows close-up view of the wall shear stress distribution near the branch corner for the no-fillet and „lightly-filleted" case. Fig. 3-16 plots streamlines overlaid on wall shear stress contours for the no-fillet, lightly-filleted and heavily-filleted cases. Figs 3-17 presents streamline plots overlaid on contours of velocity magnitude for the no-fillet, lightly-filleted and heavily-filleted cases.

Bifurcation angle of 90 degrees is not only physiological as it is seen in intercostal arteries (branch off the thoracic aorta) and renal arteries (branch off the abdominal aorta); it is also the easiest to model. When the flow characteristics of a sharp 90- degree branch model was compared with a slightly filleted branch model not much difference was seen in the flow behavior. However when the fillet angle was increased significantly, as in the heavily-filleted case, wall shear stress (WSS) was observed to increase significantly, For example, the WSS at point "A" as shown in Fig. 3-15 from 0.17 for non filleted case to 0.35 in the highly filleted case. Due to the low WSS secondary flow were seen in the region immediately above point A in branch in the no filleted and less filleted case but not in the highly filleted case. Similarly, point "B" in the wall region immediate downstream also showed comparatively low value of wall shear stress in the unfilleted and less filleted cases. However the region downstream to point "B" in all the three cases showed similar values of WSS ranging from 0.15 to 0.21.

3.5.2.2 2D Angled Case

Figures 3-17 to 3-19 show results for the two-dimensional angled bifurcation cases both with and without fillet. As before, contours of wall shear stress and velocity magnitude have also been presented .Unlike the 90-degree bifurcation case where blood undergoes a sharp transition at the branch, in case of the 65-degree angled case, blood flows through smooth transition for both the filleted as well as unfilleted cases. No secondary flows were seen in both of these cases. However the immediate region proximal to branching (around point "A" showed lower WSS in non filleted case (WSS was in the range of 0.06-0.16) when compared with filleted case (WSS was in range of 0.2-0.3). Similarly point "B" and region downstream to it showed WSS as low as (0.03-0.04) in non filleted case while (0.2-0.4) in filleted case.

3.5.2.3 3D 90 Degree Case

The flow and wall-shear stress results for the 3d 90-degree case have been presented in Fig. 3-20 and 3-21. Only one fillet radius was considered in the three-dimensional model. The flow characteristics in 3d 90-degree bifurcation model were comparable to that of 2d 90 degree bifurcation model. Secondary flows were seen at the outer wall of the branch in the region of low WSS. Nature of WSS and velocity distribution downstream were quite similar in filleted and non filleted cases as seen in figure. The values of velocity distribution were similar in the 2-d and 3-d cases but WSS were found higher by 3 times in the 3-d 90 degree cases. This can be explained by highly refined mesh in boundary wall seen in the 3d model.

Based on the results of the filleted and non-filleted cases presented above in two-dimensional and three-dimensional settings, the following conclusions may be arrived. This study suggested that for a moderate Reynolds number flow, filleted interface does not create significant impact on flow characteristics downstream of the branch. Though secondary flows were seen in non filleted or less filleted cases they were found in branches and not in the region of the artery downstream to the branch which is the main focus area in this study. However, it

was seen that the fillet angle played a significant role in the flow characteristics in branches; higher the fillet angle lesser the secondary flow. Similarly in the case of branches with take-off angle lower than 90 degrees, unfilleted branch interface didn‟t cause secondary flow in the branches and the flow downstream was also similar to that of filleted case.

Hence these results suggested that modeling of unfilleted bifurcation angles does not cause significant discrepancy in the nature of flow downstream, but only in the hemodynamics of branch flows; which is in agreement with the findings of He and Ku (1995). However, the effect of sharp corners were observed in the main channel flow downstream though limited to very small regions near the corners; which is also in agreement with the study by He and Ku (1995). Presence of sharp corners could hence have an impact in defining exclusion regions in the vicinity of branches where wall shear stress is to be calculated On the other hand, in this study only one simple branch case was modeled having radius one third of the main artery. It might be possible that for larger branches, fillets might cause significant effect on downstream flow. Fillet cases were not studied for larger branch diameter because it was not possible to create 3d 90 degree cases for them. However, it may be assumed that the analysis and conclusions in this section above may be extended to the actual artery geometry to be considered later in this study. This may particularly hold true in view of the fact that the Reynolds number considered in this section is much higher than the Reynolds number that pertain to flow conditions in the main artery simulations to be presented in the later chapters.

3.6 Reorientation of Contours for Postprocessing

The contours obtained after summing up the IVUS and angiogram images are orthogonal to the tip of the catheter and totally depend on the catheter location. The catheters are prone to twisting and turning because of the tortuous nature of the coronary vessels (Wahle et al., 1999). Catheter tries to find a position of minimal energy within the vessel thus the pullback path is much smoother than the vessel centerline (Wahle et al., 1999). Hence at any position there is a

large possibility that the IVUS image may not be representing the actual cross section oriented perpendicular to the centre line of the vessel geometry at a point but as a potentially oblique cut.

Slices orthogonal to the vessel centre lines are important to reconstruct the exact vessel morphology. This helps to accurately measure the exact wall thickness due to the possibility of measuring straight perpendicular line in between the inner and outer contour. Further, contours orthogonal to the centerline of blood vessel leads to the accurate calculation of flow velocities as well as wall shear stresses.

It was possible to obtain contours perpendicular to centerline using the methodology cited in a research paper of Vigmostad (2003). This methodology is briefly described below.

The contour or surface points of the inner lumen are considered as reference points to obtain normal planes. In order to calculate the tangent vector from the centre line, initially all the center points were splined. These center points of the inner lumen of the vessel have been represented by the dotted lines in Fig. 3-4 below. Once the equation of the spline was obtained, the first derivative of the centre line at each centre point gave the x, y and z components tangent vectors. These tangent vectors were then used to calculate the points in the outer and inner wall that are orthogonal to the line described by the tangent and the centre point of that contour. For all models of artery simulated in this study, 720 points per contour were splined into 720 axial splines using cubic B-splines. The space between each two points was further divided into 999 intervals. A binary search was then carried out such that a plane of 720 points was obtained out of the pool of 999 points, which was orthogonal to the line in between tangent(T) and centre(C) . If (P_T), be a point on the outer or inner wall then the vector (V_T) constructed in between (P_T) and (C) is given by:

$$(V_T) = (P_{Tx} - C_X)\hat{\imath} + \left(P_{Ty} - C_y\right)\hat{\jmath} + (P_{Tz} - C_z)\hat{k} \dots\dots\dots (4)$$

Here (i,j,k) are the unit vectors on the Cartesian co-ordinate system. The vector between centre and the tangent (N) is given by:

$$(N) = (T_x - C_x)\hat{\imath} + \left(T_y - C_y\right)\hat{\jmath} + (T_z - C_z)\hat{k} \dots\dots\dots (5)$$

Angle(ϕ) in between these two lines can be calculated by following formula:

$$(\phi) = (COS \frac{(N_x * V_{Tx} - (N_y * V_{Ty} - (N_z * V_{Tz})}{\sqrt{(V_{Tx})^2 + (V_{Ty})^2 + (V_{Tz})^2}\sqrt{(N_x)^2 + (N_y)^2 + (N_z)^2}}) \quad \ldots\ldots\ldots(6)$$

While determining the points forming the orthogonal plane, it turns out that most of the times the angle formed are not 90 or 270 degrees as desired. The point lies before the desired plane if the angle calculated is between 90 and 270 degrees. If the calculated angle is less than 90 degrees or greater than 270 degrees then the point is beyond the required plane.

Because of the tortuous nature of coronary arteries, many times the window of 999 points is not sufficient to determine the points forming the required orthogonal plane. Hence the search window is widened to a pool of 3000 points by splining the first four contours at a time. If the desired plane is not found then next set of four contours are taken such that the first contour in the previous search is replaced by the second counter in the previous search and a new fourth contour is considered. While performing this search it is quite possible that the newly found planes would overlap. Hence each time search is done for a new centre, the contours previously used for splining should not be used.

However, there could be several instances when the orthogonal planes as such might not get determined. In such cases, the tangent vector is rotated with respect to the point in the pool of splined points with which it makes the least angle. The tangent is rotated such that it now makes 90 or 270 degrees with that point. Binary search is carried out for this newly determined tangent to find the points in the surface that are at 90 degrees or 270 degrees to this new tangent.

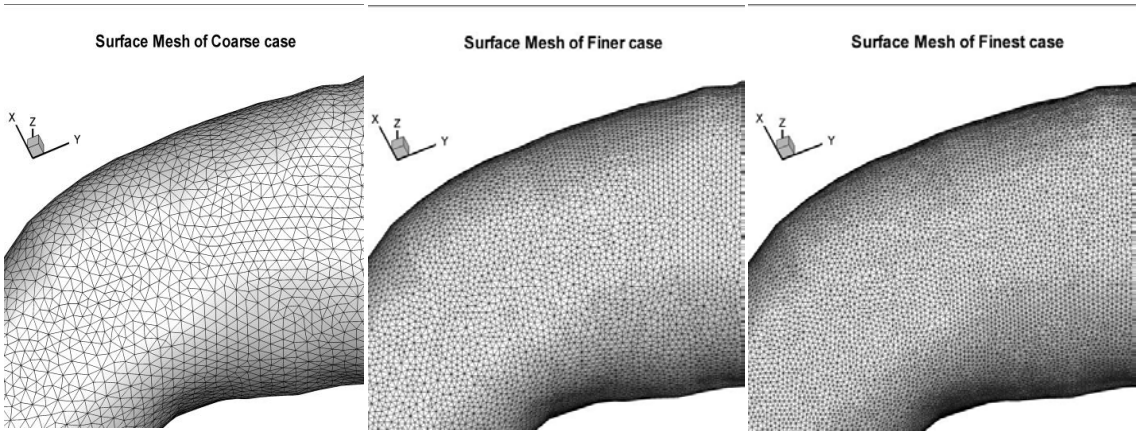

(a) **(b)** **(c)**

Figure 3-4 Close up view of (a) coarse, (b) fine, and (c) finest surface meshes used in grid independency study

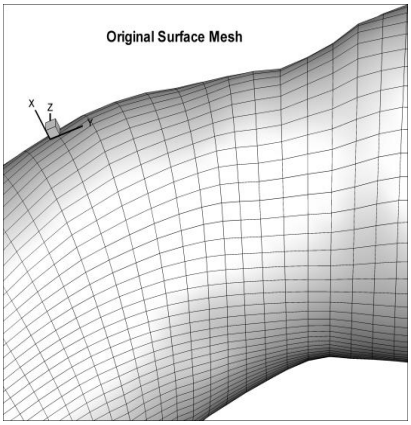

Figure 3-5 Close up view of surface mesh from original STL file

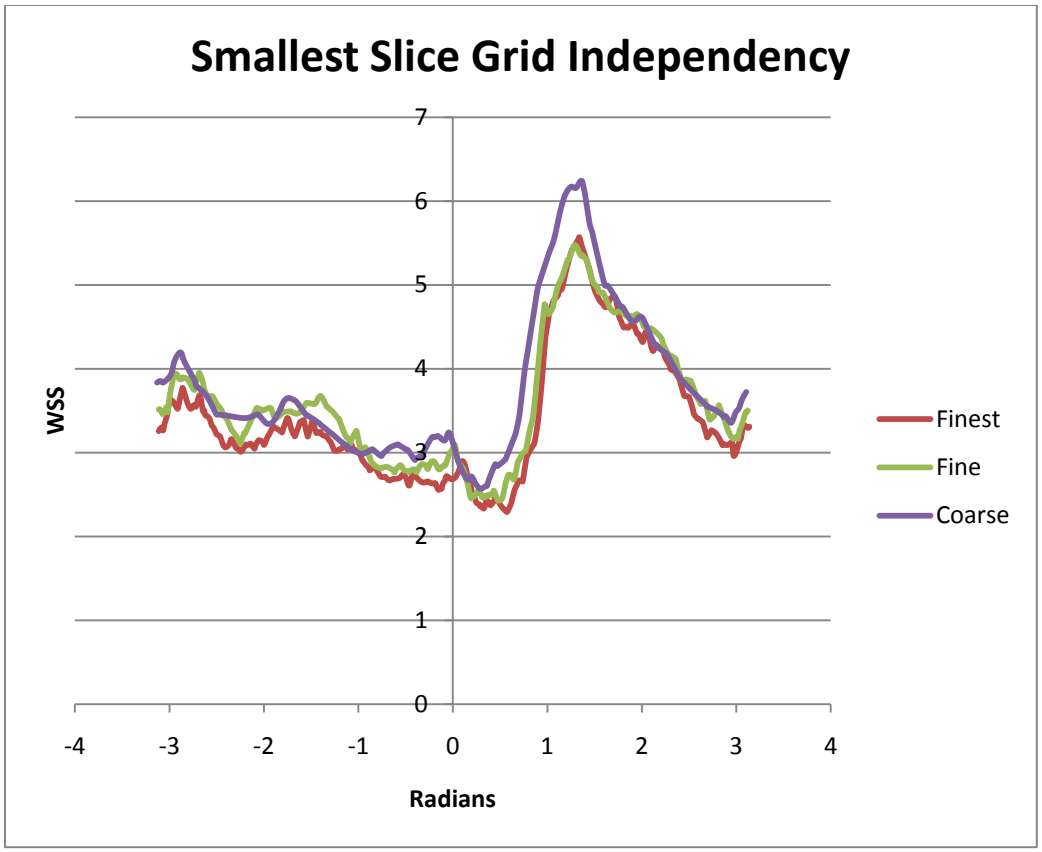

Figure 3-6 Plot of circumferential distribution of Wall Shear Stress in three cases of refinement seen in one of the cross sectional areas a representative vessel

ERROR Calculation		
	finest-finer	finest-coarse
RMSQ Error	0.2068	0.3676
% Error	1.2165	2.1623

Table 3-2 Tabulation of error calculation for smallest slice

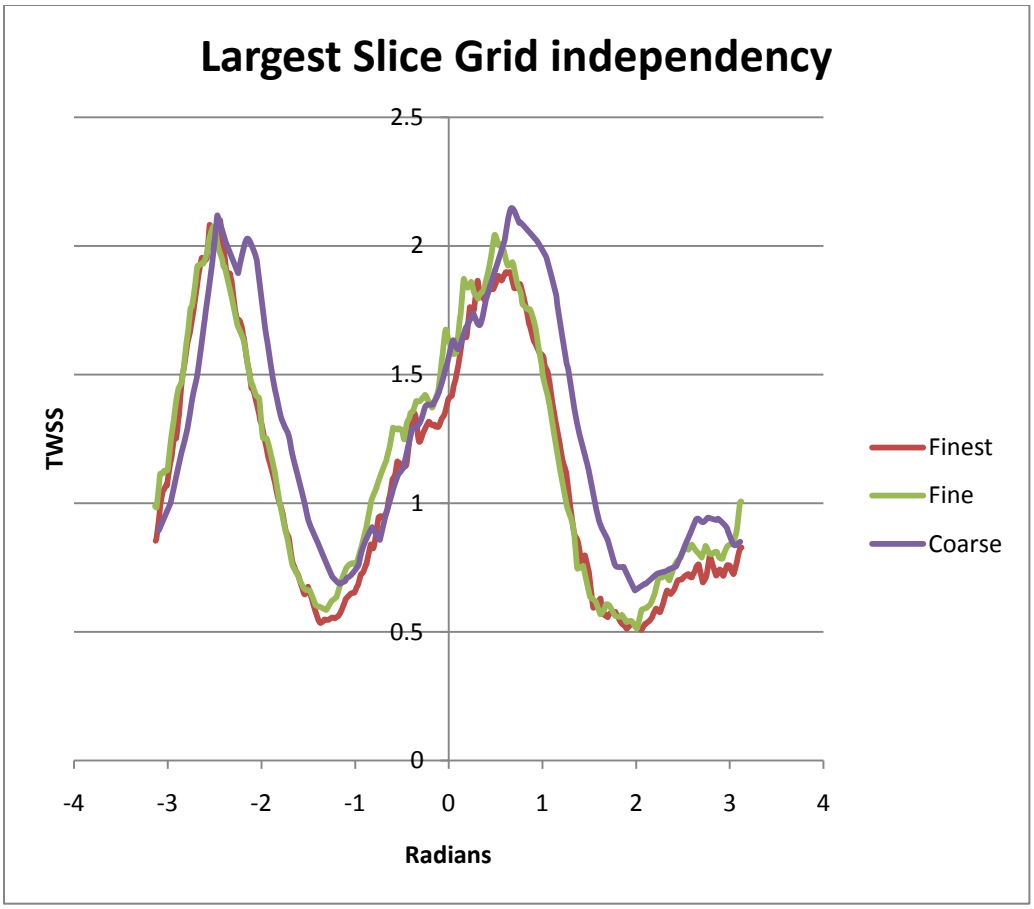

Figure 3-7 Plot of circumferential distribution of Wall Shear Stress in three cases of refinement seen in one of the cross sectional areas a representative vessel.

ERROR Calculation		
	finest-finer	finest-coarse
RMSQ Error	0.0800	0.1722
% Error	0.4355	0.9365

Table 3-3 Tabulation of error calculation for average slice

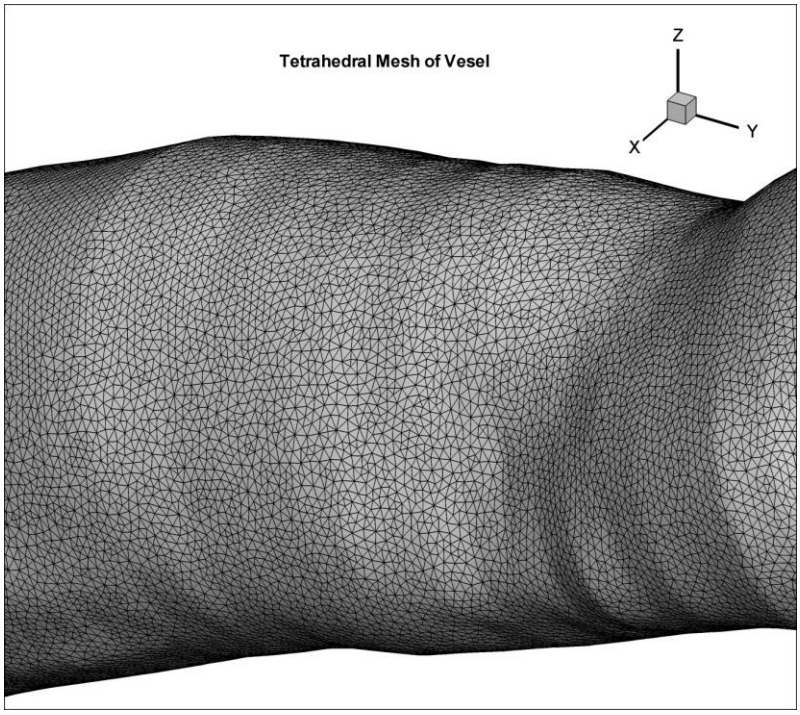

Figure 3-8 Plot of the tetrahedral mesh along a section of vessel created in Pointwise 64bit Version 16.03R1, selected from grid independency study

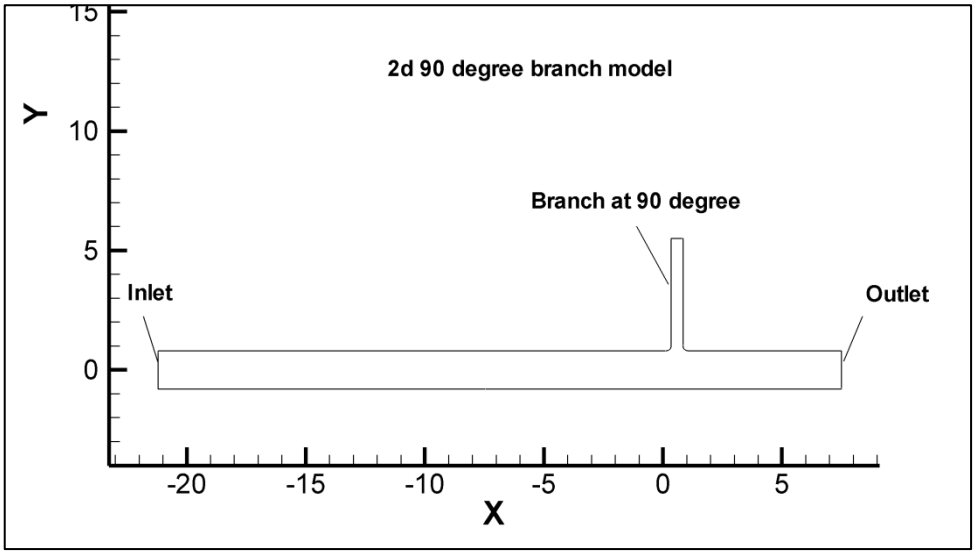

Figure 3-9 Figure showing two dimensional 90 degree artery-branch model

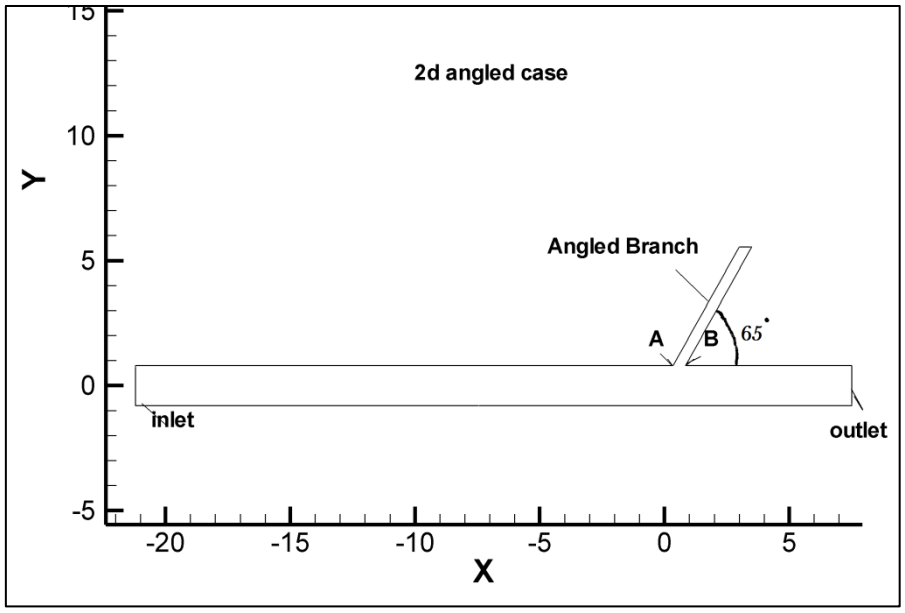

Figure 3-10 Figure showing two dimensional angled artery-branch model

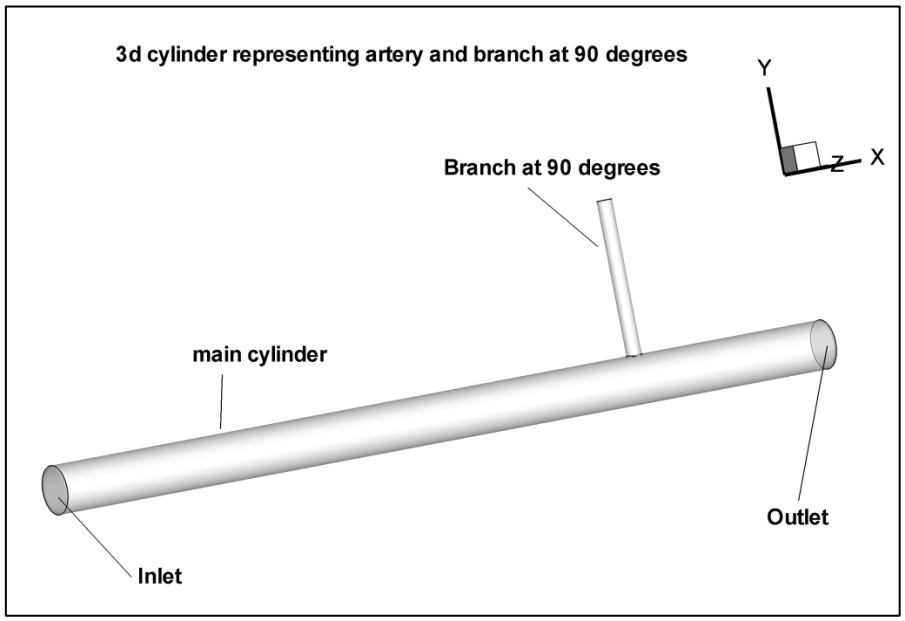

Figure 3-11 Figure showing 3 dimensional 90 degree artery-branch model

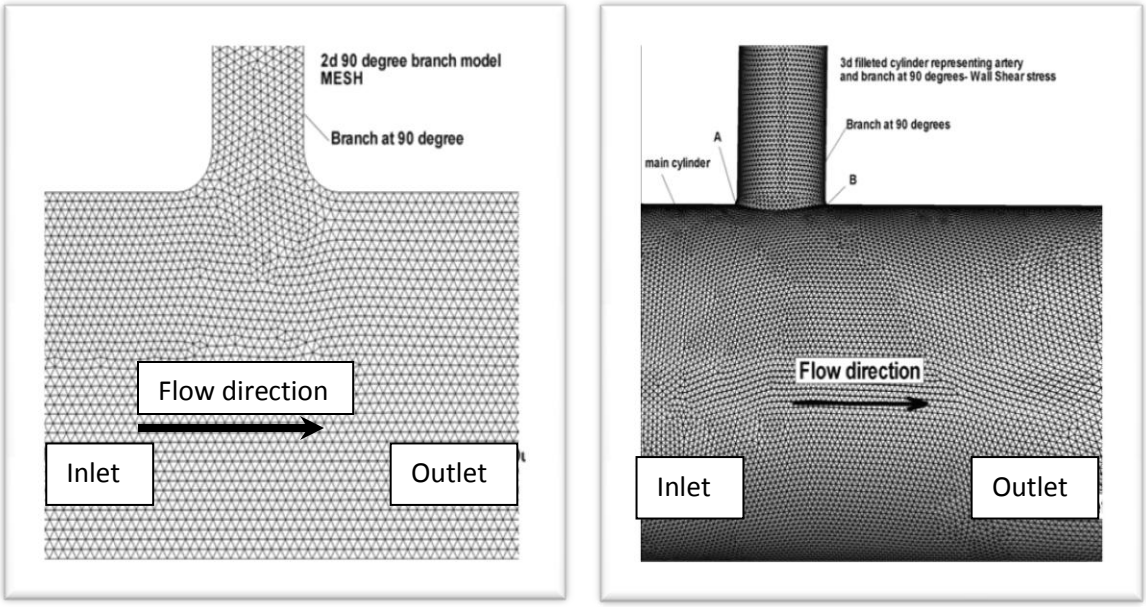

(a) **(b)**

Figure 3-12 Meshes of two dimensional 90 degree artery-branch model in (a) and in (b) z-plane view of 3 dimensional 90 degree artery branch model

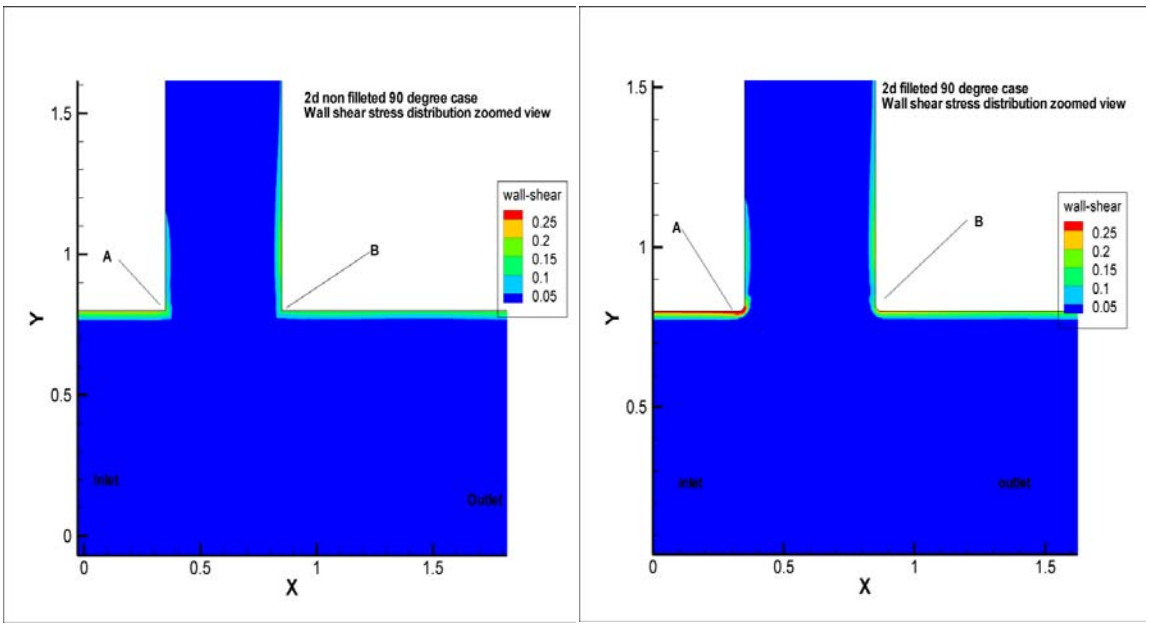

(a) **(b)**

Figure 3-13 Comparison of wall shear stress trends on unfilleted (a) and filleted (b) 2 dimensional artery-branch geometry

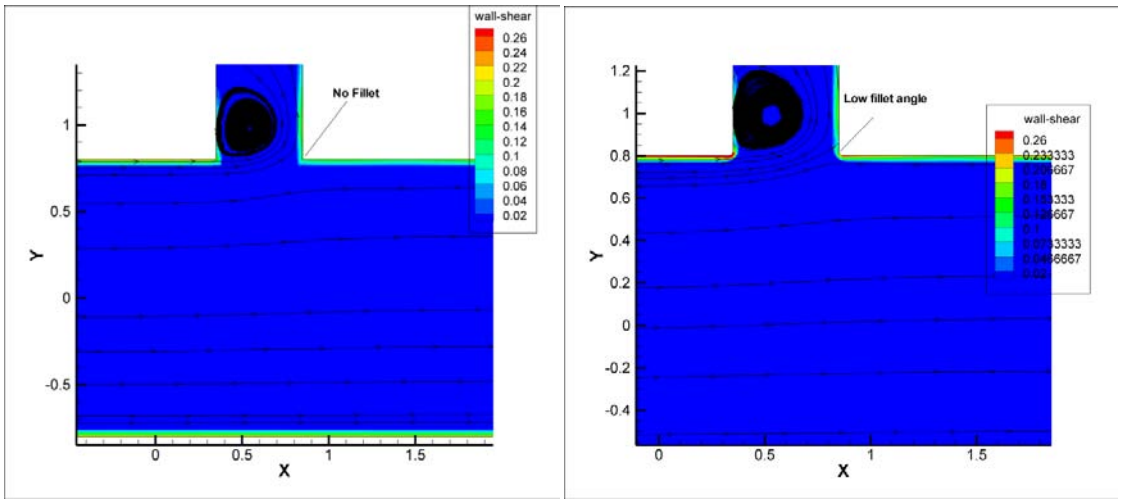

(a) 90-degree no fillet **(b) 90-degree fillet**

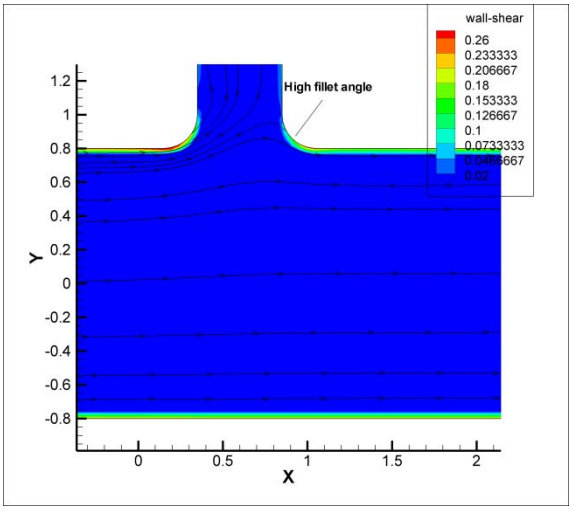

(c) High fillet

Figure 3-14 Streamlines overlaid on WSS contours for 2 dimensional 90 degree fillet cases. (a) no-fillet case, (b) low fillet case, and (c) high fillet case

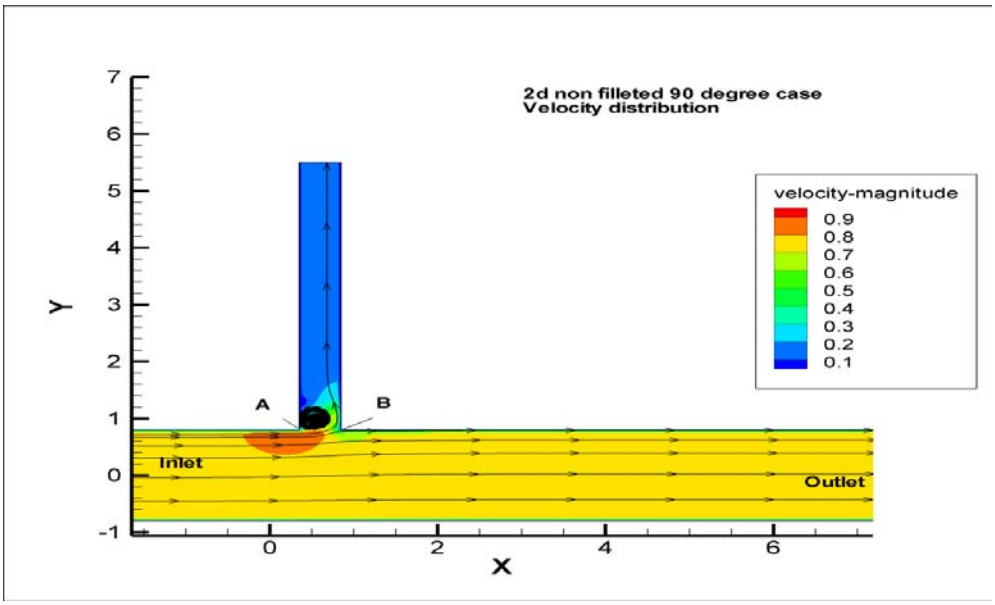

(a)

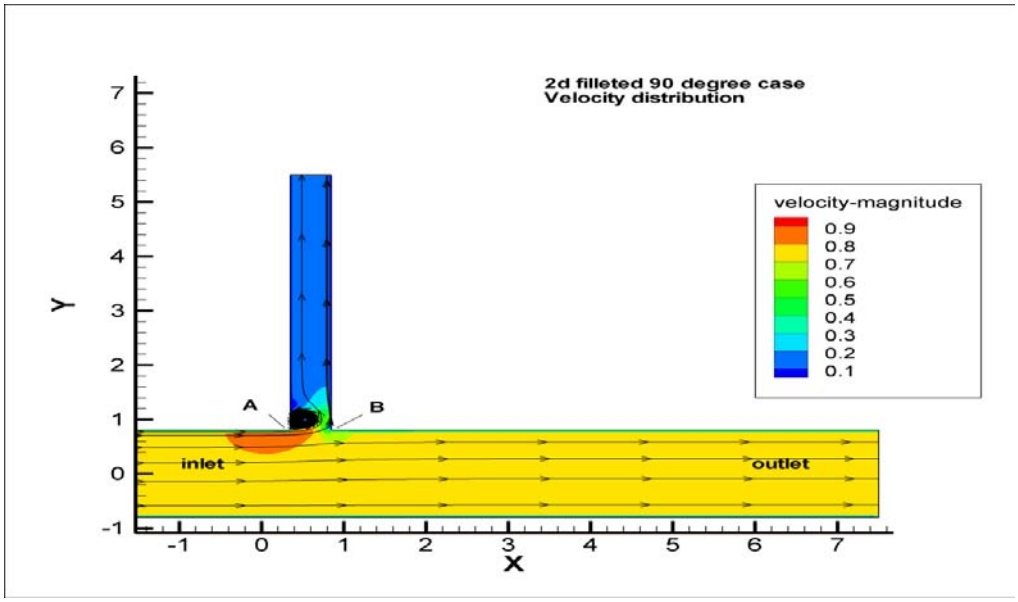

(b)

Figure 3-15 Figures in (a) and (b) are comparison of velocity profiles of filleted and unfilleted 2d 90 degree cases

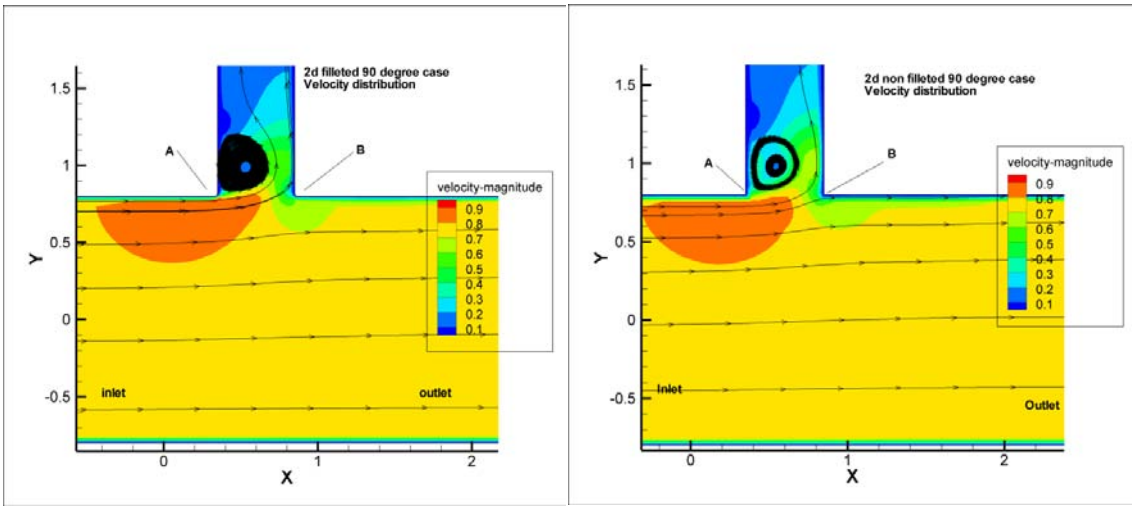

(a) **(b)**

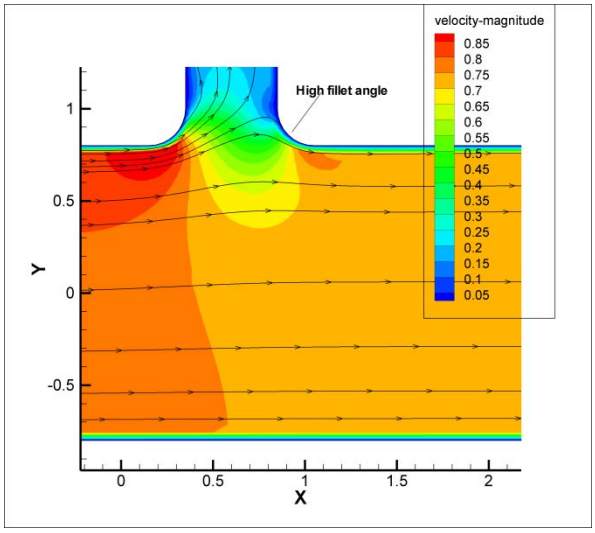

(c)

Figure 3-16 Figures (a), (b) and (c) are Close-up views of velocity profile comparison for 2d 90 degree no-fillet, low fillet and high fillet cases

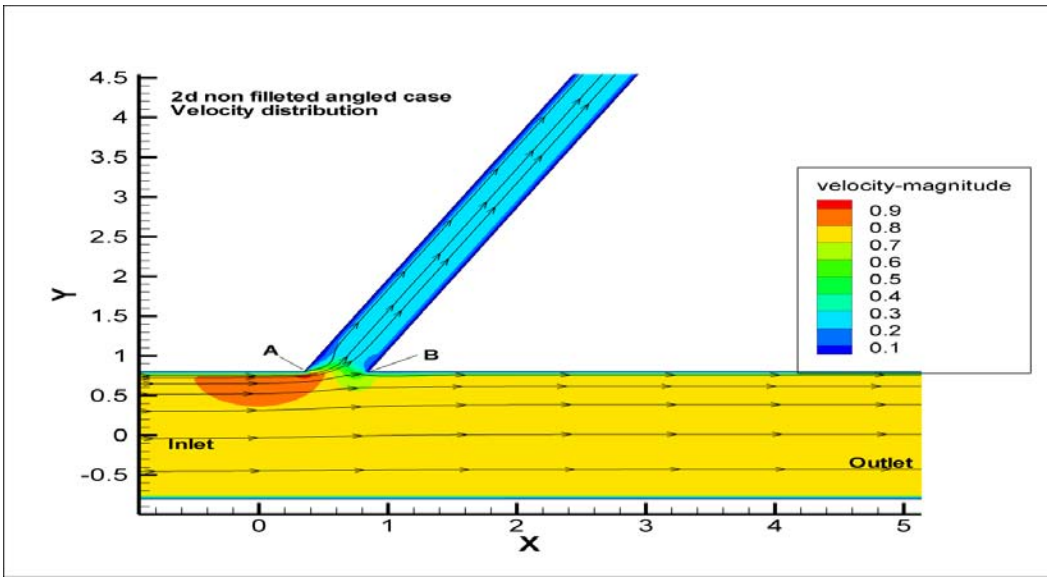

(a)

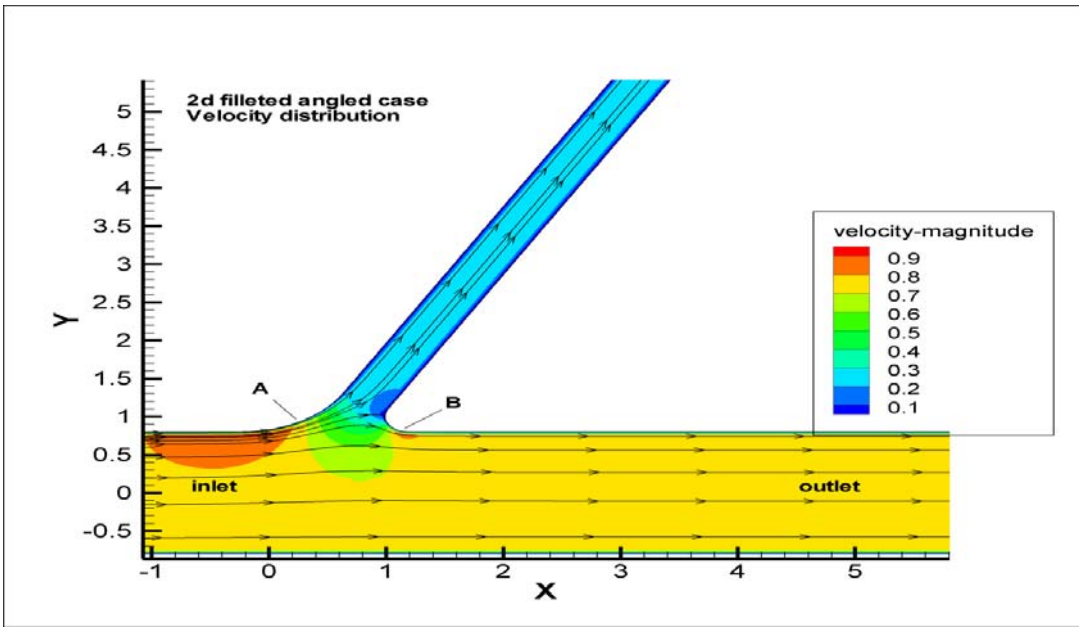

(b)

Figure 3-17 Comparison of velocity profile distribution in downstream region for (a) n0-fillet and (b) fillet 2d angled cases

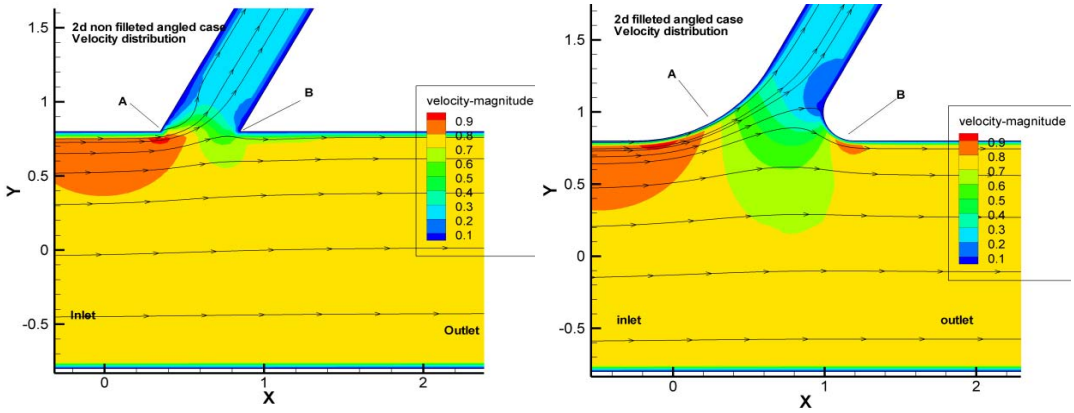

(a) **(b)**

Figure 3-18 : Close-up view of streamlines overlaid on velocity magnitude contours for 2d angled (a) no-fillet and (b) filleted cases

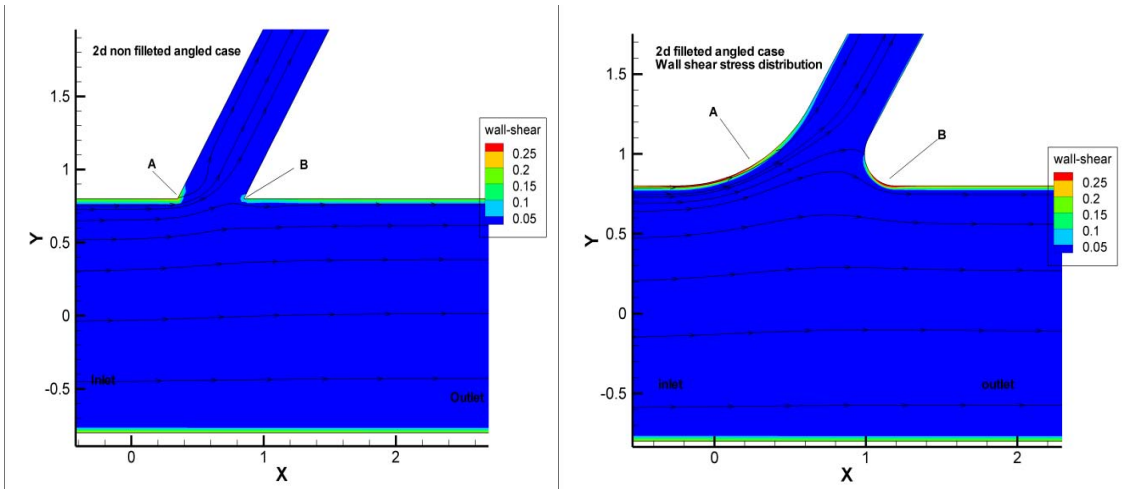

(a) **(b)**

Figure 3-19 figure of Streamlines overlaid on WSS contours of 2d angled (a) no-fillet and (b) fillet cases

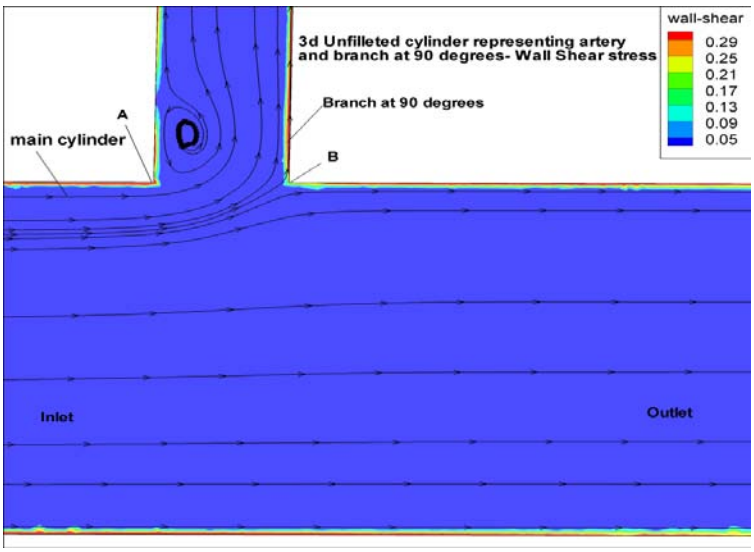

(a)

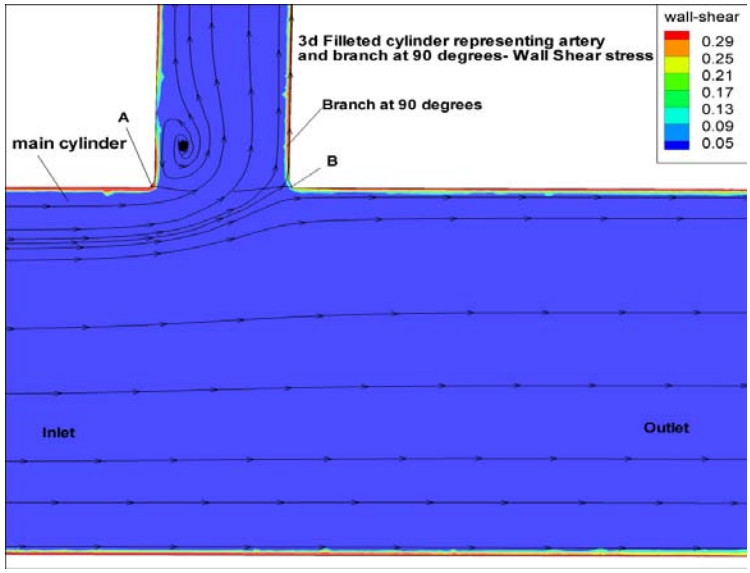

(b)

Figure 3-20 Streamlines overlaid on WSS contours in 3d 90 degree (a) (no-fillet) and (b) fillet

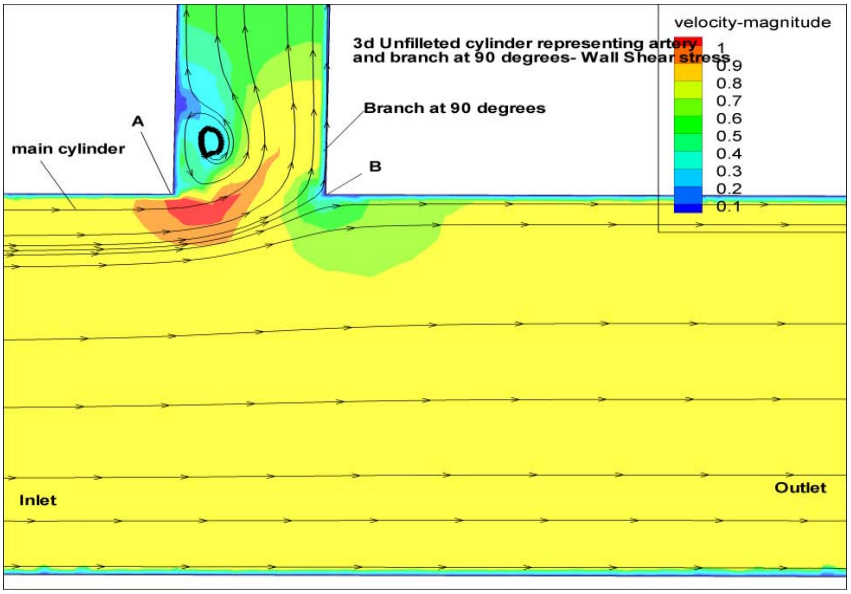

(a)

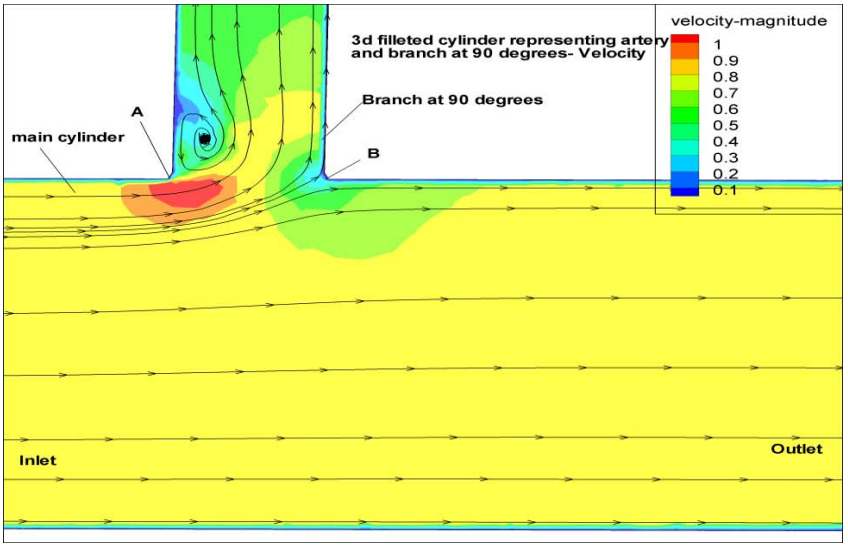

(b)

Figure 3-21 Comparison of velocity magnitude and trends of stream lines for 3d 90 degree (a) no-fillet and (b) fillet cases

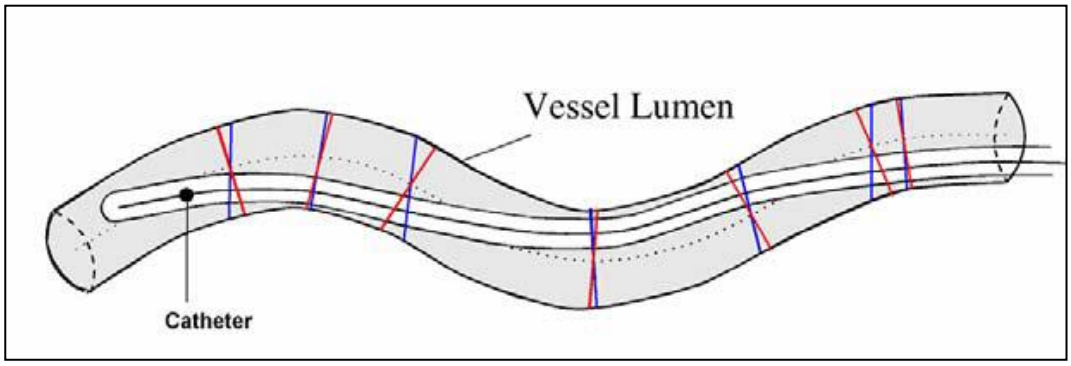

Figure 3-22 An illustration of a potential catheter path.

The blue lines show the orientation of the IVUS contours, while the red lines demonstrate the newly obtained orthogonal contours.

Source: Vigmostad S.C., "Hemodynamics and Wall Thickness in Relation to Localized Geometric Changes in Human Coronary Arteries", Masters Dissertation, The University of Iowa, Iowa City, Iowa, 2003.

CHAPTER 4 GEOMETRY AND MODEL

This chapter describes the geometry and model of the three different arteries considered in this study. Various morphometrical measurements of the artery and the branches have been presented. Various arterial nomenclature and terminologies are also described.

Blood flow was analyzed in three different coronary vessels for this study that will be referred as Vessel-A, Vessel-B and Vessel-C. Coronary arteries have highly tortuous geometry and local curvatures. These features vary not only from one location to another but also from one patient to another. All of the three vessels (branched and no branch) under consideration in this study were also seen to have totally different geometrical features which have been shown in Figures 4-1 to 4-6. Qualitatively, of the three geometries, Vessel C has the least global curvature while Vessel B has the maximum. Vessel B on the other hand has the largest number of local curvatures. Similarly, Vessel B is the longest vessel of 70.854 mm and the vessel C is the smallest vessel having length of 38.191 mm. The length of Vessel A is roughly 62.814 mm. All the above vessel length estimates are based on centerline arc-length measurements. Normally, inlets have larger cross sectional area than the outlets: this observation holds true for both Vessel A and C but not in Vessel B. As mentioned earlier, these vessels have been extended at the inlet regions by the value of ten times the inlet area and at the outlets by five times the outlet area to remove the end effects in simulations. The values of cross sectional areas and extensions at the inlets and outlets of all the vessels are listed in Table 4-1.

In each of these vessels a branch was added following the procedure mentioned in the Methodology section. These branches were added in accordance with the information obtained on their location in the vessel given by branch origin and their angular inclination with respect to principal x, y and z axes. This information about location and angular inclination of the branches for different vessels has been tabulated in Tables 4-2 and 4-3 respectively.

Altogether four cases were analyzed for each vessel. For each artery, flow through a branchless geometry was compared with the flow through the same artery with three varying sizes of branch ostiums. The three sizes of branches used were 25 %, 50 % and 75% of the local cross-sectional area of the vessel at the point of branching (see also Figure 4-8). These branches will be referred to as "Small branch", "Medium branch" and "Large branch" cases in this study. The information regarding the position of branches on the artery surface has been tabulated in Table 4-2. The cross sectional area of the vessel containing these points were computed by the number of points per contour information of the vessel lumen The cross sectional areas calculated for the branches were not representative of the physiological real size of the branch at that point. They were calculated purely for research purpose for analyzing the effect of different branch sizes on downstream flow from the region of branching. Hence altogether 12 cases were analyzed in this study. Information regarding the area of the branches used for all the vessels in this study has been presented in Table 4-4 and 4-6. The vessels under study are the segments of actual arteries. These segments have more than one branch arising from them. However to simplify the study and isolate the effect of branch sizes simply one branch has been considered for each vessel. Out of all the actual branches present in the vessel segments, the branch lying approximately at the central region was chosen for this study of the vessel segment.

The volumetric meshes in all three vessels were created using the average element size of 0.0001 m as in the fine case mentioned in the grid dependency study. A mesh for a representative artery with branch and inlets is shown in Figure 4-6. The number of nodes present in different vessel cases has been listed below in Table 4-5.

Figure 4-7 shows the side view and top view of three different branch sizes for a representative vessel has been shown. Mass outflow boundary condition was used at outlet of the main artery and branch. This requires the specification of flow rate weighting at these outlets. For simulations of no branch cases these values were maintained as 100% for the main channel as there was no flow division. On the other hand, in the case of branched flows, mass outflow ratios were calculated on the basis of the cross sectional areas of the main artery and the branch

after the point of branching. The cross sectional area of both the branch as well as the main artery (downstream of the branch) at the vicinity of branching were calculated and summed up to obtain a total cross sectional area. The ratios of these two areas were calculated with respect to the sum of the two areas in order to find the mass flow ratios. The values of these ratios for all the vessels and for different cases of branching apart from no branch cases have been given in Table 4-6.

Cross-sectional area measurements of vessels A , B and C defined in text							
Vessel	Area of Inlet (mm^2)	Area of Outlet (mm^2)	inlet diameter (mm)	Outlet diameter (mm)	Length of Inlet extension (mm)	Length of Outlet extension (mm)	Length of Vessel (mm)
A	10.8	9.50	2.80285	2.62909	28.028521	13.145451	62.814
B	7.46	12.8	2.32904	3.04799	23.29042	15.234955	70.854
C	12.4	5.71	2.99846	2.03699	29.984658	10.18495	38.191

Table 4-1 Tabulation of length and cross sectional area information of the three vessels under study

Centroid	Centroid-x	Centroid-y	Centroid-z
Vessel-A	0.0160982	-0.006388	-0.0181602
Vessel-B	0.0365646	0.0191082	0.0266605
Vessel-C	0.028884	0.00255427	0.00929887

Table 4-2 Tabulation of origin of branches in the three vessels

Angles	x axis	y axis	z axis
Vessel-A	10.3038438°	-71.894744°	14.722035°
Vessel-B	17.68221°	-54.501415°	29.62300091°
Vessel-C	33.66238559°	39.7249401°	-36.95852798°

Table 4-3 The angular inclination of branches in the three vessels in degrees

Vessel	Vessel Inlet area (mm^2)	Vessel Outlet area(mm^2)	Artery area at branch origin(mm^2)	Small branch area(mm^2)	Medium branch area(mm^2)	Large branch area(mm^2)
A	10.802	9.50416	10.8019	2.70048	5.40096	8.10145
B	7.4586	12.7657	11.6127	2.90319	5.80637	8.70956
C	12.3623	5.70533	6.33432	1.58358	3.16716	4.75074

Table 4-4 Tabulation of cross sectional areas of vessels under consideration at different regions of interest

Number of Nodes and Cells in Vessels used						
	Small Branch case		Medium Branch case		Large Branch case	
	nodes	cells	nodes	cells	Nodes	cells
Vessel A						
vessel	591243	3196178	591243	3196178	591243	3196178
branch	30723	158803	49384	258009	73770	408645
Vessel B						
vessel	637059	3519058	637059	3519058	637059	3519058
branch	52165	274737	62575	330904	70772	379077
Vessel C						
vessel	639303	3578377	639303	3578377	639303	3578377
branch	30910	159113	52384	278486	60793	318556

Table 4-5 Number of nodes present in the all the three vessels and their respective branches

Vessel Case	Branch area (mm^2)	Cross sectional area of artery at branch origin (mm^2)	sum of branch + main outlet area(mm^2)	% Mass outflow branch	% Mass Outflow main
Vessel A Small case	2.7	0.112	0.139	19.5	80.5
Vessel B Small case	2.9	0.113	0.142	20.4	79.6
Vessel C Small case	1.58	6.2	7.79	20.34	79.66
Vessel A Medium Case	5.4	0.112	1.66	32.6	67.4
Vessel B Medium Case	5.81	0.113	0.171	33.9	66.1
Vessel C Medium Case	3.17	6.2	9.37	33.8	66.2
Vessel A Large Case	8.1	0.112	0.193	42	58
Vessel B Large Case	8.71	0.113	0.2	43.45	56.55
Vessel C Large Case	4.75	6.2	0.11	43.4	56.6

Table 4-6 Tabulation of Mass flow assigned to branch and main outlets

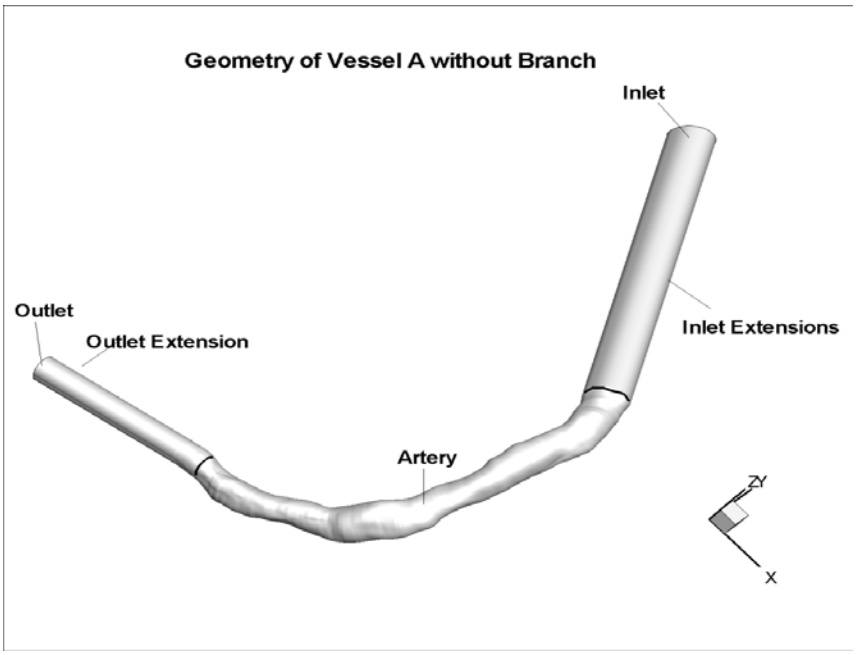

Figure 4-1 Figure of Vessel A without branch

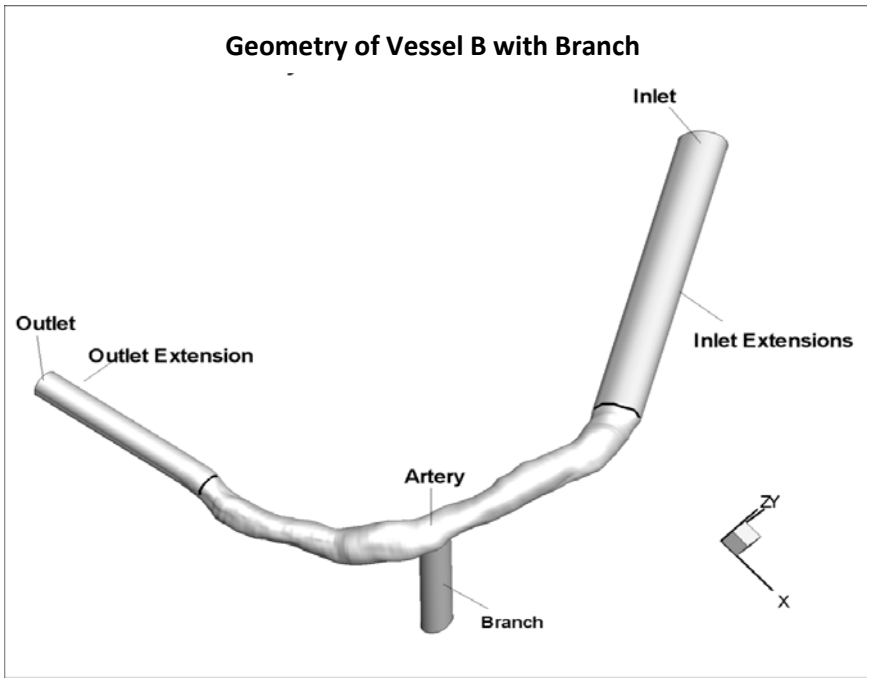

Figure 4-2 Figure of Vessel A with branch

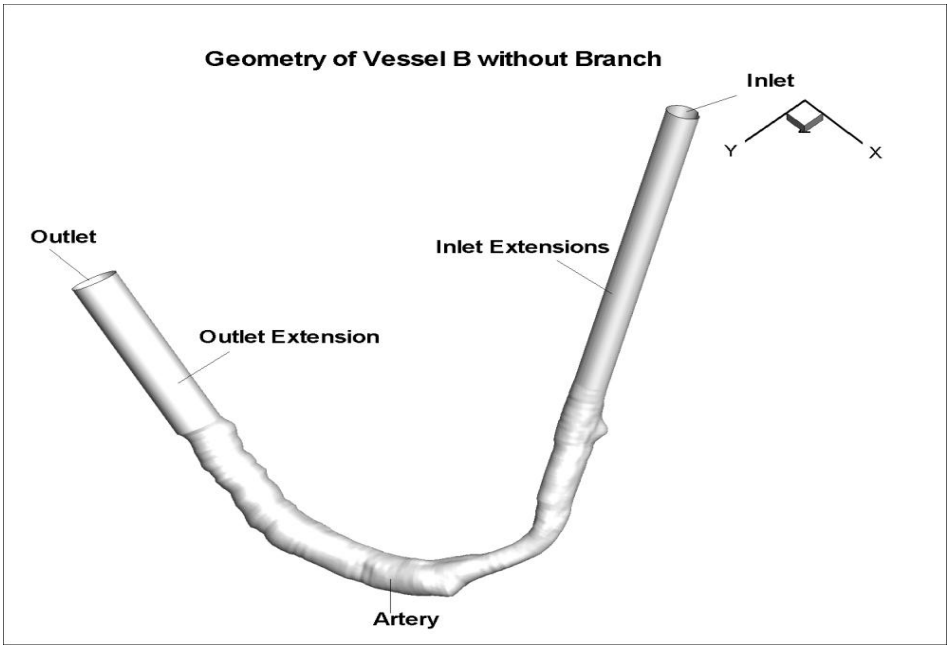

Figure 4-3 Figure of Vessel B without branch

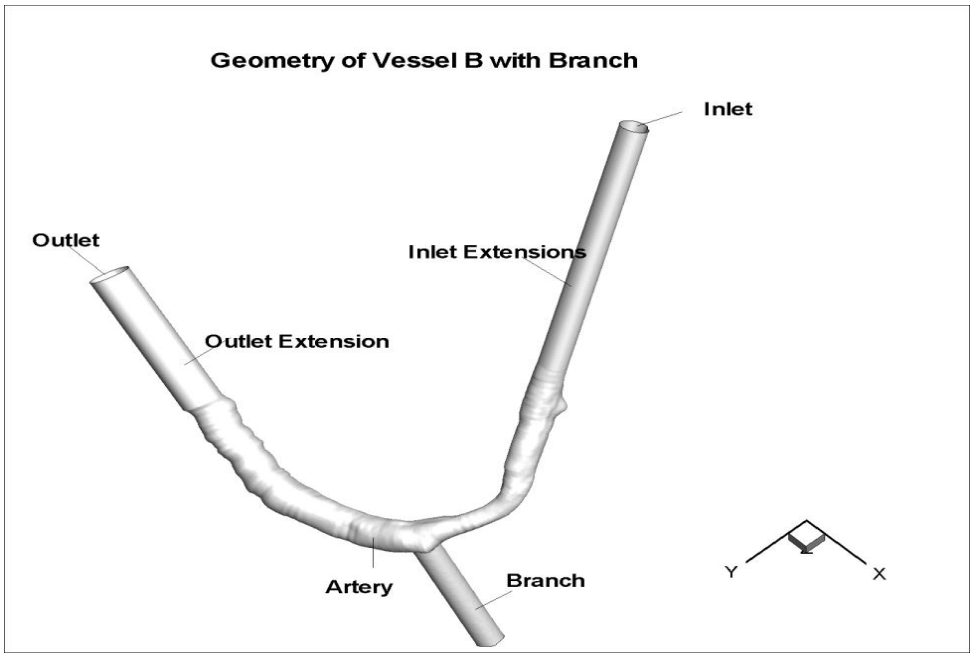

Figure 4-4 Figure of Vessel B with branch

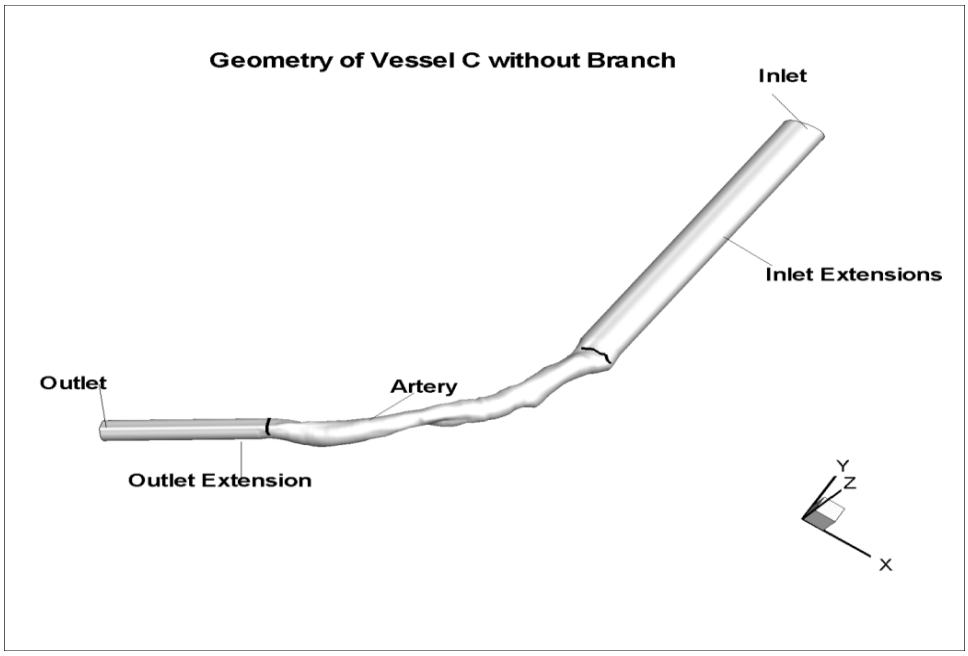

Figure 4-5 Figure of Vessel C without branch

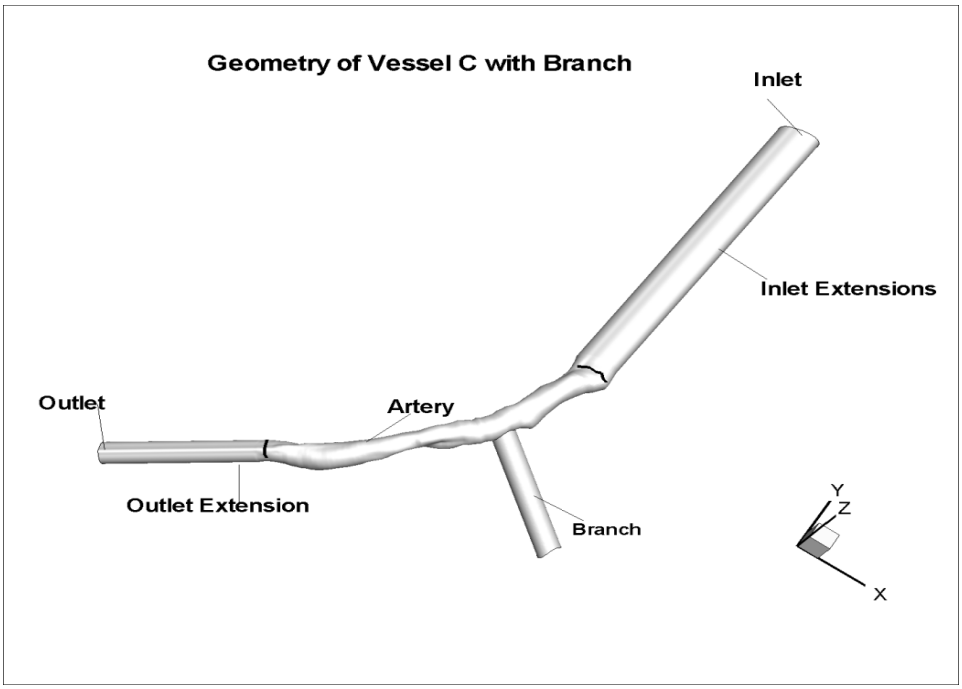

Figure 4-6 Figure of Vessel C with branch and extensions

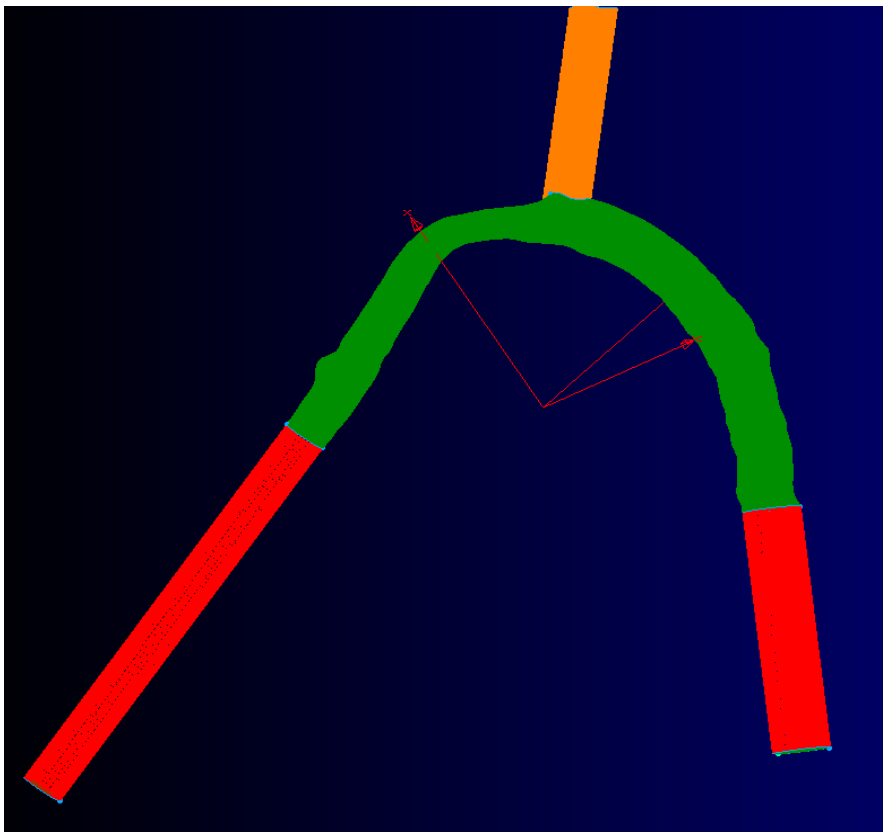

Figure 4-7 Figure of meshed model of a representative artery with branch and inlet and outlet extensions

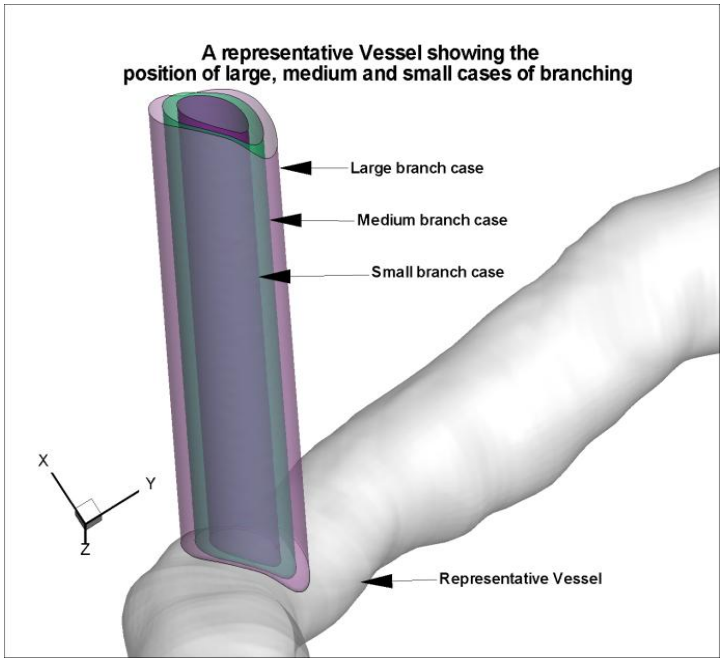

(a)

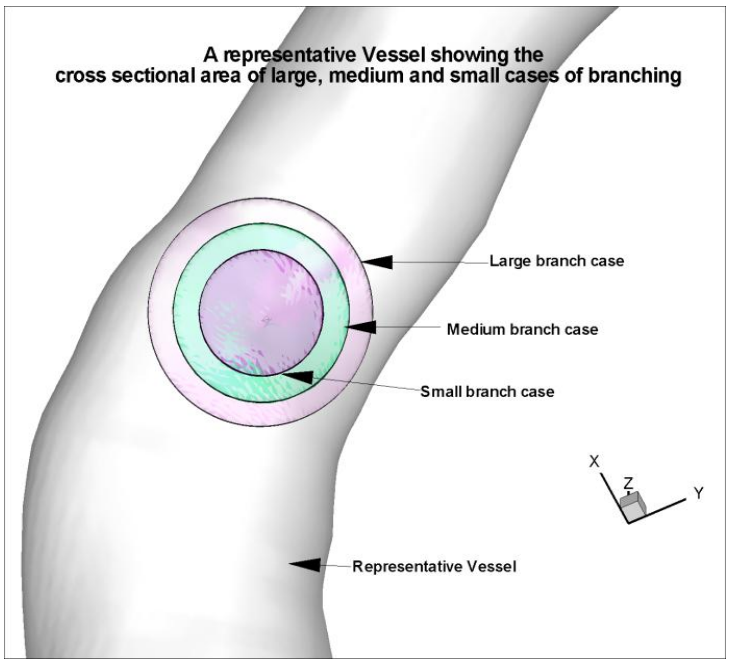

(b)

Figure 4-8 Figure (a) showing three different cases of branch (large, medium and small) attached to a representative vessel. (b) Top view of cross sections of three cases of branches on the main vessel.

CHAPTER 5 RESULTS AND DISCUSSIONS

The purpose of this study is to determine and compare the degree of impact that different sizes of branches play in flow downstream to the region of branching. Sites of branching have always been an area of interest to physicians because of the high occurrence of accumulation of plaque in these regions. These sites hold special significance to fluid analysts as well because of the generation of low wall shear stress, oscillatory wall shear stress and recirculation brought about by sudden change in geometry and division of flow. Furthermore, when branches are neglected in fluid dynamics studies, it"s important to better understand the consequences of neglecting the branches, so that results can be more appropriately interpreted.

In order to analyze the degree of effect corresponding to a branch size, it is hence reasonable to compare the amount of recirculation generated and distribution of WSS developed in that region; hence lower the values of WSS (higher the value of recirculation), higher the probability of occlusion. It is thus required to note where the wall shear stress crosses from positive to negative or from being negative to positive. Wall shear stress is a direct and effective way of detecting reverse flows which will be observed later in this chapter.

In a complicated geometry like an artery, where large local and global curvatures exist, the presence of secondary dean-vortices may be common. Hence, the observation of wall shear stress in studying flow characteristics downstream of the branch proves as a very useful tool.

In this study, flow behaviors of all cases of branching of a vessel were studied at different cross sections considered at the same distance from the origin of branch. The centers and unit normal of all contours of the vessels were calculated using the 720 points per contour information on the surface of the artery. Information as such was then used in extracting values of wall shear stress and velocity vectors from different cross sections of the artery.

Arteries have both local as well as global curvature. Hence in order to obtain the values of true WSS and velocity vectors in that vicinity, cross sections representing the original IVUS

contours were evaluated. Similarly, for each point on the circumference of a cross section in an artery, tangents were different due to the presence of local curvature. Moreover, atherosclerosis has been reported to be influenced by local shear stress values (Krams et al., 2010) hence, in this study Local Axial Wall Shear Stress (TWSS) was calculated to better examine the local fluctuations in wall shear stress values.

5.1 Parameters under Study

5.1.1 Local Axial Wall Shear Stress (TWSS)

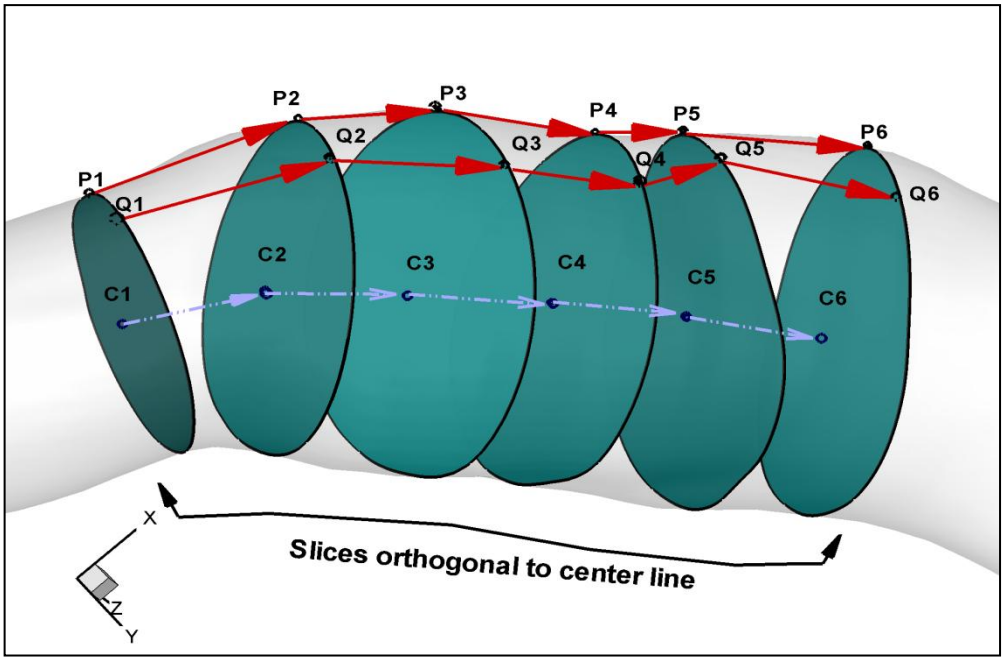

Figure 5-1 Figure showing Slices orthogonal to the center line of vessel along with points on the circumference

Local axial wall shear stress (TWSS) can be determined by taking a dot product of components of wall shear stress at a point and tangents to that point. If the components of unit tangent to each and every point in the circumference of the plane is represented by t_x, t_y, and t_z

and the x, y and z components of wall shear stress are τ_1, τ_2 and τ_3, respectively, then the $TWSS$ can be calculated as shown below.

$$TWSS = t_x\tau_1 + t_y\tau_2 + t_z\tau_3 \dots\dots (3)$$

An illustrative figure of slices orthogonal to the center line of a representative vessel has been shown in figure 5-1. In the first slice to the left, P1 and Q1 are first two points taken in clockwise direction on the circumference. Similarly, P2 and Q2 are the corresponding two points taken on second slice and so on. When calculating TWSS, a vector joining the first points on the slices is calculated; for example for slice 1 and 2, a unit vector joining points P1 and P2 (colored by red solid arrow) is calculated. This vector will be referred to as a tangent joining the two points P1 and P2. Each and every point on the circumference also has corresponding wall shear stress values. A dot product of tangent and wall shear stress at a point such as P1 is taken to calculate TWSS at that point, which gives a measure of local axial wall shear stress. Same process is followed for all points on each and every slice. Previously, while calculating the wall shear stress at a point on the circumference a dot product of wall shear stress at a point and vector passing through the center of the slice would be taken (Vigmostad, 2003). In figure 5-1, vector joining centers C1 and C2 (colored by dashed blue arrow) would specify the direction vector in such approach. Calculation of TWSS is more representative of local axial wall shear stress than the previous approach of measuring vector along centerline, as the previous one takes in to account the orientation of each and every point on the surface of the vessel.

5.1.2 Reverse Flow and Secondary Flow

As explained earlier, in the downstream regions after branching velocity profiles are skewed towards the divider wall giving rise to low wall shear stress in the outer wall and hence causing recirculation in those regions. Checking for the presence of negative axial or "z velocity" (when individual slices are converted to a 2D x-y plane) or reverse flow is another straight

method of determining the presence of recirculation in the cross sections. In the same way secondary flow is a behavioral property of curved tubes. Hence this study was also aimed at analyzing the presence of Dean vortices in the convoluted coronary and the way branching affected their presence.

5.2 Results

It has been reported in literature that branch vessels only have effects till 3mm downstream (Gijsen et al., 2008, Ritcher et al., 2004) and hence excluding the results up to one diameter of the side branch downstream from the point of bifurcation has been assumed to be a reasonable approximation in hemodynamic studies. However, in that study, only a single model of Lower Anterior Descending (LAD) artery and its bifurcation was examined, and the vessel was one in which very little curvature existed. Hence to more thoroughly evaluate the effect of different sizes of branch ostiums, flow dynamics were examined in cross sections/slices at various positions downstream to the branch. It was also expected that the presence of branch would impact on upstream flow; hence flow dynamics in the regions upstream were also analyzed.

The methodology that was utilized to obtain these slices was described earlier in Chapter 3. Figure 5-1 shows the slices obtained in representative artery geometry in both upstream and downstream regions of the branch. The centerline points have also been marked in this figure. In the results discussed below cross sections or slices have been addressed by numbers for instance slice 62 in figure 5-3. All the slices have been numbered from the outlet to the inlet such that the slice at the outlet would be addressed as slice 1 for a particular vessel. This approach of numbering is consistent in all the three vessels considered in this study.

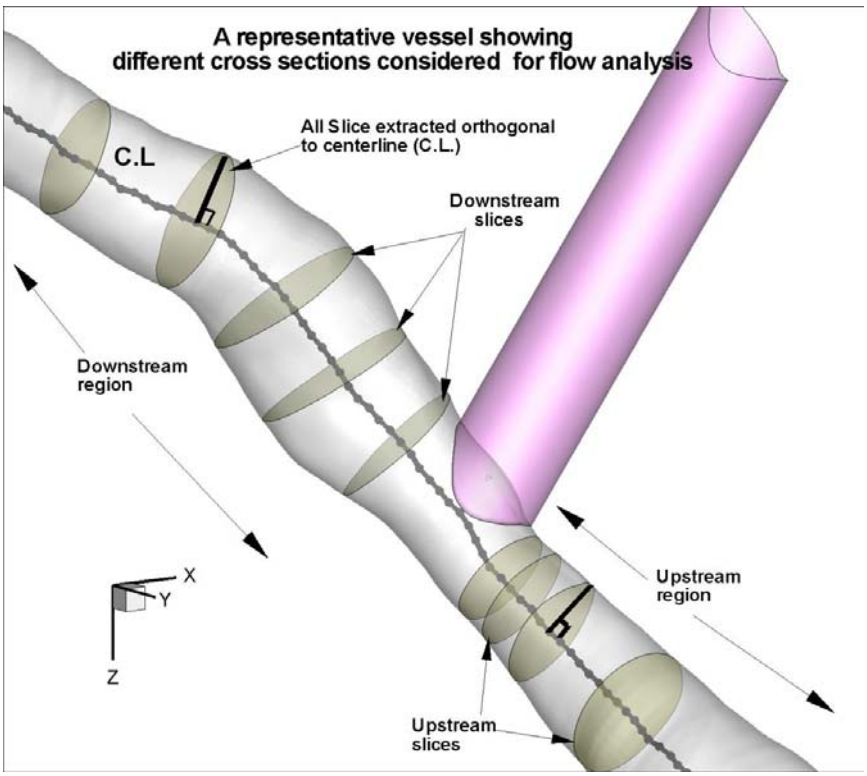

Figure 5-2 A figure of geometry of a representative Vessel showing positions of different downstream and upstream slices orthogonal to center line.

5.2.1 Results and Discussions for Vessel A

5.2.1.1 TWSS in Vessel A

5.2.1.1.1 Downstream

Results of the local axial wall shear stress for vessel A in the downstream region are shown in Figures 5-3 to 5-6. As would be expected, the shear stress magnitudes downstream to the site of branching were varied for no-branch, small branch, medium branch and large branch cases. In part, this was due to the changes in flow rate associated with each of these cases. For example, in the large branch case in vessel A, only 58% of flow was sent through the downstream main artery while the remaining 42% flowed through the branch. Hence the shear stress magnitudes are lower than the smaller branch case; more precisely, larger the branch size

lower the value of local axial wall shear stress. Shear stresses for all the cases of branching appeared exhibit similar trends at considerable distance downstream from the site of branching, where the all cases analyzed appeared to vary by certain order of magnitude only. However, as one moved closer towards the branch in the downstream region; though the basic trend of shear stress remained the same for all cases, few distinguishing peaks were observed in the branched cases.

For slice at 9 mm (slice 50), only large branch showed negative shear stress in a very small region near about 4 to 5 radians. For slices considered after a downstream distance of about 9 mm (slice 50), shear stress on the wall was positive through-out the circumference. This observation has been clearly shown in Figure 5-6; where TWSS values of all the cases of branching at a distance of about 18 mm (slice 32) have been plotted. In this way, based on TWSS, one could argue that the impact of the branch died after distal distance of 9mm for the large artery. For the medium branch, this impact wore off at 8.5 mm, and for the small branch, after 7 mm.

Slices 32 and 50 discussed above were downstream slices far away from the origin of the branch. As one observed the regions closer to the branch, various differences could be noticed between the different branch-sizes considered when compared to the no branch case. For example, in Slice 62 (at downstream distance of 3.02 mm, Figure 5-3), two peaks were observed. However, shear stress also crossed the negative axis before attaining these peaks; once in the continuous region before 0.8 radians and beyond 4.4 radians and then again in regions in between 2.2 – 3.2 radians. The two regions in the circumference of the slice where the shear stress was negative lied in the either sides of the branch. This can be clearly seen in Figure 5-2. For further analysis, the TWSS plot may be compared between the green and pink/rose lines of Slice 62 (at downstream distance of 3.02 mm). In the large branch case (rose/pink line), the negative TWSS peak value reached was around -0.5 N/m^2 at about 4.8 radians. For the smaller branch case, the negative value of TWSS was merely -0.1 N/m^2 at the circumferential location of about 5.2 radians. Hence, TWSS was observed to decrease with an increase in branch size in the

regions of the circumference lying on the either sides of the branch. Large branch case had TWSS value (0.2-(-0.1), where 0.2 is TWSS magnitude for no branch case and -0.1 is TWSS magnitude for large branch case in N/mm^2, comparison of TWSS values will be done in this manner throughout the chapter) lower by 3 times on average except for in a narrow region of circumference. Similarly on average the medium branch case had TWSS value lower by 1.4 times and the small branch case by a fraction of 0.5. However in a small region of circumference, TWSS was observed to elevate with an increase in branch size in the region of the circumference lying in the direction of the branch. TWSS value was seen to elevate by about (3.5-0.7) 5 times for the large branch case. The TWSS values were seen to increase by (2.9-0.7) about 4.14 times and (1.9-0.7) 2.7 times for the medium and small branch cases. TWSS values in the region of the circumference, opposite to branch was observed to be positive. This trend was observed till about 9 mm distance downstream from the branch origin.

Similarly, in slices at a distance of 5.02 (slice 58), the no branch TWSS curve behaved very differently when compared to the branched cases in Figure 5-4. In this slice, for example, two peaks of local axial wall shear stress were observed in the region of the circumference lying in the direction/side of the branch and opposite to the branch. The trend observed for this slice is comparable to the trend seen in Figure 5-2 for slice 62. The first peak was observed near around 1.8 radians while the second peak, much larger in magnitude was observed around 3.8 radians. The first peak was observed to decrease with the increase in the size of branch while the second peak was observed to increase with the increase in size of branch. Also, in the branch cases, the WSS became negative beyond roughly 4.8 radians and before 1.2 radians. The magnitude of negative TWSS increased with the increase in size of branch.

An interesting observation regarding the local axial wall shear stress (TWSS) plot was that for further downstream slices (like 32) the larger branch showed the least magnitude of TWSS compared to other cases. But as one moved closer to the branch, while still looking at more proximal downstream locations, the peaks of the large branch shear stress in both positive

as well as negative direction (for example Slice 62 at a distance of 3.02 mm), was the largest compared to all other cases. This effect was observed to decrease with the size of branch.

5.2.1.1.1 Upstream

Figures 5-7 to 5-9 show the wall shear stress plots for upstream locations. Three locations have been shown. Slice 73 was at an upstream distance of 2.51 mm and was the closest slice to the branch that was investigated. It was intuitive that the shear stress variation with the circumferential angle coalesces and will behave the same for further upstream locations. For example, slices at upstream distances of 3.52 mm and beyond (see Figures 5-8, 5-9). But it was the goal of this section to report upstream wall shear stress plots towards two objectives. First, study of the effect of branch and its effect on the flow even in upstream locations. Given the complexity of the artery geometry and the resulting inertial flow effect (given that the Reynolds number of the flow was 114), the branch might have effects on upstream locations. Second, the shear stress plots at further upstream locations were also recorded for completeness of the analysis.

Before 5.02 mm upstream distance (slice 78) no effect of branch was seen. At a distance of 3.52 mm upstream (slice 75), this distance was slightly more than the size of the largest branch diameter (3.21 mm); TWSS in a certain region of the circumference were higher for branched cases. The TWSS values in this region decreased with the decrease in branch size. The values of TWSS in that region was higher from the non branched case (2.15-1.6) by a factor of 1.3 for large branch case, by a factor of 13 percent for medium branch case and (1.8- 1.6) by 1.125 for small branch case. NOTE: Slice 73 upstream higher shear is due to the proximity of the branch to this slice as the diameter of the branch is the smallest in the larger branch case and hence a significant increase in the observed TWSS.

At a distance of about 2.51 mm (slice 73, see Figure 5-7) from the branch TWSS for large branch case was observed to increased by (5.7-2.2) by a factor of 2.6. TWSS for medium

and small branch cases were observed to increase by a relatively low factors of 1.3 (2.9 – 2.2) and 1.2. It was notable that the value of TWSS was significantly high in the large branch case than in medium or small branch case. This might be due to the fact that this slice is closer to the periphery of large branch case than the medium or small branch case. This accounted for the possibility of higher TWSS for both medium as well as small branch cases at cross sections more upstream than this. However those slices were not considered in this study.

Hence in upstream regions, the effect of branch was seen in a small range as compared to the downstream cases. The effects wore off after an upstream distance of in a range of small distance of about 3.5 mm, 4 mm and 4.5 mm for small, medium and large branch cases.

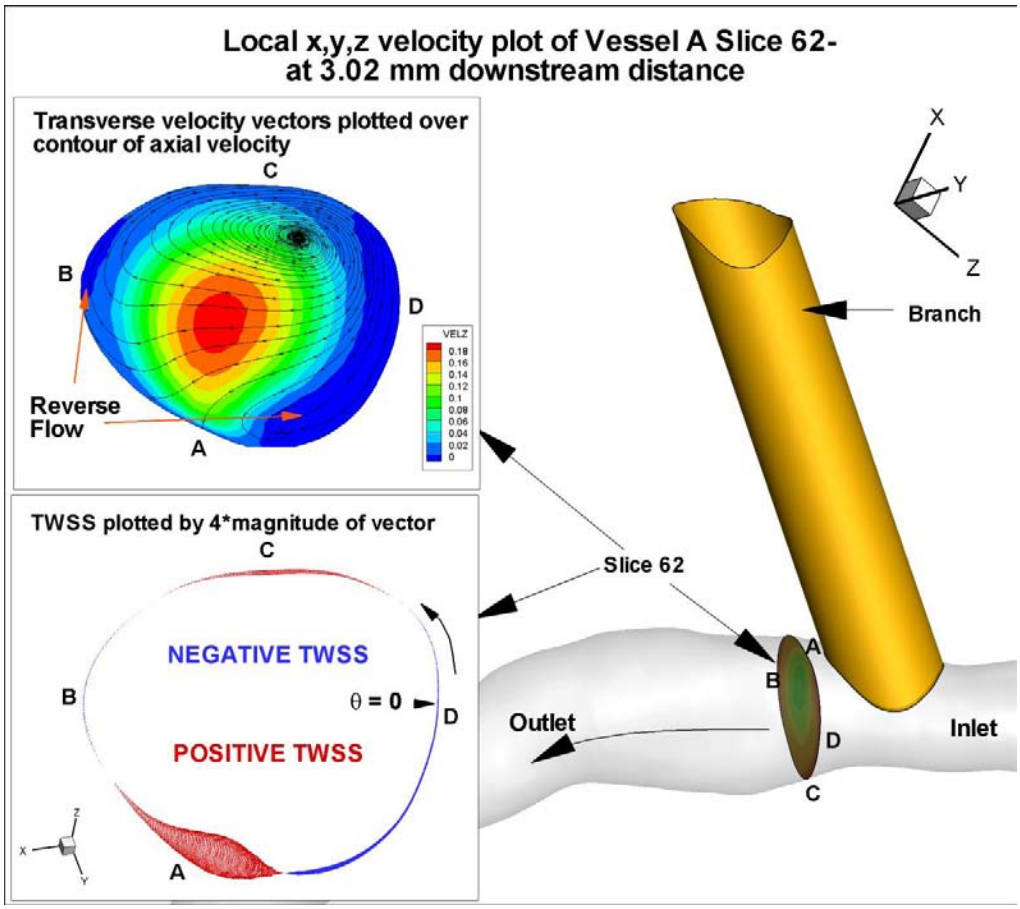

Figure 5-3 Figure showing the position of slice (slice 62) at a downstream distance of 3.02 mm and the regions of reverse flow and transition of TWSS

5.2.1.2 Reverse and Secondary Flow in Vessel A

5.2.1.2.1 Downstream

The plots of transverse velocity vector for downstream cases have been shown in figures 5-19 to 5-26. At the downstream distance of 3.02 mm (slice 62) axial or z-velocities were found to be negative at one small and one large region in the cross sectional-area at the sides of the branch. This can be clearly seen in Figure 5-19. The value of negative z velocity increased with the increase in branch size. The lowest z-velocity observed was in the large branch case and it was -0.0187 m/s. Similarly, for medium branch case the lowest axial velocity was -0.0093m/s

and for small branch case it was -0.00166m/s (Figure 5-20). No branch case only had positive z velocity. Two secondary flows were observed in this slice for all cases. These secondary flows were hence caused purely due to curvature of the original geometry. These secondary flows observed were hence the Dean‟s Vortices. Similar phenomenon was observed in the slices further downstream however, in a decreasing order. For example, at 5.02 mm (slice 58) downstream as seen in Figures 22 and 23, the Dean vortices were present in all the cases of branching for this slice, but the magnitude of z velocity was seen to decrease slowly. The magnitude of lowest axial velocity at this point as seen in figure 5-32 and 5-33 was -0.016 m/s, -0.01 m/s and -0.002m/s for the large, medium and small branched cases respectively. The negative z velocity was seen to decrease completely by slice 50 at a distance of 9 mm downstream. The axial velocity plot for above slice in figure 5-22 shows that in downstream flows after a certain region there is no reverse flow due to branching and hence no negative axial velocity (Figure 5-23-26) were seen. Further. flow was also observed to grow symmetrical in more distal slices. For example, flow in slices 62, 58, and 50 were skewed towards the divider wall but in slice 32 it was almost symmetric for all the branch sizes.

Interestingly, secondary flow was clearly seen in no branch case at the slice (50) 9.0 mm downstream of bifurcation, but in the branched cases only trends of secondary flow were observed. This observation can be clearly seen in Figure 5-23. In the regions further downstream, as shown in Figure 5-25 of slice 32, the nature of flow in all the cases of branching was observed to the same, however, the magnitude of velocity vectors were lower than in no branch case which could be because of less amount of flow passing through the main channel as explained earlier.

5.2.1.2.2 Upstream

In the slice at about 2.51 mm (slice 73) upstream to the branch neither secondary flow nor negative axial velocity were observed in all the cases of branching. The nature of the flow

can be seen in Figure 5-27 and 5-28. In these plots of transverse velocity vectors no concrete effect of branching was seen. Transverse velocity plots for slices upstream have been shown in Figure 5-27 and 5-28.

5.2.2 Results and Discussions for Vessel B

Out of the three vessels that were considered in this study vessel B was the longest. As discussed earlier, this vessel has an inlet area smaller than its outlet. Since this vessel had the largest local as well as global curvature out of three, it was no surprise that this vessel exhibited particularly interesting flow behaviors.

5.2.2.1 TWSS in Vessel B

5.2.2.1.1 Downstream

The downstream TWSS plots for vessel B have been reported in Figures 5-10 to 5-12. At a distance of 2.01 mm downstream (slice 68) from the branch center, TWSS values for the branched cases were seen slightly higher than the no branch case at almost half of the circumference in the side of the circumference towards the branch. However, in the other half, in the region opposite to the branch side, they decreased considerably and turned slightly negative. The range of the TWSS was (-0.4 N/m^2 to 4.0N/m^2). The highest variance was seen for the large branch case and it decreased for the medium and the small branched cases. The maximum variance seen for large branch case was 14 times of no branch case; where the value of TWSS for large branched case was 3.9 N/m^2 as compared to 0.3 N/m^2 no branch case. For medium branch case the highest value of TWSS was 3.45N/m^2 and for small branch case it was 2.5N/m^2, which was 8.8 and 6.25 times higher than the no branch case. Similar trends were seen few slice downstream as well. An example of this could be seen in Figure of slice 64 at a downstream distance of about 4.02mm from the branch origin. This trend was observed until the distance of

about 7.5 mm (slice 57) but in decreasing order. The cross sections more distal to the branched cases were observed to have lower TWSS in the entire circumference such that higher the branch size, lower the TWSS, as seen in Figure 5-12 of slice 56 at 8.04mm distance downstream. In this figure an illustrative sub-figure showing the contour of WSS has been shown. It could be seen that the peak of WSS (black line representing the circumference of the slice lying in red region representing high WSS values) observed in all the cases of branch sizes were due to the local curvature.

5.2.2.1.2 Upstream

The branched cases showed lower values of TWSS in about half of the circumference at a distance of 2.01 mm upstream as shown in Figures 5-13. The value of TWSS for large branch case was lower by (-4.4/– 0.2) two orders of magnitude compared to the no branch case at a point in the circumference. The TWSS values were lower by roughly four times (-1.2/-0.2) and roughly 1.6 times (-0.7/-0.2) for medium and small branch cases respectively, again in comparison with the no-branch case. Hence, with the increase in size of branch lower values of TWSS were observed in the regions of the circumference towards the branch. Similar trend was seen up to few slices upstream but in decreasing order. The effect was however not seen after an upstream distance of about 4 mm for large branch case and after about 3.5 mm for medium and small branch cases. As shown in Figure 5-14 of slice 82, at a distance of 4.5 mm downstream the plots for all the cases of branching coalesced. Hence, larger the size of branch larger the range of impact was seen in upstream direction as well.

5.2.2.2 Recirculation and Secondary Flow in Vessel B

5.2.2.2.1 Downstream

The results of transverse velocity vectors in downstream slices are shown in Figures 5-29 to 5-34. At a distance of 2.01 mm downstream from the branch origin, secondary flows were seen in all cases of branching. Presence of branch of different sizes did not alter the nature of secondary flow. However, the value of axial velocity was observed to differ in each case of branching. The lowest value of axial velocity was seen for the largest branch case and it was -0.04m/s. This value decreased subsequently with decrease in branch size. Minimum value of axial velocity observed for medium and small branch cases at this distance were -0.035 N/m^2 and -0.018 N/m^2. The value was zero for no branch case. Axial velocity profile was observed to be skewed towards the divider, with most of the flow being positive. However though in a small region of the cross sectional area, negative axial velocities were also observed in the direction opposite to the branch or in the outer wall. The strength of the axial velocity was higher for lower branch cases in the direction of flow whereas it was lower in the region of negative or reverse flow (see Figure 5-30). Similar trends were observed until few slices downstream. When the velocity vectors in slice 64 (4.02 mm downstream) were plotted, it was seen that the negative axial velocities, representative of reverse flow, were still present in all branched cases. However, the magnitude had decreased. It can clearly seen in Figure 5-32 that the magnitude of axial velocity has decreased to -0.033 N/m^2 in the largest case while -0.02 N/m^2 and -0.0004 N/m^2 for the medium and small branched cases. This trend was seen to diminish in regions more distal to branching. Negative z velocities completely disappeared after a distance of 7.5 mm, 6.5 mm, and 4.5 mm downstream from the point of branching. This was clearly seen when a slice (56) at about 8.04 mm downstream was plotted as shown in Figure 5-34. The entire region was seen to have positive value of axial velocity though skewed towards the divider wall. Similar to the case of Vessel A, velocity profile became symmetric as one moved more distal from the site of branching.

5.2.2.2.2 Upstream

As seen in Figure 5-43, at a distance of 2.51 mm upstream (slice 77), axial velocity was observed to be negative for all the cases of branching including no branch case. Hence this reverse flow could be a result of high curvature of Vessel B. The magnitude of negativity was however higher for large branch case and the least for no branch case, Hence, reverse flow observed at this point could be due to the cumulative effect of curvature as well as branching. Following were the maximum values of negative z velocities observed in large, medium, small and no branch cases respectively:-0.173m/s,- 0.01325m/s,-0.0107m/s,-0.0045m/s. However, in the subsequent regions beyond 3 mm, negative axial velocities were not seen in Vessel B. No variation in flow properties were observed in regions more upstream which has been clearly shown in Figure 5-36 while plotting slices at a distance of about 5 mm (slice 82) upstream. It is important to note that in the case of vessel A, upstream regions were devoid of any negative z velocities. Further, curvature plays major role in generating reversed flow and Vessel B qualitatively had the highest curvature in the three Vessels under study.

5.2.3 Results and Discussions for Vessel C

Vessel C comparably had the simplest geometry (qualitatively) out of three vessels under study. It was not only shortest but also had smallest overall cross sectional area. This vessel also had minimum curvature of the three. Below are the discussions on the results obtained after analyzing the TWSS, transverse velocity vectors and axial velocity at different upstream and downstream slices for this vessel.

5.2.3.1 TWSS in Vessel C

5.2.3.1.1 Downstream

Downstream slices of Vessel C have been plotted in figures 5-15 and 5-16. TWSS values for entire downstream region were observed to be positive for this Vessel which is quite contrary to the observations made for Vessels A and B. These values for branched cases were observed to be lower than the no branch case in downstream regions as expected due to lower amount of outflow. However for most parts in the circumference, the trend that TWSS followed was similar. A slice was considered at a distance of 2.51 mm (slice 45) downstream from the branch origin as shown in Figure 5-15. Despite of proximity of this slice to the site of branching, at this cross section, TWSS values for branched cases were observed to be lower than the no branch case throughout the circumference. This could have occurred due to high Reynolds number as the cross sectional area of Vessel C is considerably smaller than other two vessels for the same amount of mass inflow. However, TWSS values were observed considerably lower in one third region of the circumference (from 2-3 radians and 4 -6.28 radians) than in the no branch cases. Lower values of TWSS were observed in the regions of the circumference lying at the either sides of the branch. The regions of the circumference opposite to the branch and in the direction of branch were observed to have higher TWSS values. The variation was seen to increase with the increase in branch size. The highest variation observed with respect to no branch case was 0.45 (4.2/1.9) for large branch case, 0.52 (4.2/2.2) for medium branch case and 0.67 (4.2/2.87) for small branch case. In the regions downstream, the effect of branching was observed to decrease. For instance in the cross sections analyzed at a distance of 3.02 mm (slice 44) downstream, the trends of small branch appeared to be almost similar to that of no branch case but TWSS curves of medium and large branch cases had slightly different features in the region in between 1-2.5 radians. The large branch case appeared to behave the same as the other cases of branching after a distance of about 3.5 mm. To support it further, the cross sections at 4.52 mm (slice 41) was considered where the trend of TWSS for all the cases of branching appeared

similar. Further downstream, the TWSS value decreased with the increase in size of branch. This variation in magnitude was obviously due to the flow of less amount of fluid in the main channel with the increase in branch size.

5.2.3.1.2 Upstream

At a distance of about 6 mm (slice 62) upstream from the branch origin, TWSS plots for all the branched as well as no branch cases were observed to almost overlap as shown in Figure 5-18. However as the distance decreased to about 4mm (slice 58), at different points around the circumference, branched cases were observed to have either slightly higher or slightly lower values of TWSS when compared to the no branch case. As the site of branching approached closer, the variance in TWSS values were seen to increase. At a distance of 2.51 mm upstream (Figure 5-27) of branch the highest variation in between large branch and no branch case was calculated to be (4.05/3.1) 1.3 times for largest branch case, (3.7 /3.1) 1.19 times for medium branch case and (3.5-3.1) 1.13 for small branch case.

Surprisingly, the values of TWSS for this vessel though were lower than no branch case at regions, never became negative. For the same mass inflow rate assumed for all three vessels, vessel C had the highest Reynolds number. This could strengthen the argument that reverse flows are more prominent in the regions of flow where viscous forces are dominant.

5.2.3.2 Recirculation and Secondary Flow in Vessel C

5.2.3.2.1 Downstream

When cross sections of all the cases of Vessel C at a downstream distance of 2.51 mm (slice 45, see Figure 5-37) were compared it could be seen that secondary flow was more prominent in the branched cases. It could be seen in Figure 5-37 that at this slice, no-branch case did not show secondary flow. However, only slight trend of secondary flow was seen in small

branch case. This trend was observed to increase to small secondary flow in medium branch case and finally to a complete secondary flow in large branch case. These secondary flows were seen to degrade after a short distance downstream. When another slice further downstream at a distance of 4.52 mm (slice 41) from branch origin was considered, it could be clearly observed that there were no trends of secondary flow at any cases of branching. This slice has been shown in Figure 5-39. Same observation was made in regions further downstream from the point of branch origin. Surprisingly, negative axial velocity which was observed as a prominent factor in the regions closer to the branching in downstream flow were completely absent in this vessel. As observed in Figure 5-38, no negative axial velocities were seen in the distance of about 2.5 mm. However, when a cross section in the region of branch was considered, negative axial velocity due to recirculation was clearly seen.

5.2.3.2.2 Upstream

On comparing the flow behavior for all the cases of branching at upstream region from the branch origin, it could be seen that presence of branch did not have any impact on the flow behavior. Everything from the transverse velocity range, their distribution and axial velocity were observed to be same. This comparison has been clearly shown in Figure 5-40 and 5-41 where slices of different cases at upstream distances of 2.51 mm and 4.02 mm (slice 55and slice 58) have been plotted. When these upstream were compared, existence of secondary flow could be clearly seen in slice considered in Figure 5-48 for all the cases of branching, but it was absent in the case of slice considered in Figure 5-49. However, these secondary flows were present due to geometrical factors and not branching.

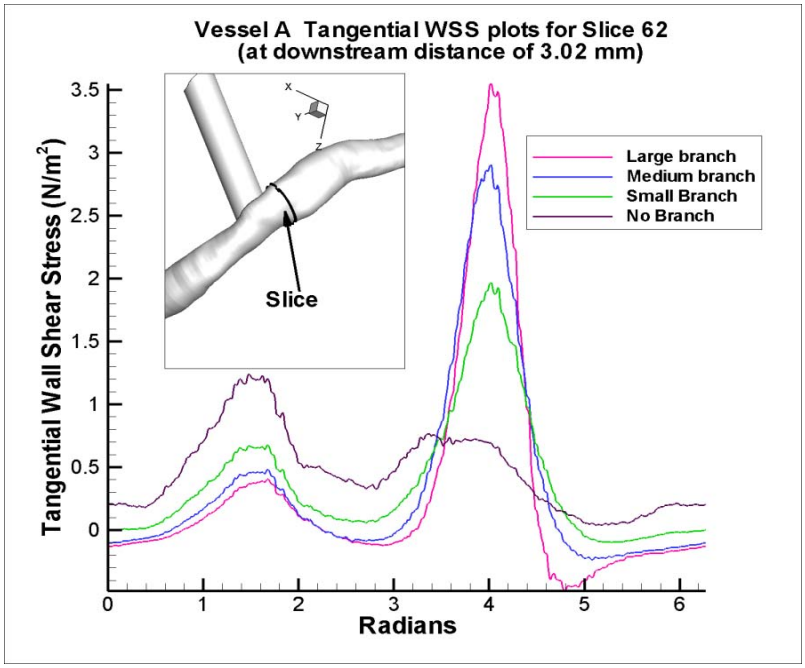

Figure 5-4 Plot comparing TWSS at about 3 mm downstream from branch origin in vessel A for all cases of branching

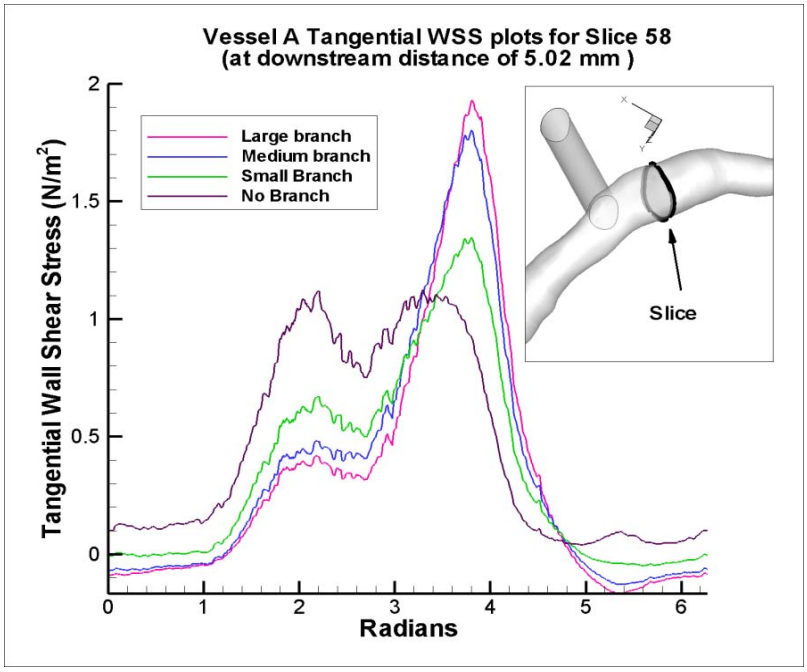

Figure 5-5 Plot of TWSS at about 5 mm downstream distance from branch origin in vessel A for all cases of branching

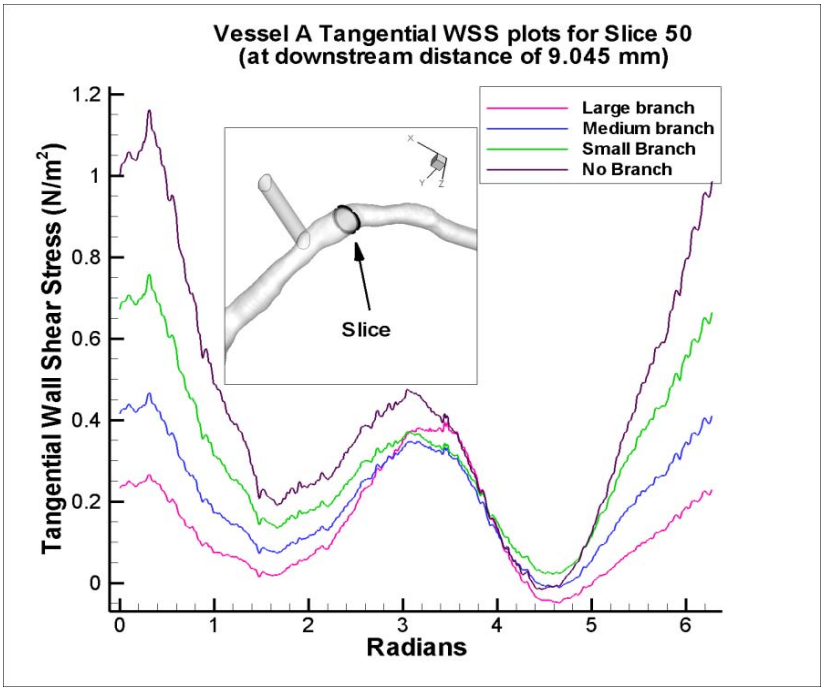

Figure 5-6 Plot of TWSS at about 9 mm downstream from branch origin in vessel A for all cases of branching

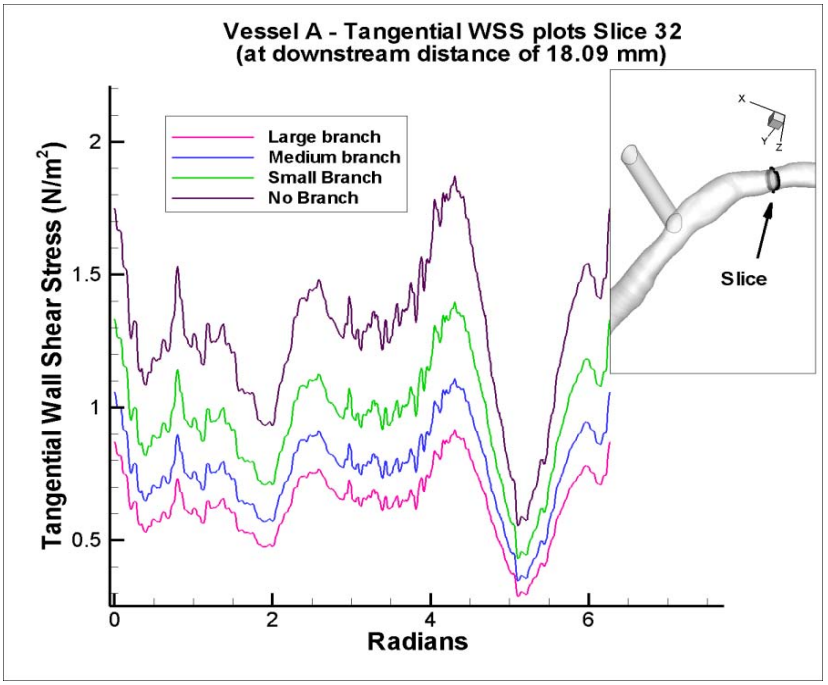

Figure 5-7 Plot of TWSS at about 18 mm downstream from branch origin in vessel A for all cases of branching

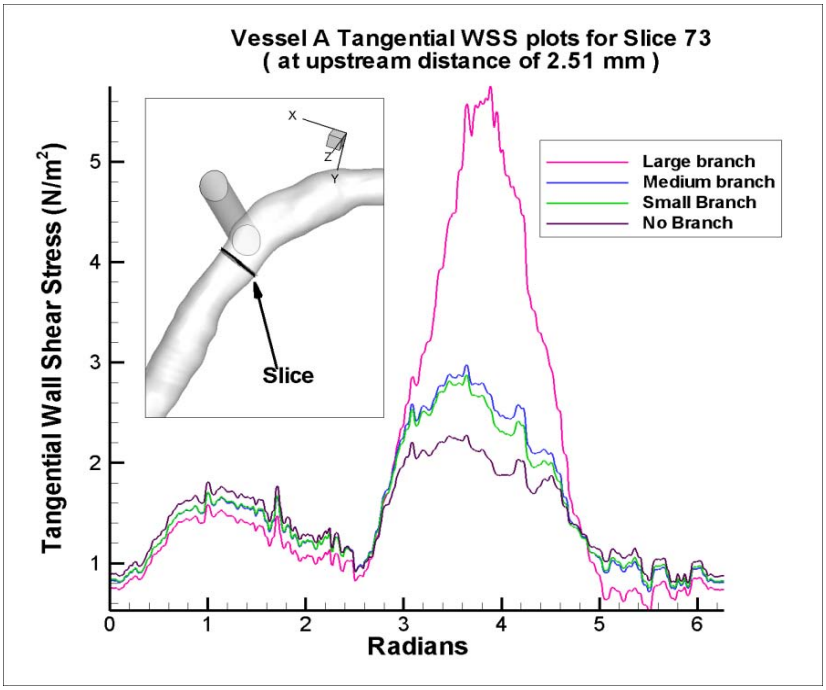

Figure 5-8 Plot of TWSS at about 2.5 mm upstream distance from branch origin in vessel A for all cases of branching

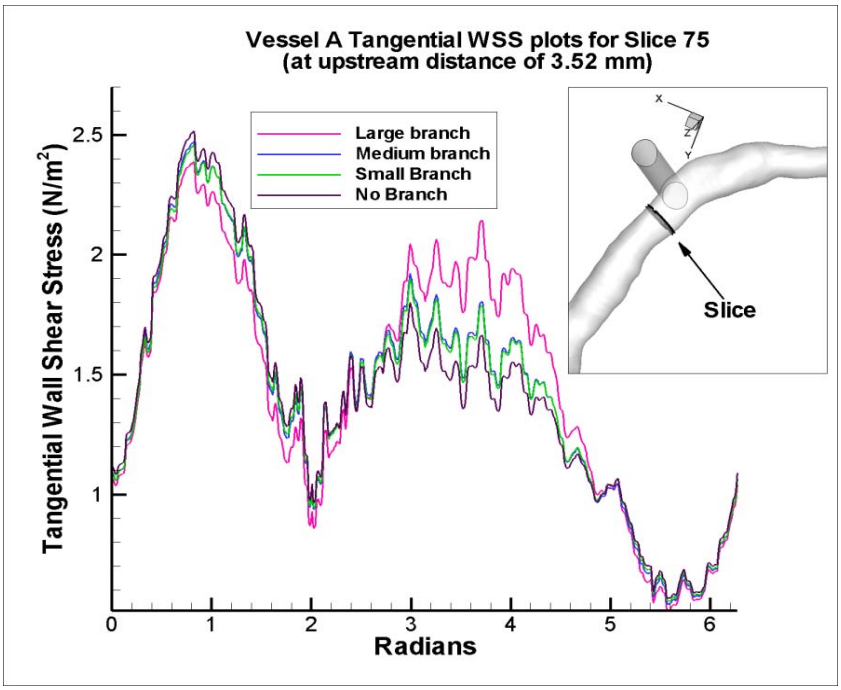

Figure 5-9 Plot of TWSS at about 3.5 mm distance upstream from branch origin in vessel A for all the cases of branching

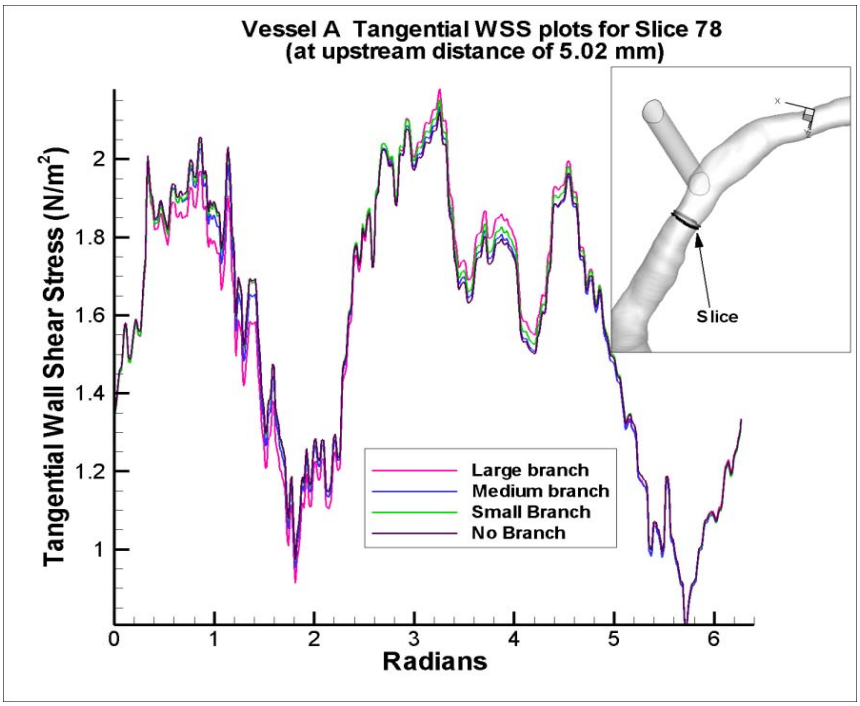

Figure 5-10 Plot of TWSS at 5 mm upstream from branch origin in vessel A for all cases of branching

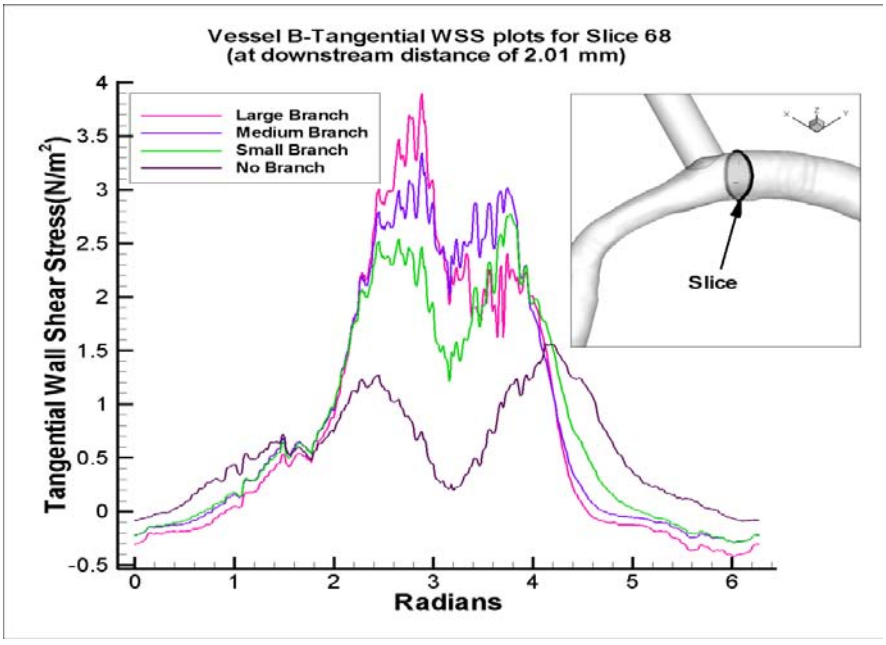

Figure 5-11 Plot of TWSS at a downstream distance of about 2.01 mm in vessel B from branch origin for all cases of branching

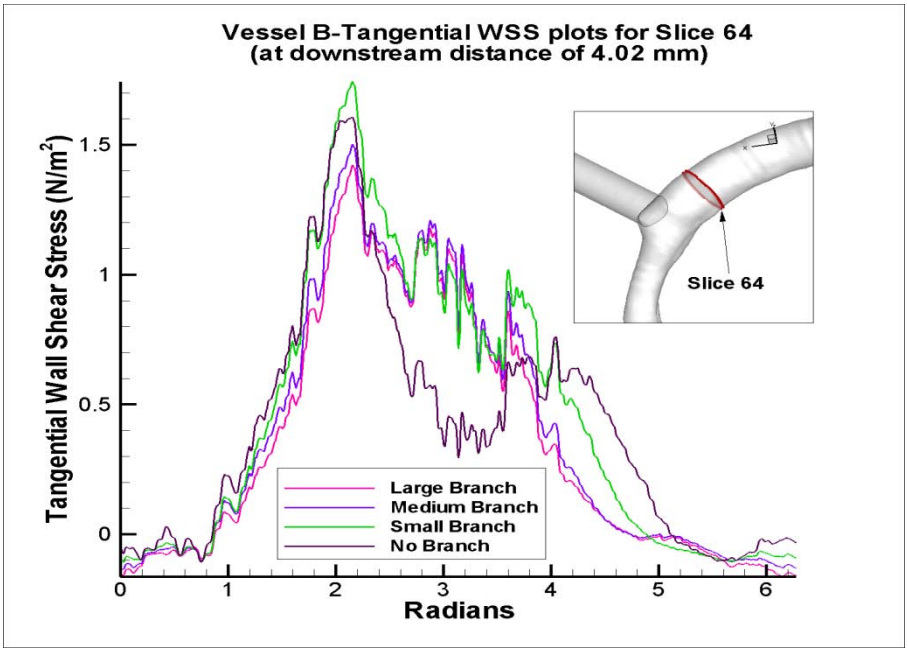

Figure 5-12 Plot of TWSS at a downstream distance of 4.02 mm from branch origin in vessel B for all cases of branching

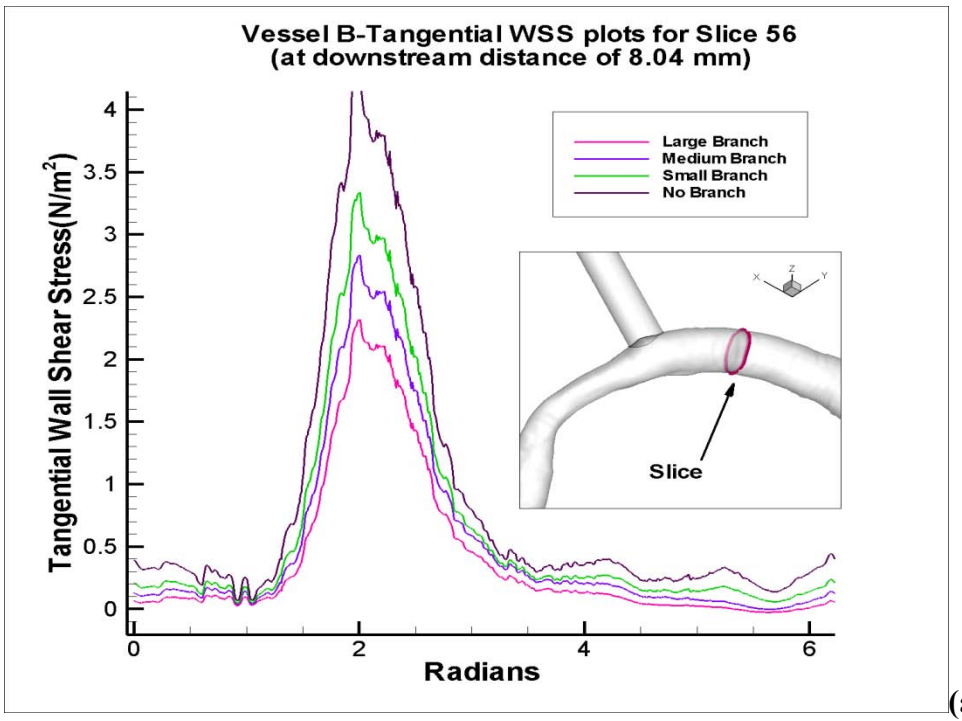

(a)

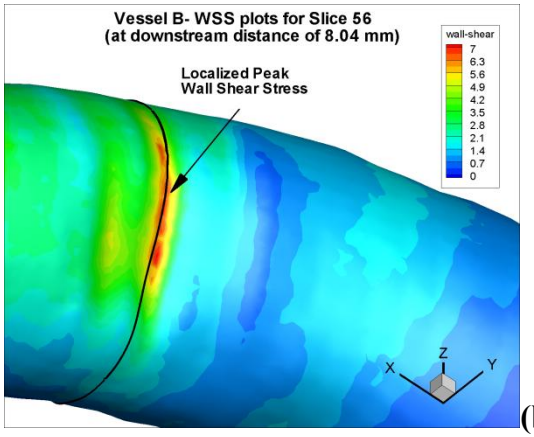

(b)

Figure 5-13 Figure (a) is a plot of TWSS at a downstream distance of 8 mm from branch origin in vessel B for all cases of branching. (b) plot showing local curvature causing high wall shear stress in the slice of interest.

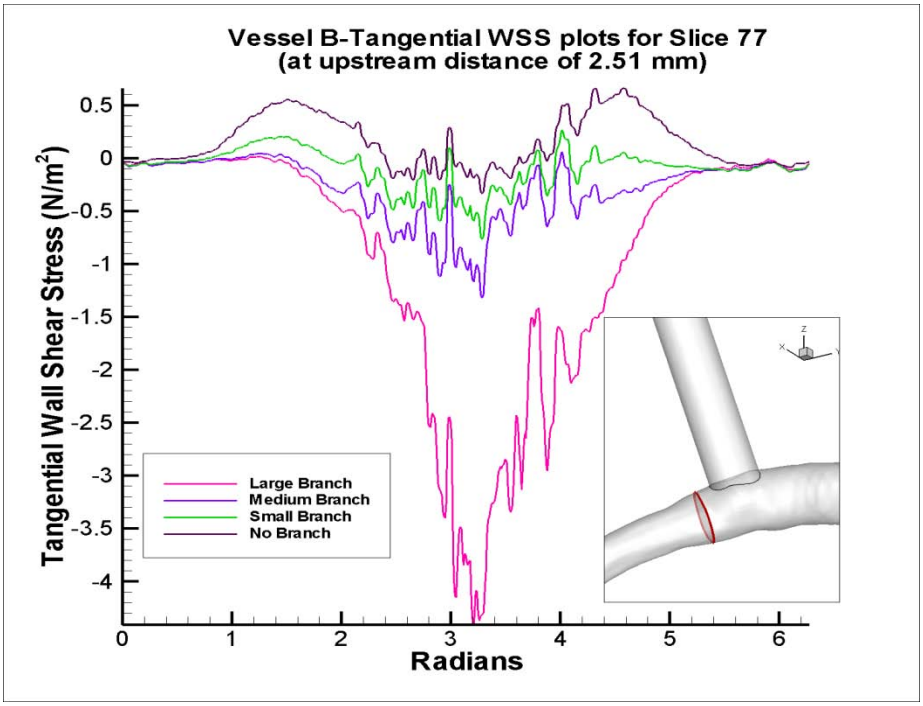

Figure 5-14 Plot of TWSS at an upstream distance of 2.51 mm from branch origin in vessel B for all cases of branching

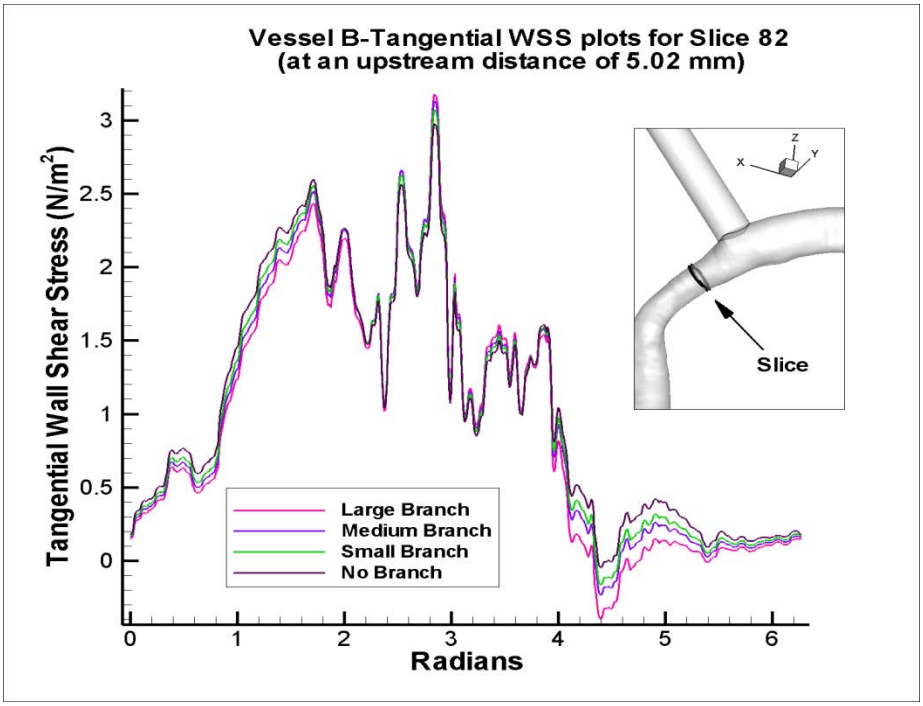

Figure 5-15 Plot of TWSS at an upstream distance of about 5 mm from branch origin in vessel B for all cases of branching

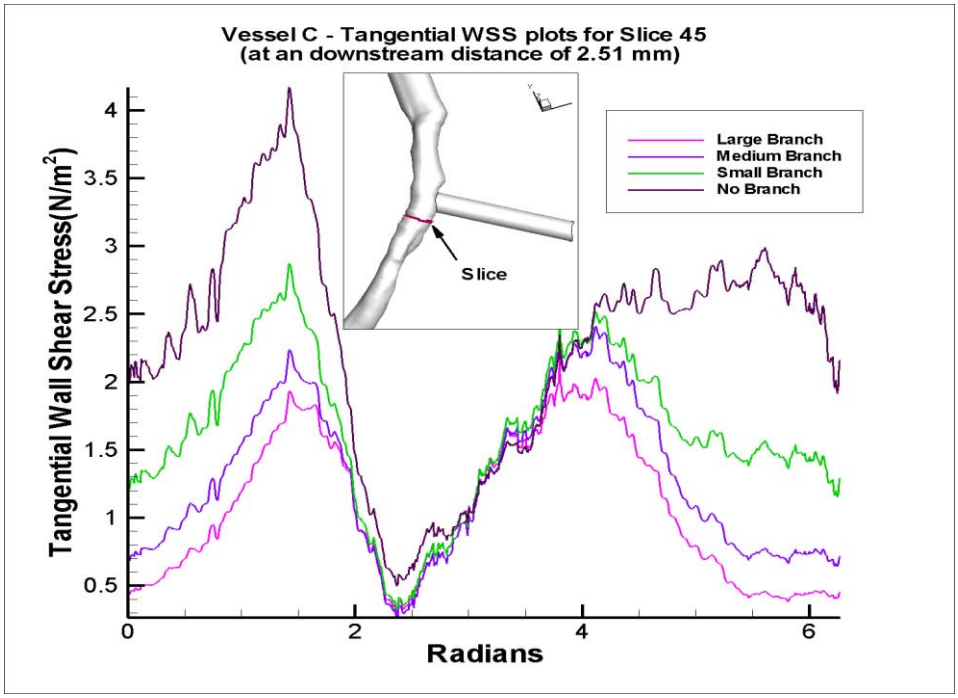

Figure 5-16 Plot of TWSS at a downstream distance of 2.51 mm from branch origin in vessel C for all cases of branching

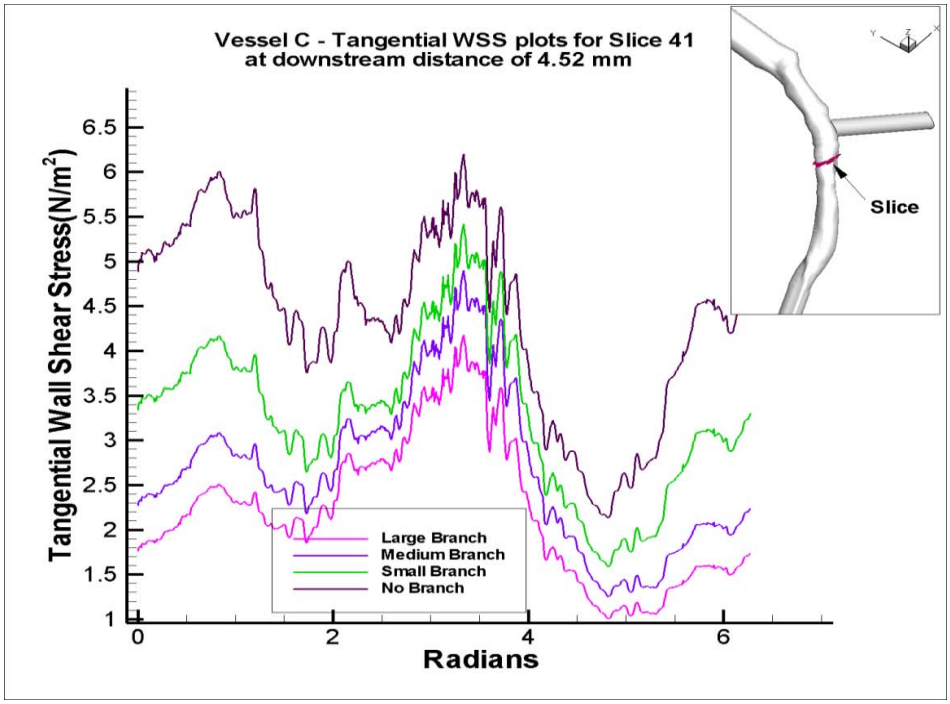

Figure 5-17 Plot of TWSS at a downstream distance of 4.52 mm from branch origin in vessel C for all cases of branching.

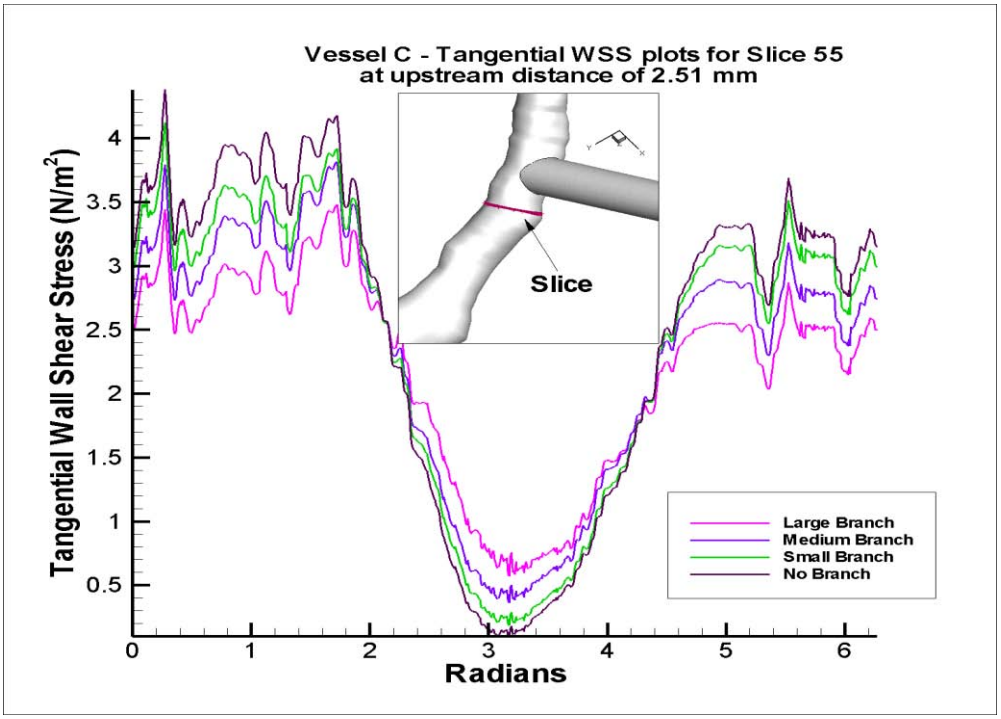

Figure 5-18 Plots of TWSS at an upstream distance of 2.51 mm from branch origin in vessel C for all cases of branching

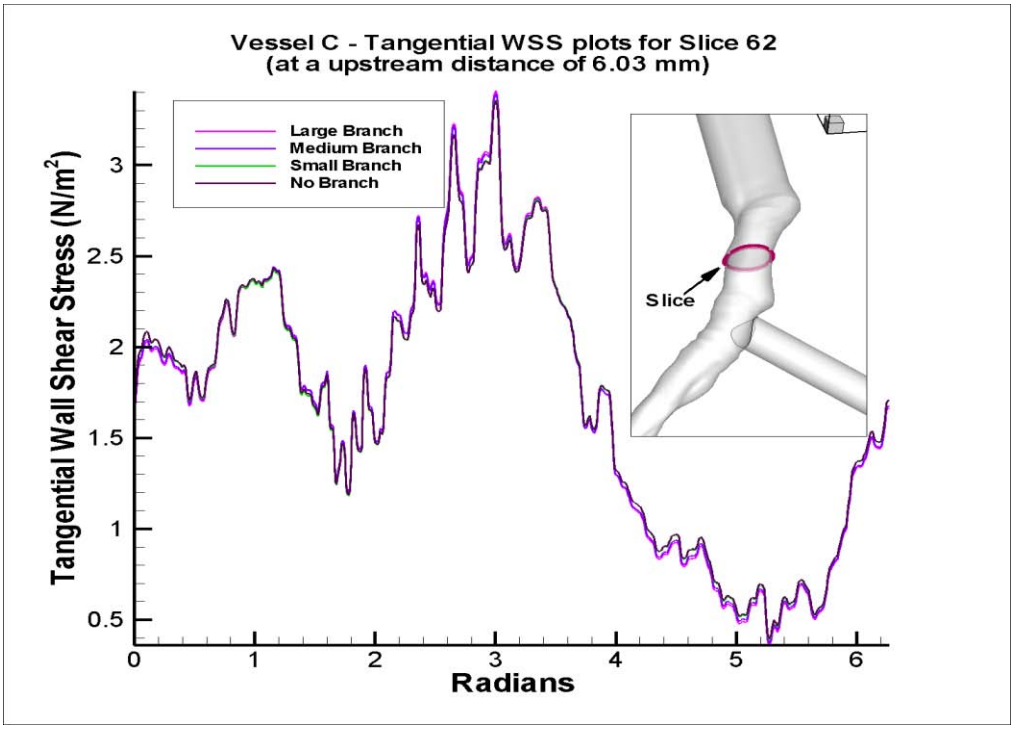

Figure 5-19 Plot of TWSS at a upstream distance of about 6 mm from branch origin in vessel C for all cases of branching

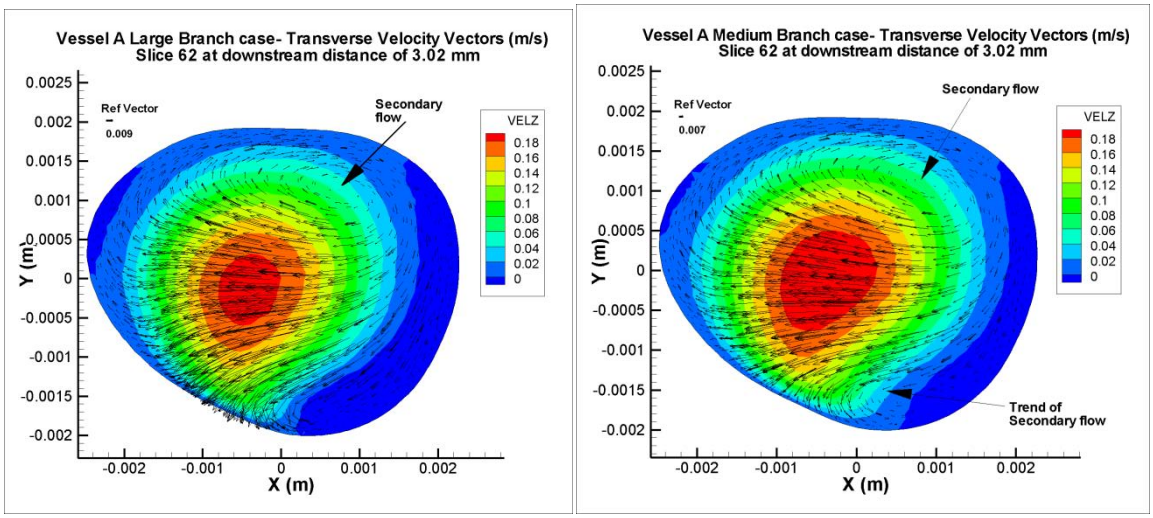

Figure 5-20 Plots of slices at a downstream distance of 2.51 mm from the branch origin showing Transverse velocity vectors overlaid on the contours of axial in Vessel A for all cases of branching

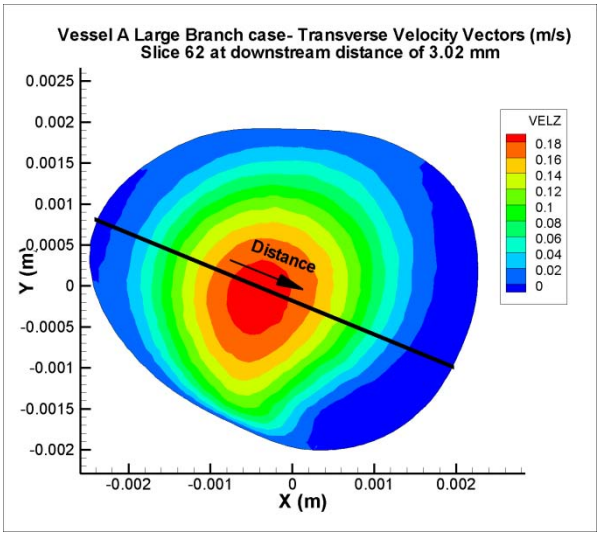

(a)

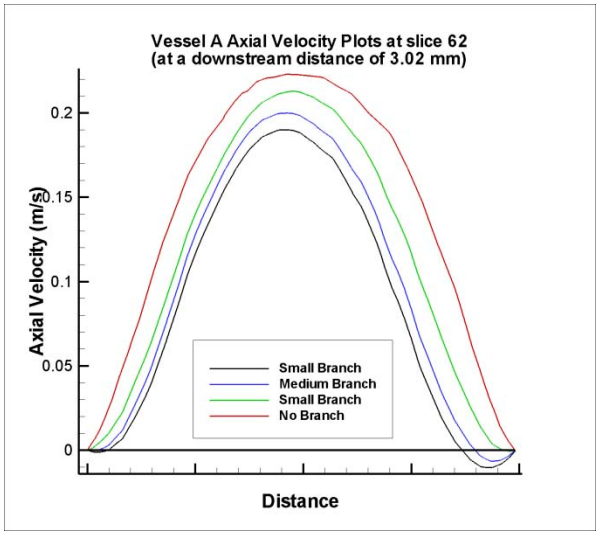

(b)

Figure 5-21 Axial velocity distribution in an extracted in in Vessel at 3.02 mm downstream distance

Figure (a) shows the line extracted from cross section of slices at 3.02 mm distance downstream of branch origin for different cases of branching in Vessel A. Figure (b) shows comparison of axial velocities in those slices.

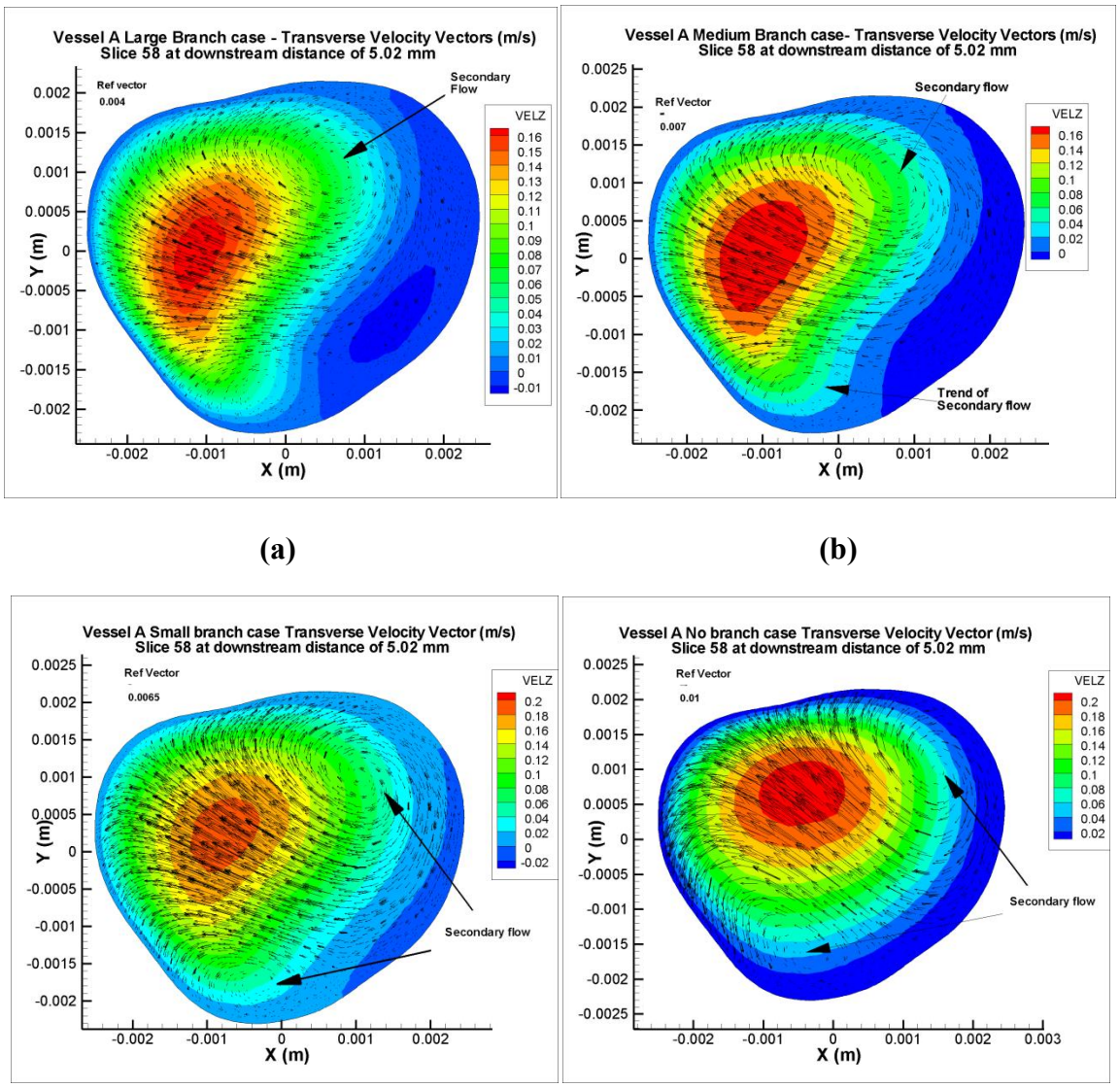

Figure 5-22 Plots of slices at a downstream distance of 4.52 mm from the branch origin showing Transverse velocity vectors overlaid on the contours of axial in Vessel A for all cases of branching

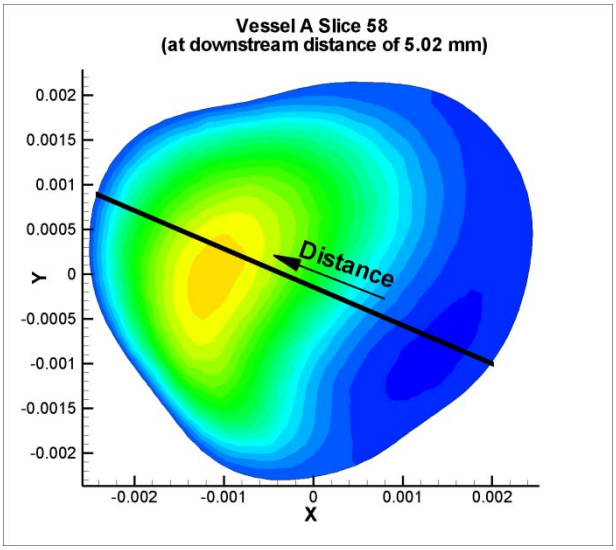

(a)

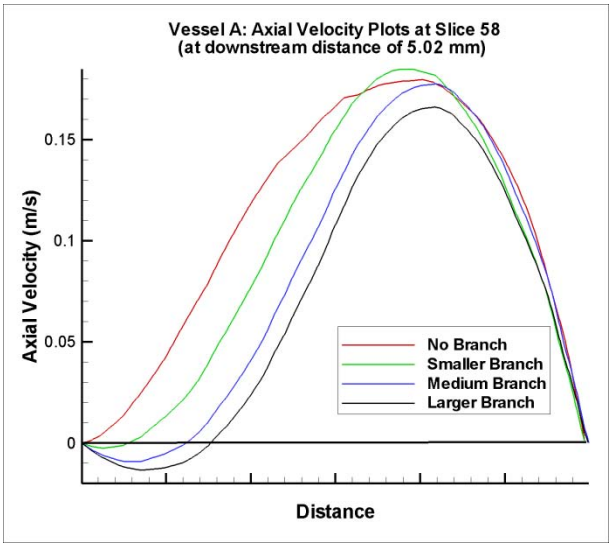

(b)

Figure 5-23 Axial velocity distribution in an extracted in in Vessel at 5.02 mm downstream distance

Figure (a) shows the line extracted from cross section of slices at 5.02 mm distance downstream of branch origin for different cases of branching in Vessel A. Figure (b) shows comparison of axial velocities in those slices.

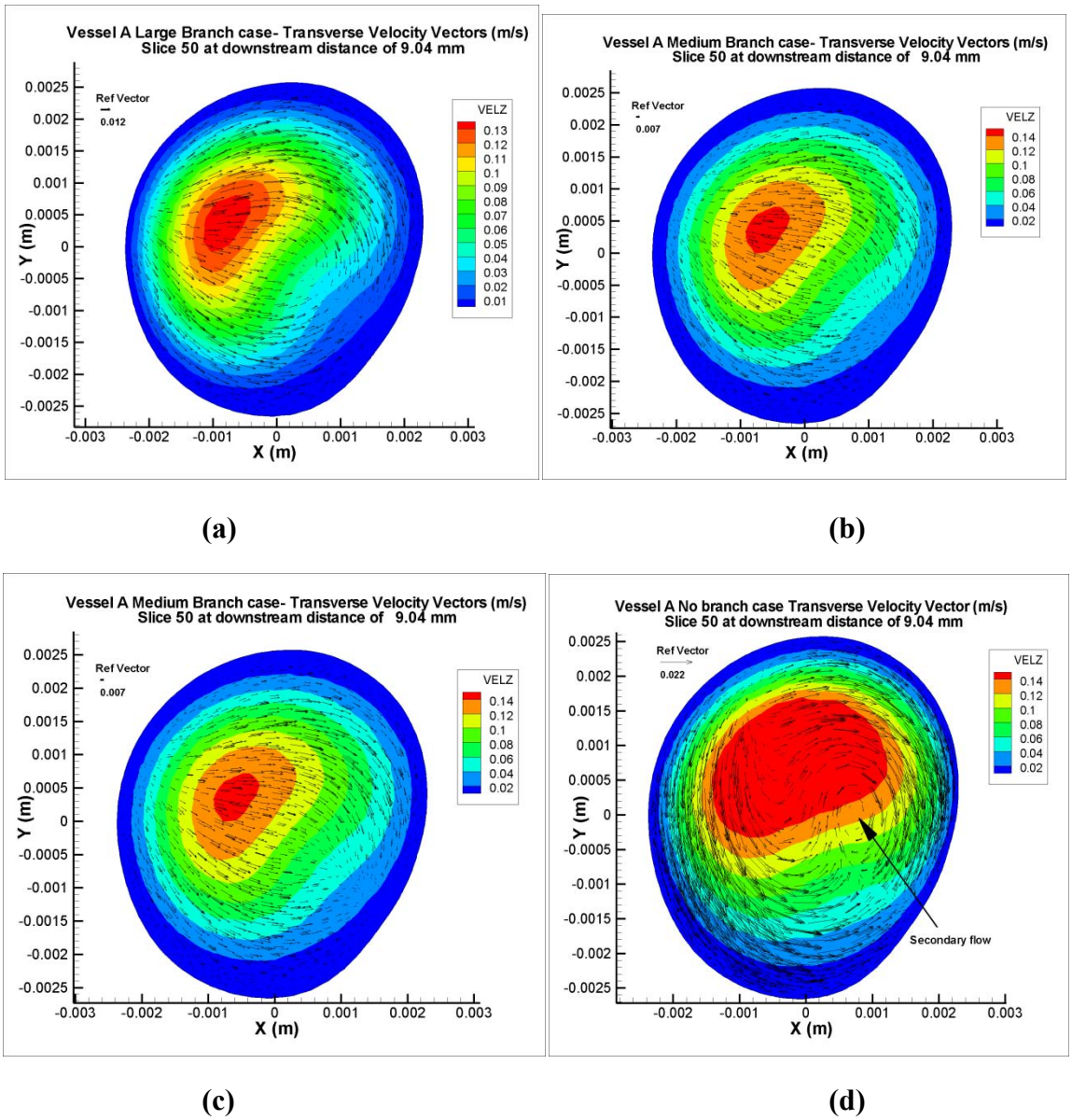

Figure 5-24 Plots of slices at a downstream distance of 9.04 mm from the branch origin showing Transverse velocity vectors overlaid on the contours of axial in Vessel A for all cases of branching

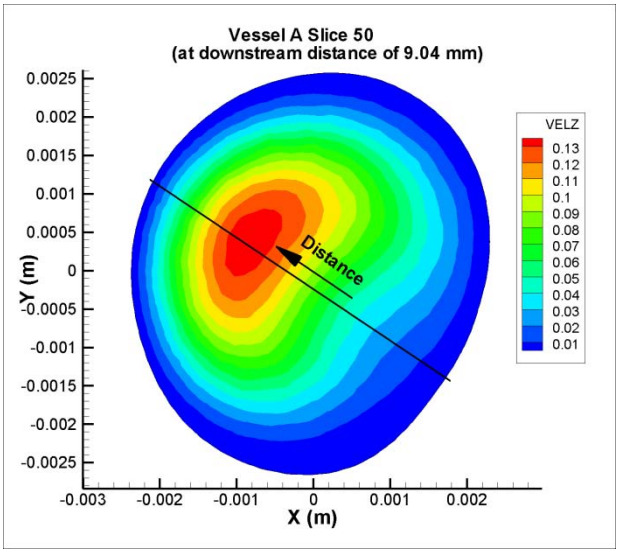

(a)

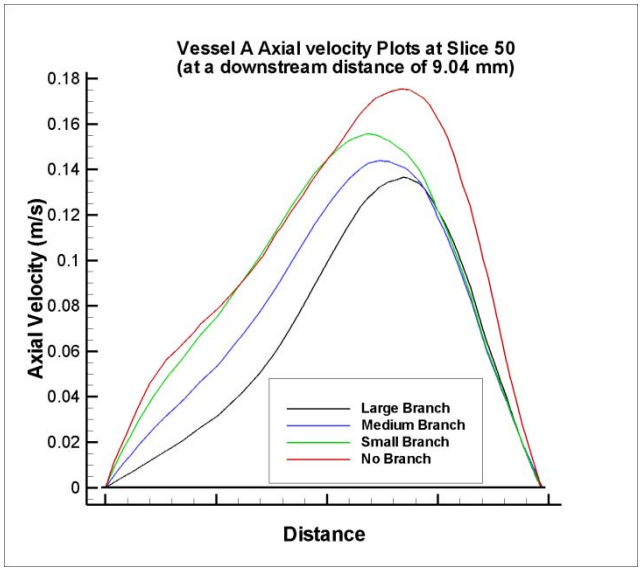

(b)

Figure 5-25 Axial velocity distribution in an extracted in Vessel at 9.04 mm downstream distance

Figure (a) shows the line extracted from cross section of slices at 9.04 mm distance downstream of branch origin for different cases of branching in Vessel A. Figure (b) shows comparison of axial velocities in those slices.

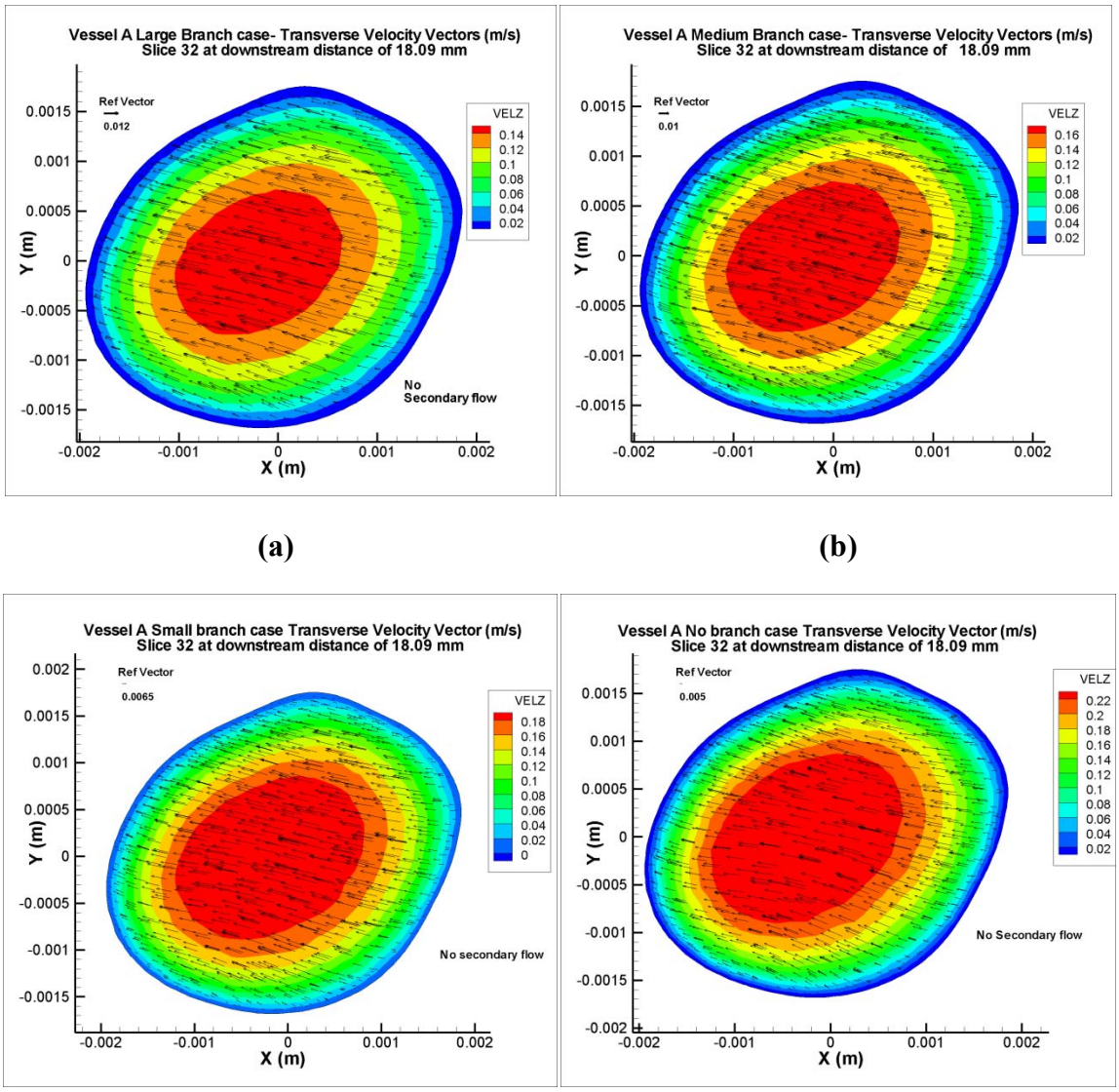

Figure 5-26 Plots of slices at a downstream distance of 18.09 mm from the branch origin showing Transverse velocity vectors overlaid on the contours of axial in Vessel A for all cases of branching

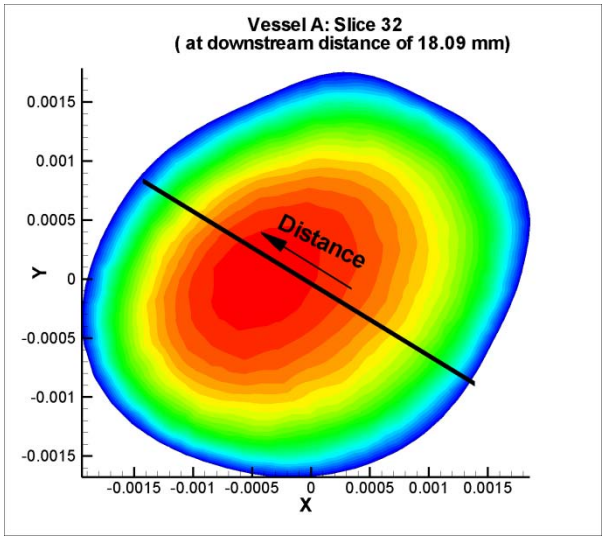

(a)

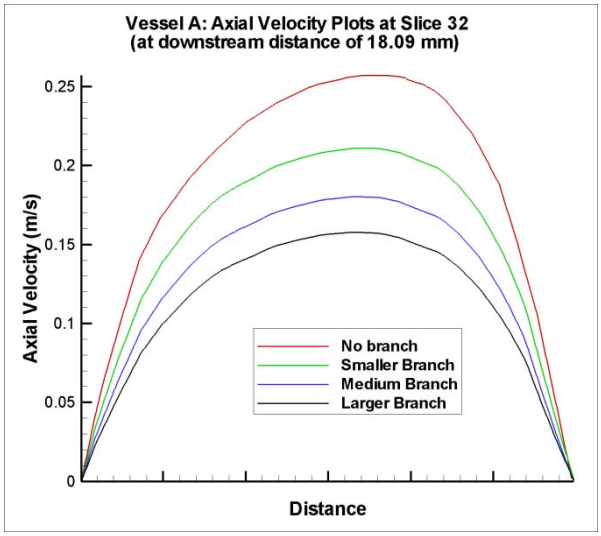

(b)

Figure 5-27 Axial velocity distribution in an extracted in Vessel A at 18.09 mm downstream distance

Figure (a) shows the line extracted from cross section of slices at 18.09 mm distance downstream of branch origin for different cases of branching in Vessel A. Figure (b) shows comparison of axial velocities in those slices.

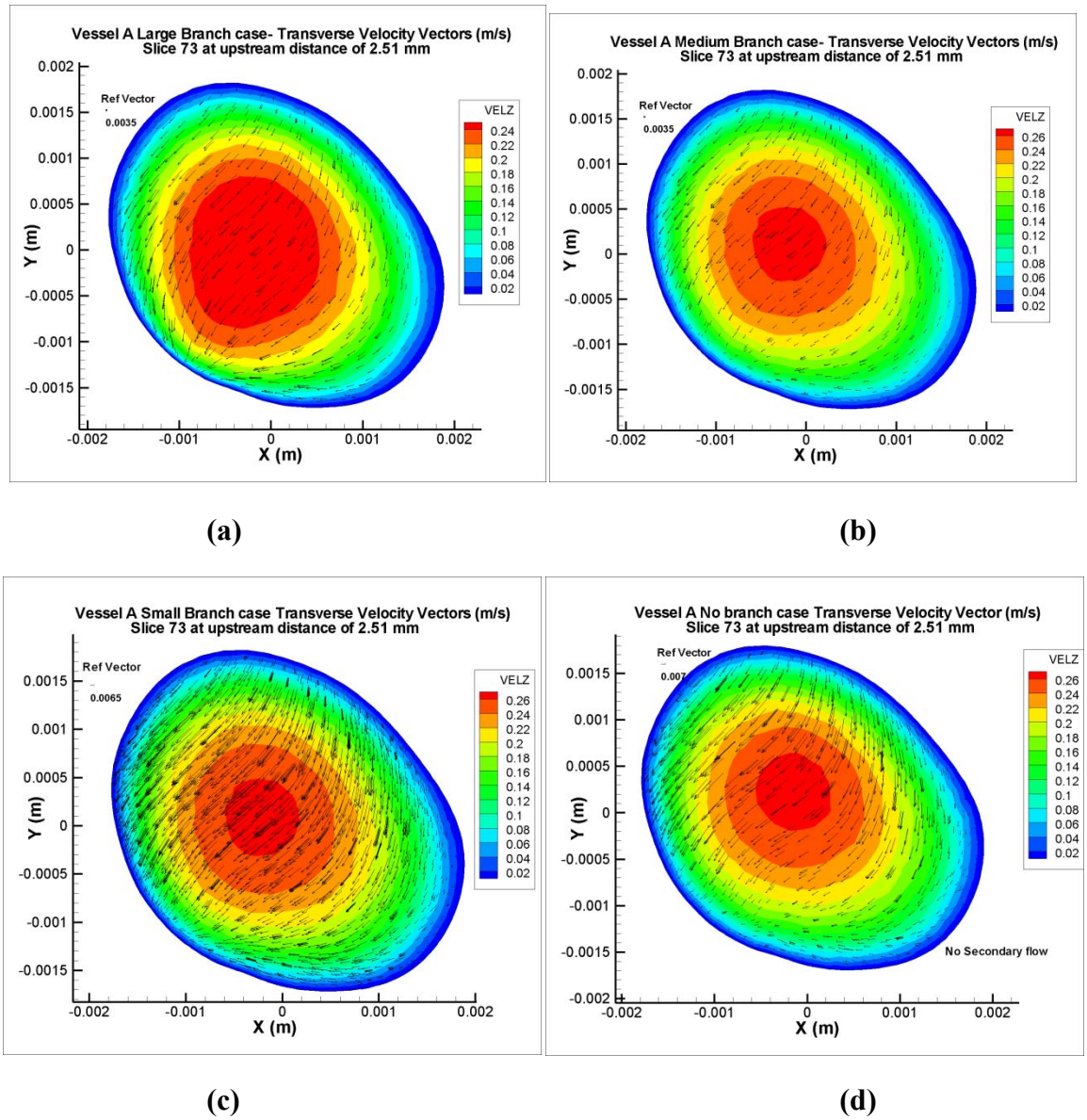

Figure 5-28 Plots of slices at a upstream distance of 2.51 mm from the branch origin showing Transverse velocity vectors overlaid on the contours of axial in Vessel A for all cases of branching

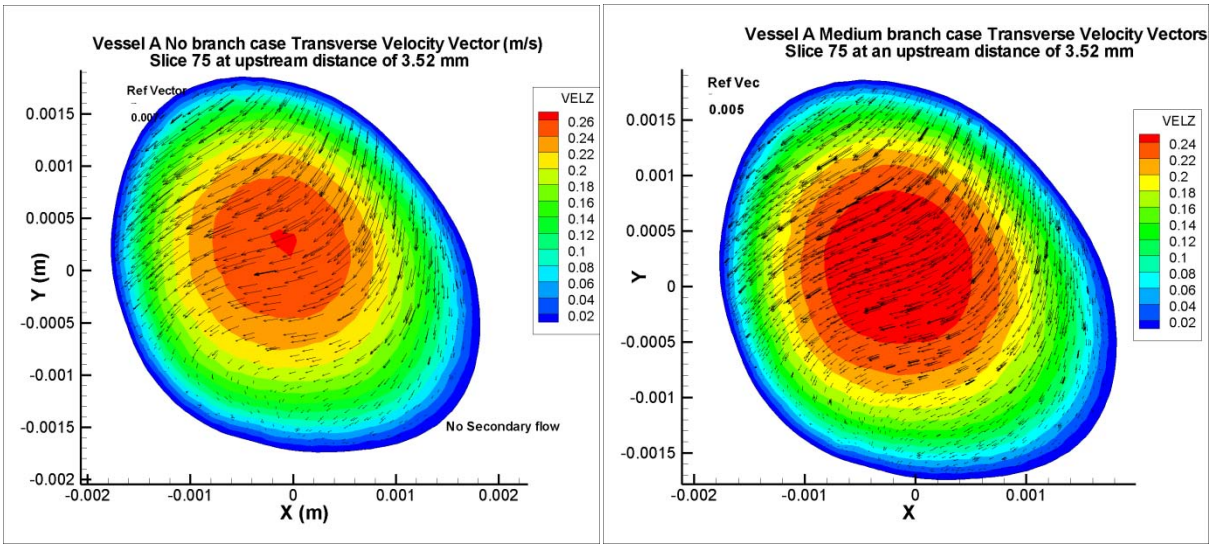

(a) **(b)**

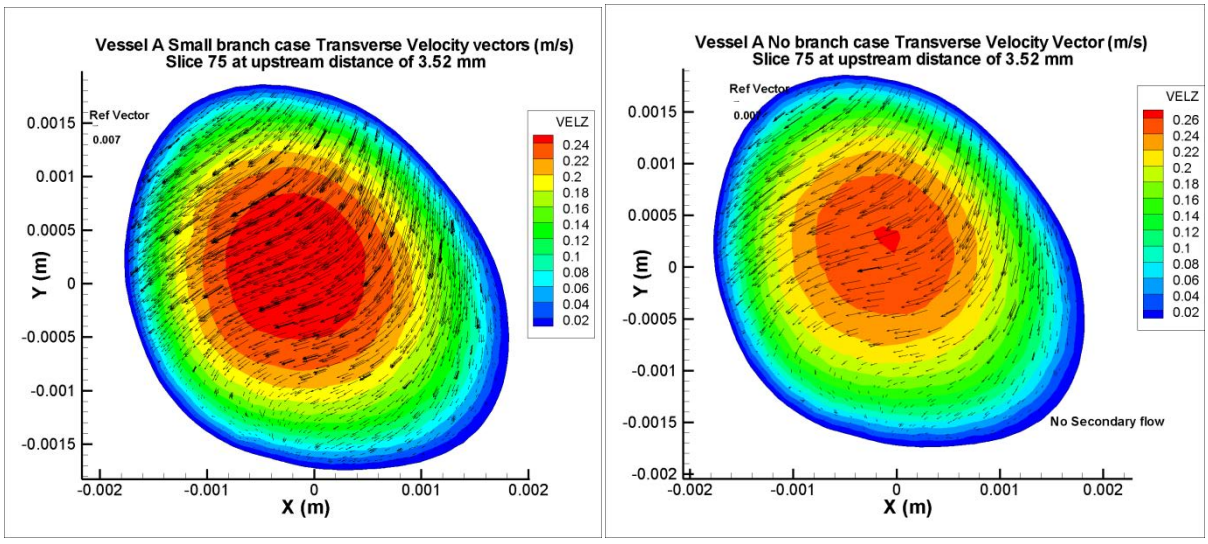

(c) **(d)**

Figure 5-29 Plots of slices at a upstream distance of 3.52 mm from the branch origin showing Transverse velocity vectors overlaid on the contours of axial in Vessel A for all cases of branching

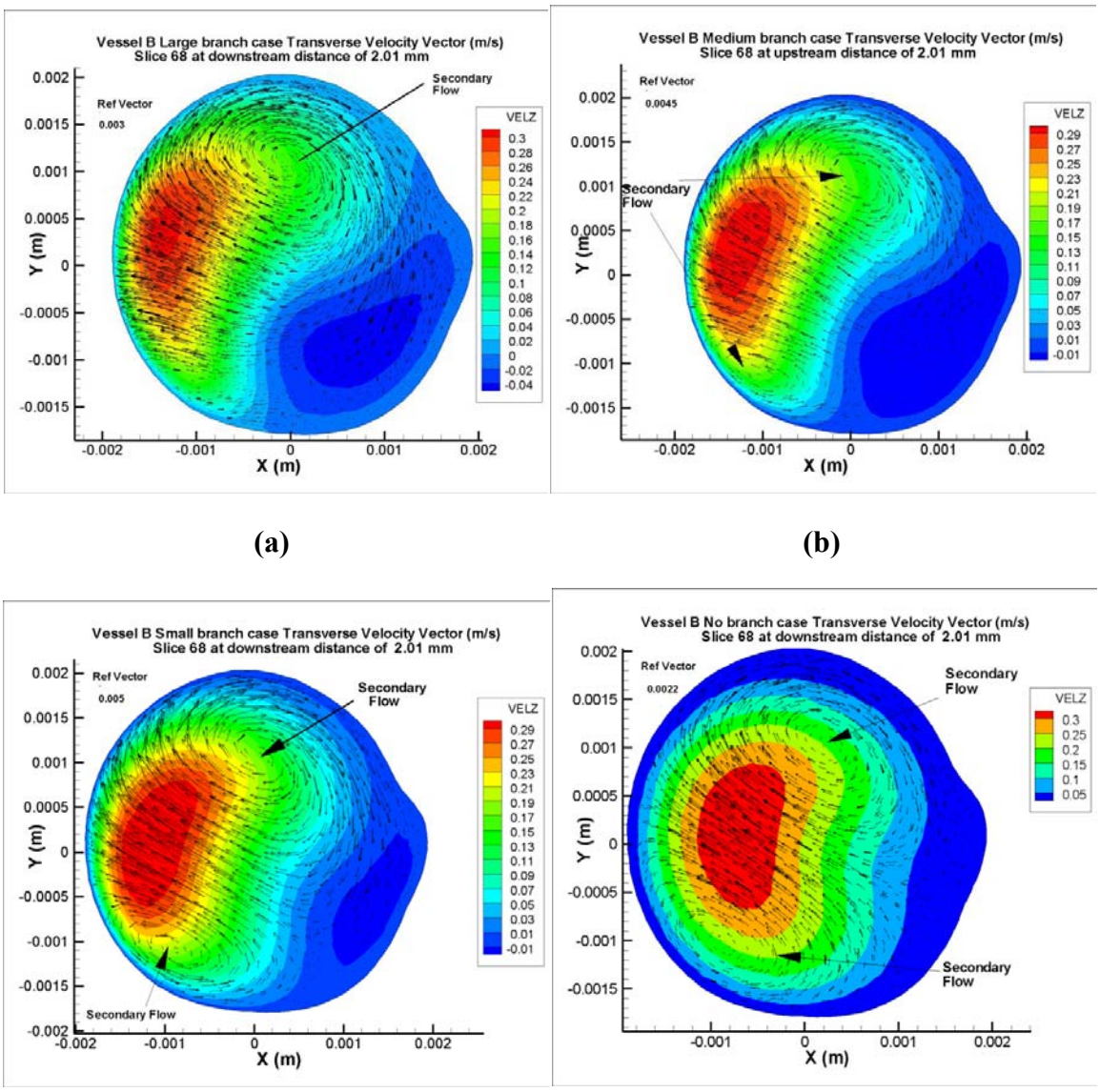

Figure 5-30 Plots of slices at a downstream distance of 2.01 mm from the branch origin showing Transverse velocity vectors overlaid on the contours of axial in Vessel B for all cases of branching.

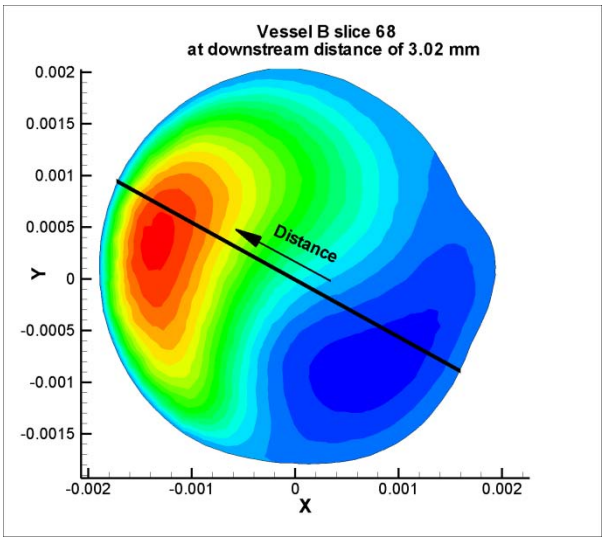

(a)

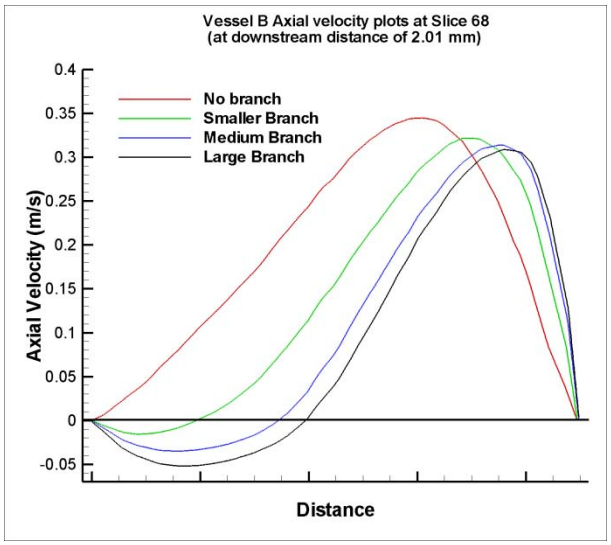

(b)

Figure 5-31 Axial velocity distribution in an extracted in Vessel B at 2.01 mm downstream distance

Figure in (a) shows the line extracted from cross section of slices at 2.01 mm distance downstream of branch origin for different cases of branching in Vessel B. Figure in (b) shows comparison of axial velocities in those slices.

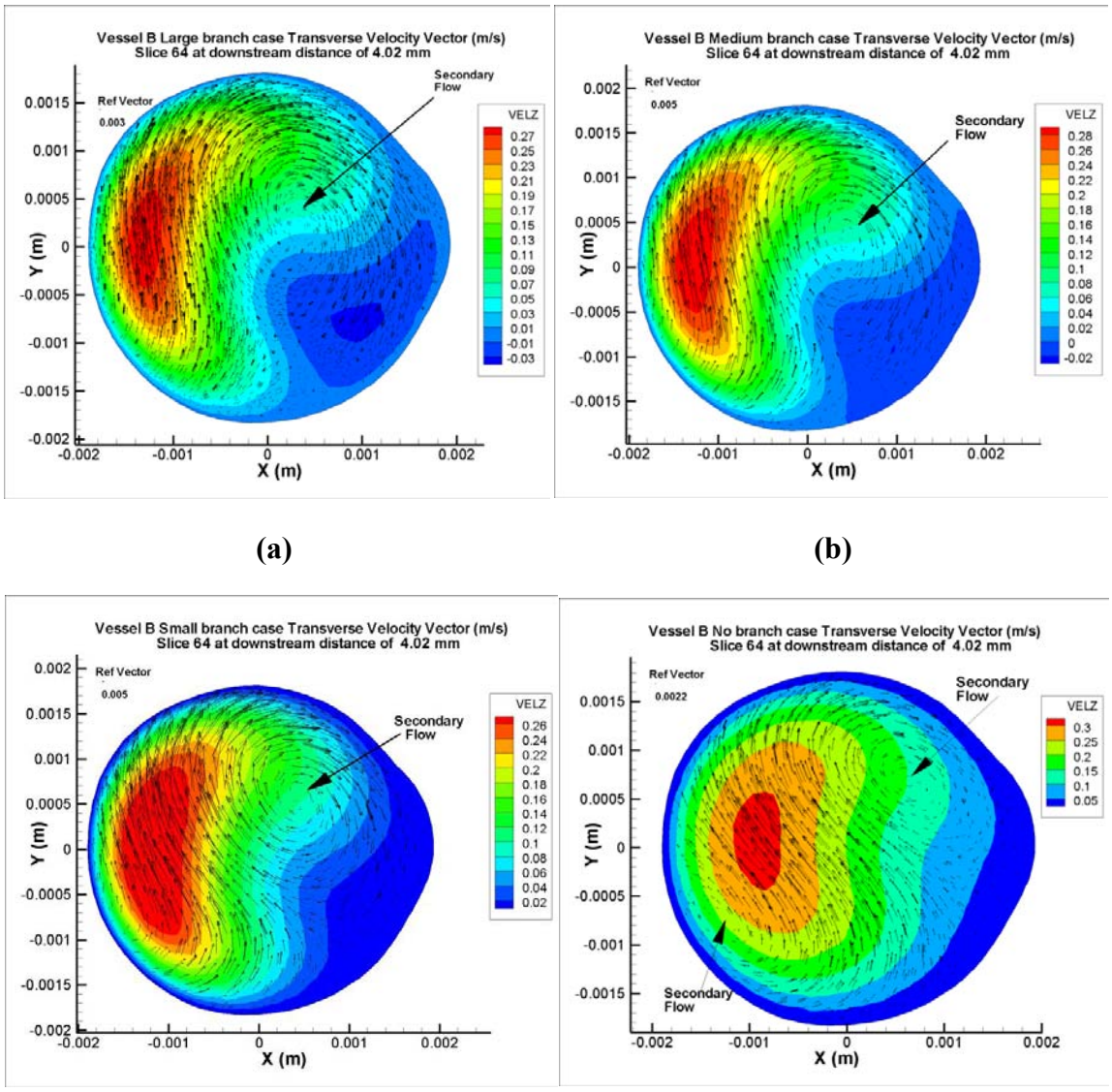

Figure 5-32 Plots of slices at a upstream distance of 4.02 mm from the branch origin showing Transverse velocity vectors overlaid on the contours of axial velocity in Vessel B for all cases of branching

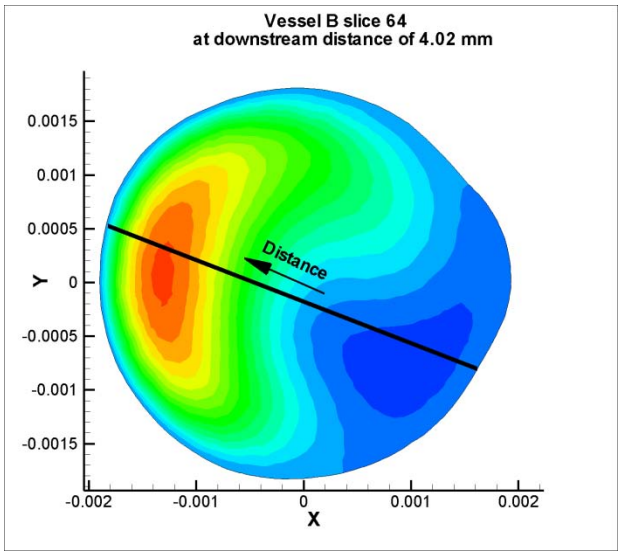

(a)

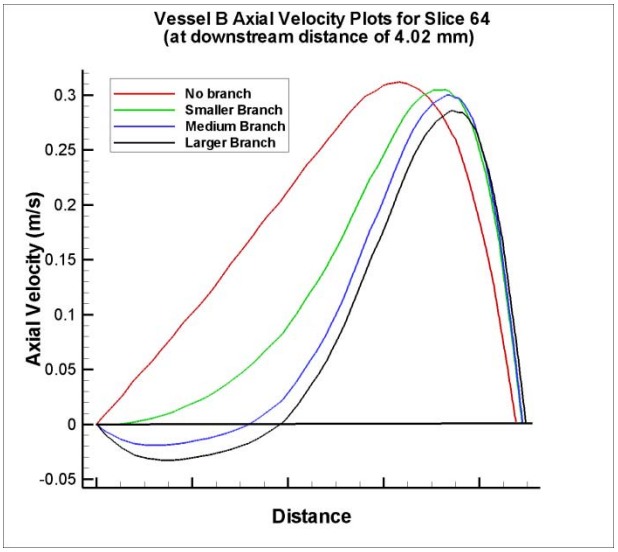

(b)

Figure 5-33 Axial velocity distribution in an extracted in Vessel at 18.09 mm downstream distance

Figure in left shows the line extracted from cross section of slices at 4.02 mm distance downstream of branch origin for different cases of branching in Vessel B. Figure in right shows comparison of axial velocities in those slices.

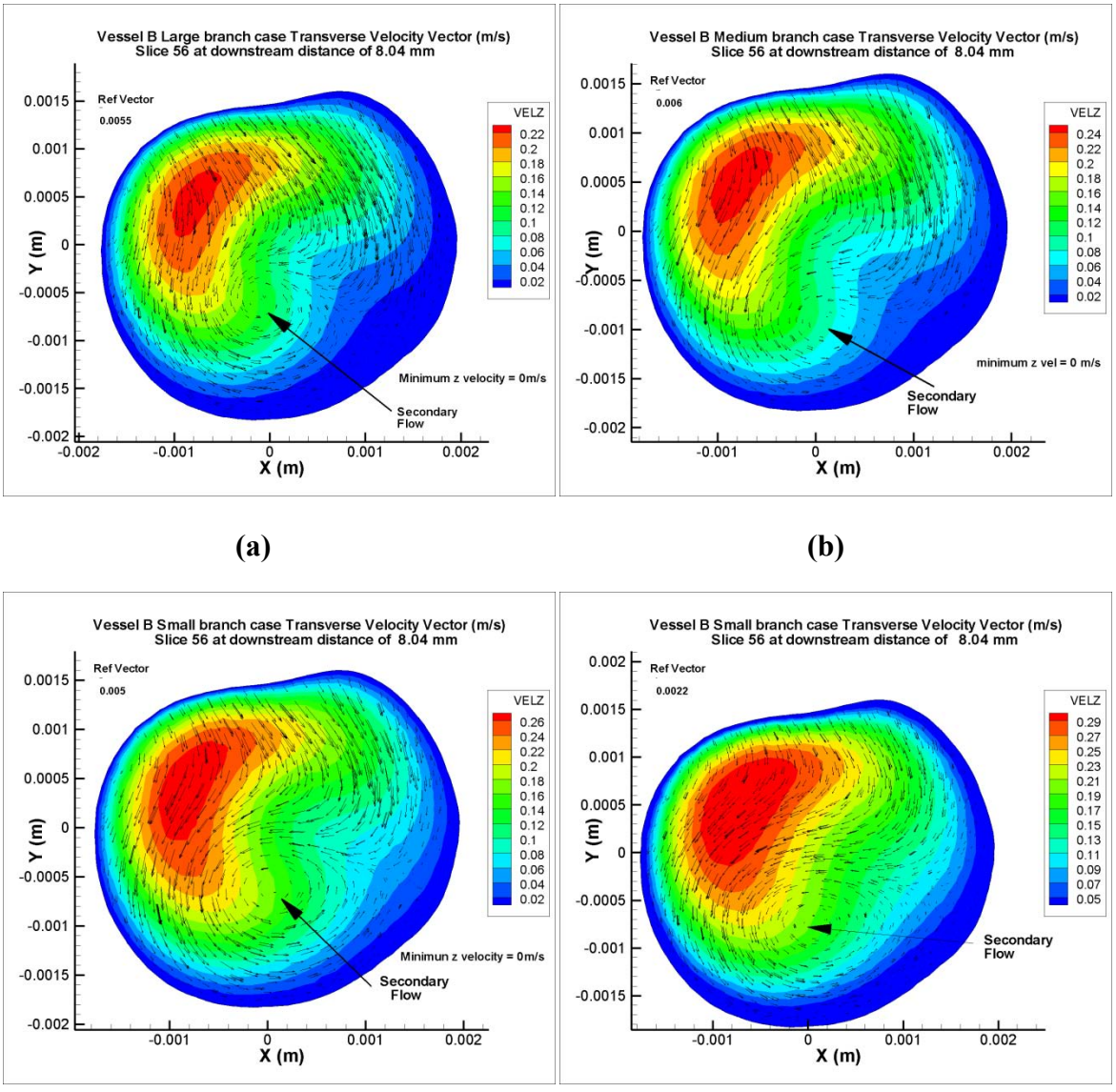

Figure 5-34 Plots of slices at a upstream distance of 8.04 mm from the branch origin showing Transverse velocity vectors overlaid on the contours of axial velocity in Vessel B for all cases of branching

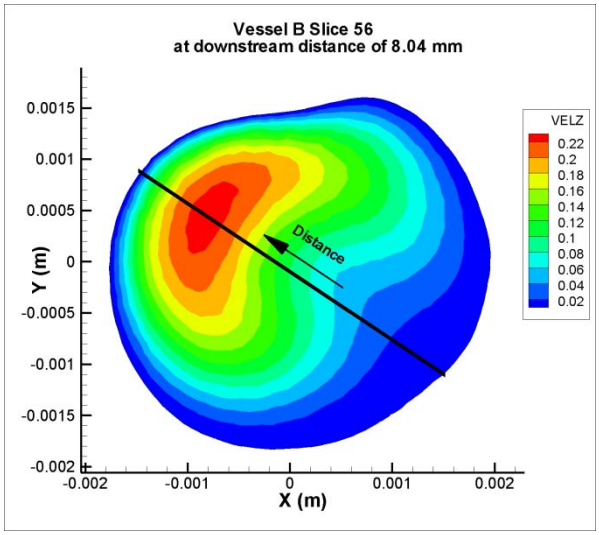

(a)

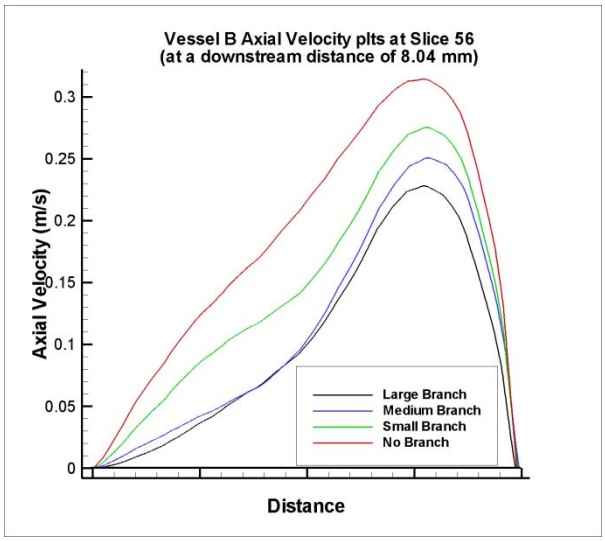

(b)

Figure 5-35 Axial velocity distribution in an extracted in Vessel B at 8.04 mm downstream distance

Figure in (a) shows the line extracted from cross section of slices at 8.04mm distance downstream of branch origin for different cases of branching in Vessel B. Figure in (b) shows comparison of axial velocities in those slices.

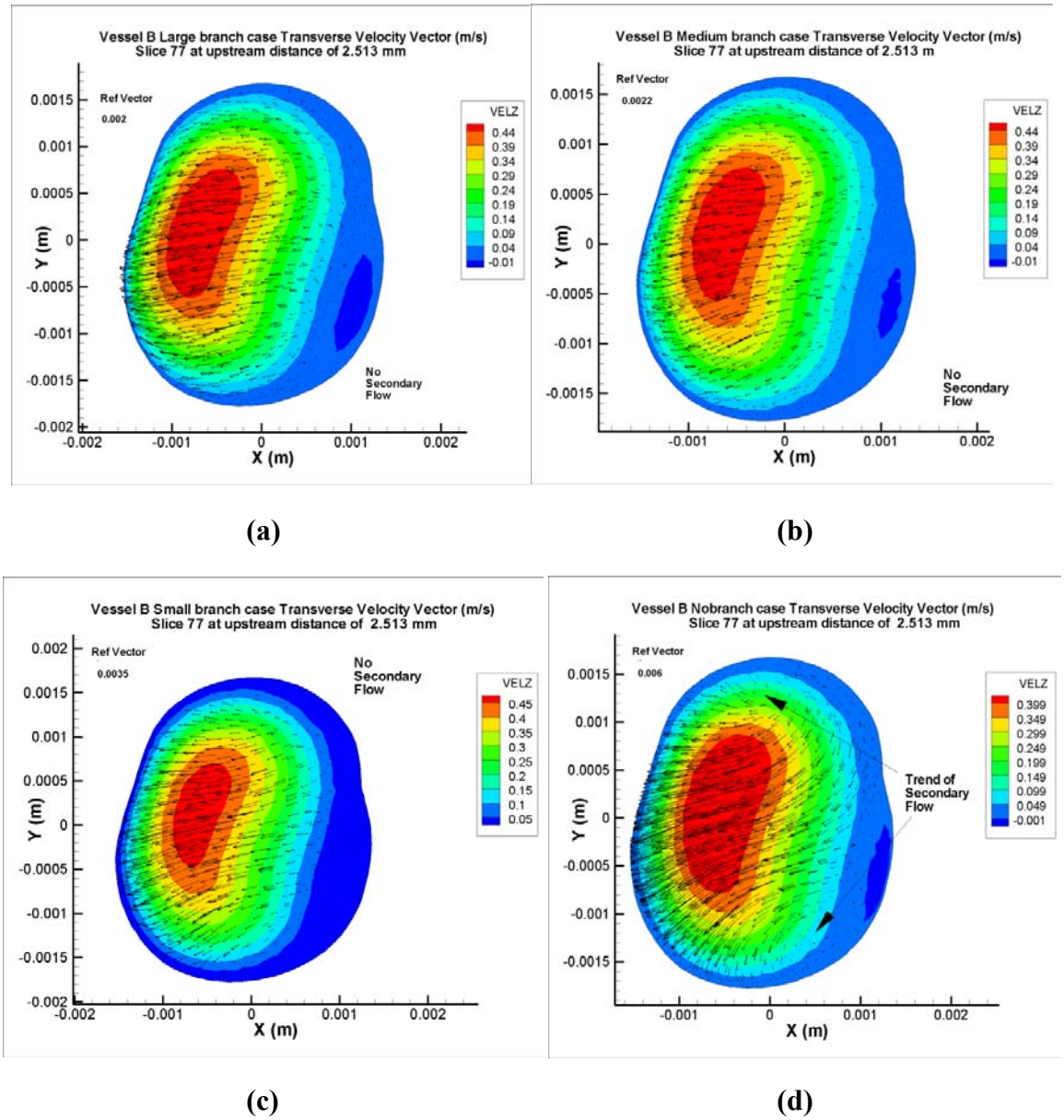

Figure 5-36 Plots of slices at a upstream distance of about 2.5 mm from the branch origin showing Transverse velocity vectors overlaid on the contours of axial velocity in Vessel B for all cases of branching

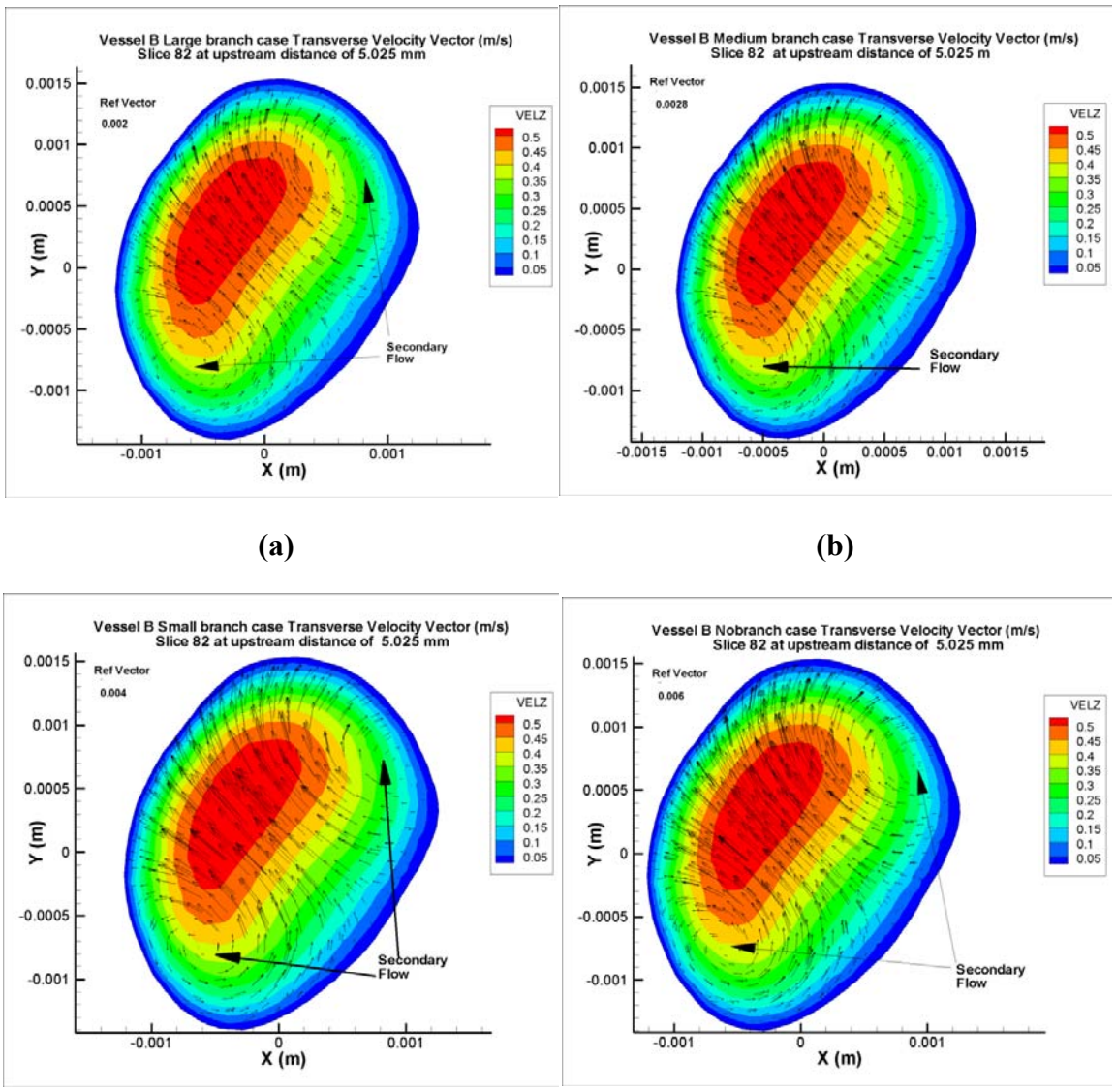

Figure 5-37 Plots of slices at a upstream distance of 5.025 mm from the branch origin showing Transverse velocity vectors overlaid on the contours of axial velocity in Vessel B for all cases of branching

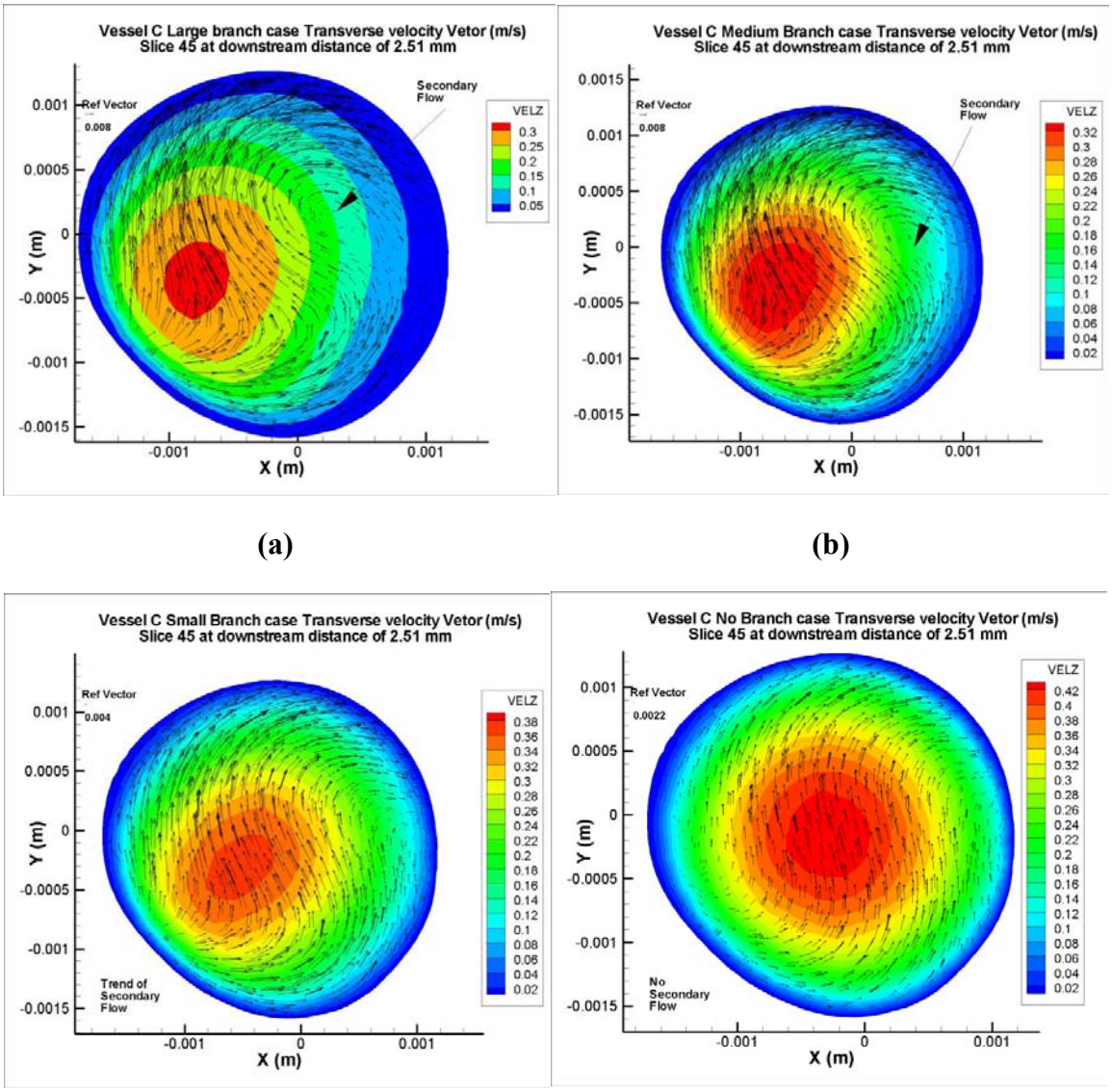

Figure 5-38 Plots of slices at a downstream distance of 2.51 mm from the branch origin showing Transverse velocity vectors overlaid on the contours of axial velocity in Vessel C for all cases of branching

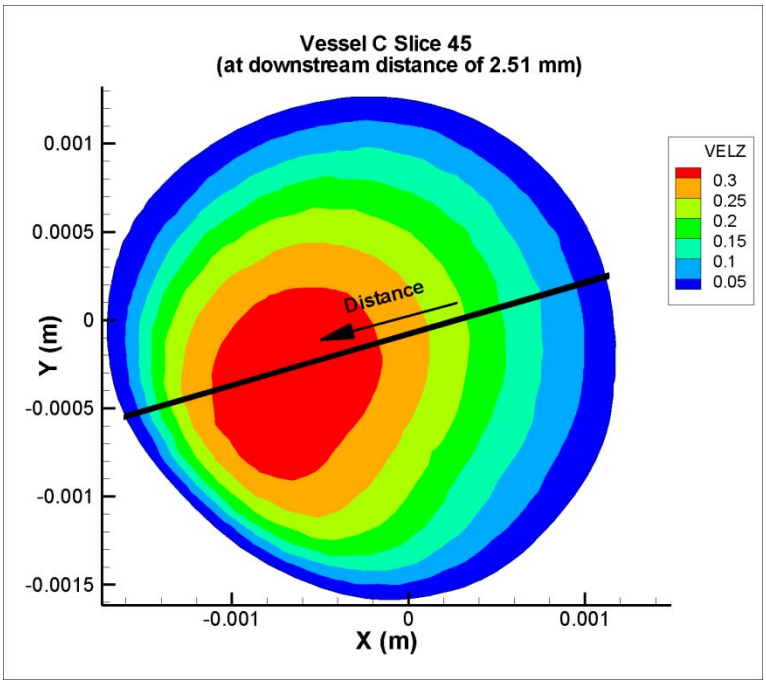

(a)

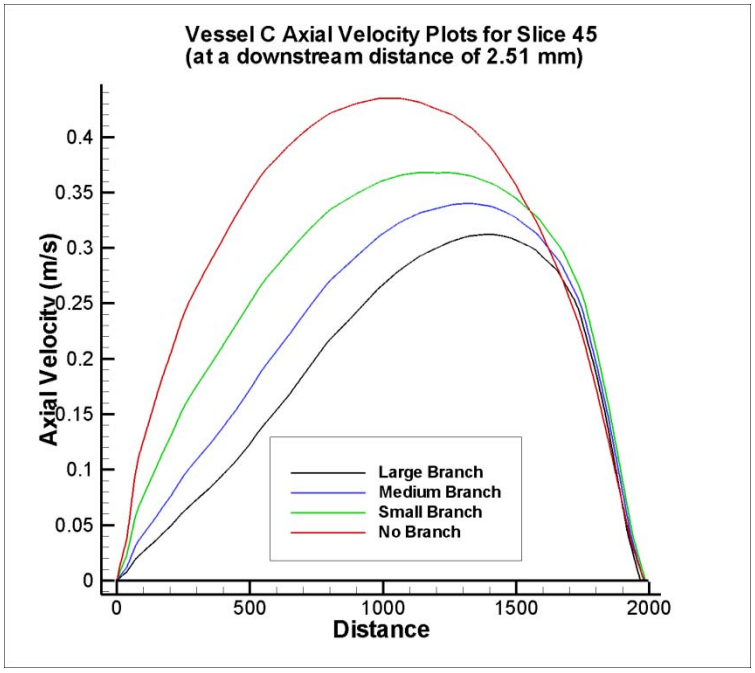

(b)

Figure 5-39 Figure in (a) shows the line extracted from cross section of slices at 2.51mm distance downstream of branch origin for different cases of branching in Vessel C. Figure in (b) shows comparison of axial velocities in those slices.

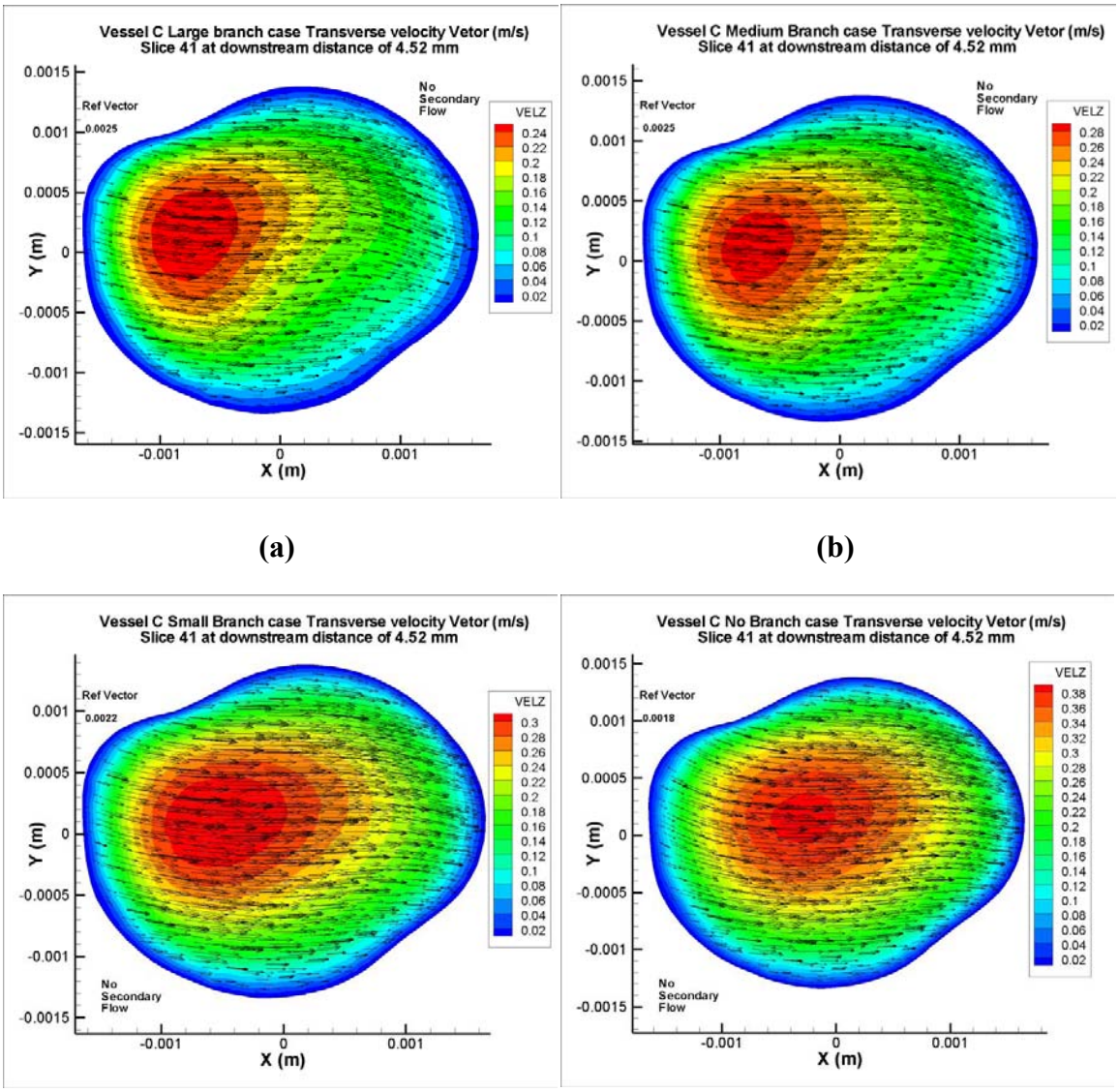

Figure 5-40 Plots of slices at a downstream distance of 4.52 mm from the branch origin showing Transverse velocity vectors overlaid on the contours of axial velocity in Vessel C for all cases of branching

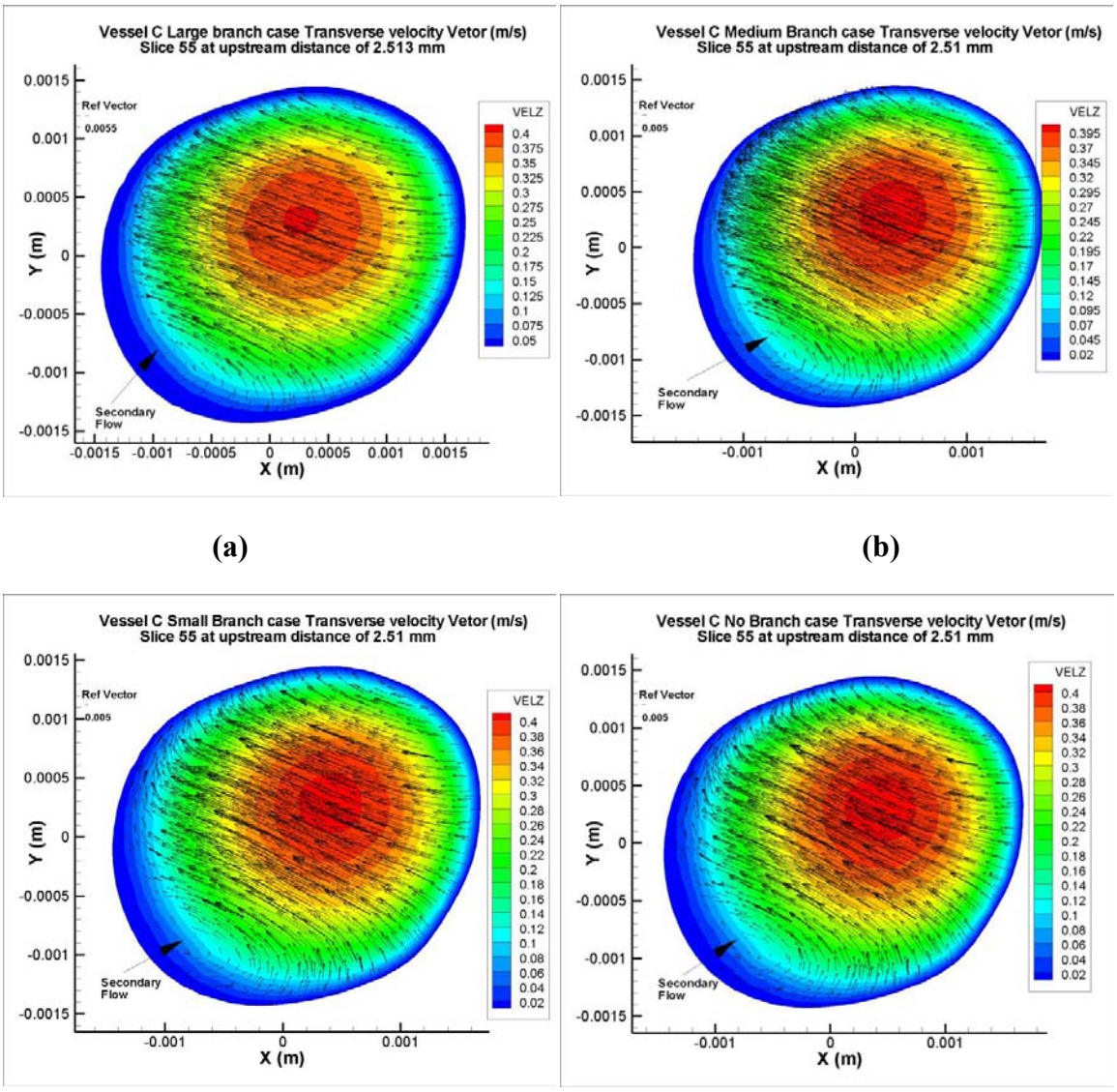

Figure 5-41 Plots of slices at a upstream distance of 2.51 mm from the branch origin showing Transverse velocity vectors overlaid on the contours of axial velocity in Vessel C for all cases of branching

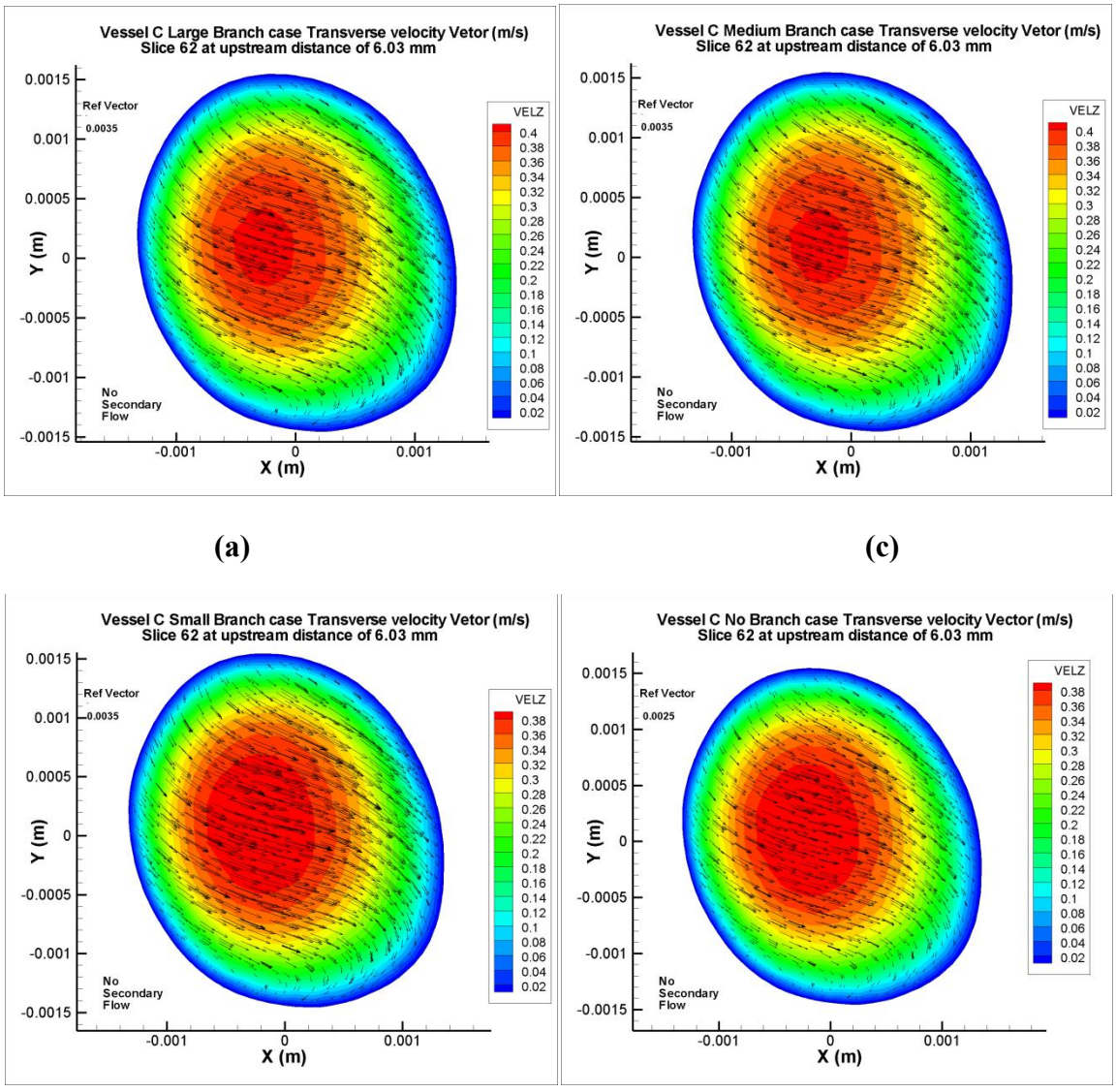

Figure 5-42 Plots of slices at a upstream distance of 6.03 mm from the branch origin showing Transverse velocity vectors overlaid on the contours of axial velocity in Vessel C for all cases of branching

CHAPTER 6 CONCLUSIONS AND FUTURE WORK

6.1 Conclusions

Studies have always shown a high correlation in between the progression of lesion and WSS (Krams et al., 2010). More advanced studies have clearly indicated the existence of accumulation of lesion in the regions of low WSS, flow separation, and in the regions where there was departure from axially aligned unidirectional flow (Zarins et al., 1983, Krams et al., 2010). Caro et al. (1971) have suggested that because of low shear rate there occurs a significant retardation in the transportation of circulating materials away from wall, resulting in what is called the accumulation of lipids in the intimal linings of vessel. Branches are one of the most important factors that affect the flow patterns (Mayers et al., 2000, Krams et al., 2010)). Because of the sudden transition in the geometry for blood flow, the velocity profiles in the region downstream to the bifurcation are skewed towards the divider wall. This subsequently gives rise to low wall shear stress in the outer walls of bifurcation and hence causes flow to separate (Chandran, 2006). Regarding the effect of branches, researchers have mainly focused on the effect of bifurcation angle and position of bifurcation. Significantly less attention has been given to the size of the branching arteries. In these studies, the most common assumption done by researchers to simplify the model creation has been to neglect the existence and hence effect of any branches in the main artery (Steinman et al., 2001, Wentzel et al. (2003), Wahle et al. 2006).

In this study, the role that various branch dimensions play on downstream blood flow in the main channel has been studied to determine whether some branch sizes can be reasonably neglected when considering WSS distribution, and whether larger branches must be included for reasonable hemodynamic studies. Reversed flow, local axial wall shear stress and secondary flow patterns were the key factors examined at numerous distal locations for comparing

differences in blood flow due to branching. To provide a complete picture to the effect of branching, a few cross-sections upstream to branching were also considered.

6.1.1 Nature of TWSS Distribution

In the main channel downstream to branching, TWSS was seen to decrease with the increase in branch size. While this in part could be due to the reduction in flow in the channel because of branching, in the regions near to branch origin, at certain portion of the circumference towards the divider wall which is in accordance with the study reported by Gijson et al. (2009). The TWSS values were seen to elevate by the factor of two orders for the branched cases. The factor increased as the branch size increased. This feature was seen to degrade with increase in downstream distance. Shear stress on either sides of the divider wall was found to be considerably lower than in the rest of the circumference in all the vessels studied. It even reached to negative values for vessels with large cross sections like Vessel A. Regions of negative wall shear stress were also observed in outer wall like in Vessel B. Hence it could be argued that depending on the global curvature the region of low wall shear stress could vary from sides of the divider wall to the outer wall.

For the vessel with smallest cross sectional area, the branch effects were seen in a much smaller region downstream. This claim can be justified by comparing the results of Vessel A and B with vessel C. The effect of large branch in terms of TWSS fluctuation was observed until almost 9.0 mm (slice 50) for vessel A, and 7.5 mm (slice 57) for vessel B while for vessel C the effect was seen till only about 3.5 mm (slice 43) downstream. It should be noted that the cross sectional area of the main vessel A, B and C at the point of branching were 11.2 mm^2, 11.3 mm^2, 6.2 mm^2. Similarly the diameter of large branch cases for all the three vessels were roughly 3.2, 3.3 and 2.46 mm. Hence larger the branch size, and larger the cross sectional area at the branch origin, larger the influence of branches in downstream region. Further, it was notable that though vessel B had almost the same cross sectional area as vessel A at the point of branching, in the

former case branch seemed to effect on relatively small distance. This might be due to the highly tortuous geometry of vessel B.

For all the three vessels, TWSS values were seen to be altered by the presence of branch until a short distance of about 4 mm in upstream region (4.5 mm upstream for vessel A, 4 mm for vessel B, 4 mm for vessel C).

6.1.2 Nature of Velocity Distribution

The regions in the circumference of the vessel exhibiting negative wall shear stress corresponded to the regions in the cross sections where flow reversals were seen. Hence low local axial wall shear stress was seen as a direct indicator of reverse flow. The strength of the negative z-velocity therefore directly correlated with the negative values of wall shear stress.

Occurrence of secondary flow, generally a result of geometrical feature (mainly the artery curvature), was seen to be altered in the presence of branches. In a region where otherwise no secondary flow was observed, presence of a branch seemed to introduce secondary flow. This phenomenon was observed at a distance of 2.51 mm downstream of branch origin in vessel C. On the other hand, a phenomenon opposite to above was also observed. In the case of vessel A at a distance of about 8.5 mm downstream from the site of branching, the presence of the branch diminished the fully developed secondary flow observed in the no branch case to transverse vectors showing only no trends of secondary flow.

The effect of branch on velocity distribution was not confined in regions downstream only. They were observed to have effects in upstream regions too, however in a narrow range. In both the vessels A and B, axial velocities were found to be negative in a small interval of about 3 mm upstream from the branch origin. Similarly, the larger branches were seen to generate more negative z velocities and hence more reverse flow. The summary of the distance downstream until where effect of branch were seen for all the cases have been tabulated in Table 6-1.

Plaque accumulation and atherosclerosis are mostly seen in the regions having low wall shear stress and flow reversals (Zarins, 1983, Krams et al., 2010) In this study we have seen that even the smaller branches generated considerably low wall shear stress and reverse flows in the regions closer to site of branching. The impact grew with the increase in size of branch ostium. Hence it can be argued that larger values of branch ostium could lead to very low values of TWSS and hence higher probability of atherosclerosis. With the increase in branch size the region of influence also increased. In the same way, the strength of reverse flow and hence plaque accumulation also increased with the increase in cross sectional area or decrease in Reynolds number.

	Small Case (mm)	Medium Case (mm)	Large Case (mm)	Length of Vessel (mm)	Area of Vessel at branch site (mm^2)
Vessel A	7.03	8.54	9	62.814	10.8
Vessel B	4.5	6.5	7.5	70.854	11.61
Vessel C	2.51	3.02	3.54	38.191	6.33

Table 6-1 Summary of distance downstream to the site of branching until where the effect of branch were observed (qualitative) with respect to variation in TWSS

6.2 Limitations of Current Study

This study of analyzing the role of branches in the downstream flow of the coronary arteries was carried out but not without limitations. Several assumptions made like assuming blood to be a Newtonian fluid to simplify the simulation have been discussed below.

6.2.1 Unfilleted Geometry

It has been discussed earlier in methodology section that the geometric models developed in this study, lacked filleted branch-artery interface. The software used for carrying out mesh generation in this study lacked the feature of creating filleted 3-d interface region joining the artery and branches. This limitation could be alleviated if surface mesh of branch could also be obtained. In this study a cylinder of constant diameter has been added to the main arterial tube to model the branch. Though the surfaces of the main vessels were derived from an actual artery, branches were not. Due to the lack of filleting tool in Pointwise V16, models with sharp interface regions were used. However, fillet study reported in the CHAPTER 3 METHODOLOGY suggests that sharp interfaces affect the branch flows. However, its effect in the main channel flow downstream is limited to very small regions near the sharp corners which is in agreement with the study by He and Ku (1995). It could hence have an impact on defining exclusion regions in the vicinity of branches where wall shear stress is to be calculated. Also, this effect is much less in the case of angled (not at 90 degrees) branches, which was the case in this study. However, since the information about the exact fillet angle in the vessels studied were not available and simply one branch and main channel diameter ratio was studied in this section, hence more elaborate studies with different fillet angles and surface ratios may be needed to fully understand this.

6.2.2 Absence of Data on Physiological Boundary Conditions

Inlet and outlet velocities as well as pressure conditions vary throughout the artery. For accurate simulation of blood flow, it is necessary to supplement the model with this information. Normally these values are difficult to estimate as limited by *in vivo* settings. Hence, an accepted value of 100 ml/s as mass inlet was used with reference to a similar research done in arteries by Vigmostad in 2003.

6.2.3 Steady Flow Assumption

Although it is well known that the blood waves are pulsatile in nature, a steady state simulation was carried out in this study due to lack of such time variant input data. But, the main objective of this work was to study the effect of branch and its size on the downstream flow. Such an analysis remains scarce in literature and the current model helps reveal various phenomena related to downstream secondary and reverse flows that were previously unknown.

6.2.4 Hot Spots

The method used to solve flow required an offset distance of about 10^{-7} or lower to exist in between the branch and the artery surfaces (for detailed information refer FLUENT manual – Chapter 7- Unconventional meshes). While solving flow using this interface approach, high shear stress was observed in the localized region of intersection or interface purely due to the presence of offset distance. Although these values were localized only in the interface region and not in the downstream or upstream region of branching and the data extracted remained unaffected, the approach is not physiological. Hence, it may be desirable to model the branch and artery geometry as a single entity, particularly in pulsatile flow computations.

6.2.5 Motion of Coronary Artery

Coronary arteries are subjected to motion due to respiration as well as the motion of the heart. However, these motions were not considered in this study. Since, the objective of this study was to analyze significance of the presence of different branch sizes, assumption of a vessels free of any motion was made which is reasonable for current study.

6.3 Future Approach to CFD Analysis for Coronary Arteries

To alleviate the limitations faced in flow analysis in coronary arteries a new method has been developed but not yet fully tested. This method would require information about the points along the surface of the artery and the rest of the computing would be done by a software package written in Fortran 90 and then solved in in-house code ELAFINT3D (Eulerian Level-set-based Algorithm For Interfacial Transport in 3D). The methodology adapted in this new approach would not require any mesh generation software for either surface or volume meshing, a step that has in involved significant challenges and limited the modeling in past and present studies. Because this was a significant effort developed by the Masters candidate, the approach is discussed below.

6. 3.1 Generating Surface Mesh for Preprocessing

A different approach of reconstructing the vessel contours was undertaken after reading in the data from IVUS and angiogram imaging. A data of a vessel with 720 points per contour was taken along with the information of the tangential vector to the centre line of respective contours. All the points in a contour were arranged into 720 axial splines by cubic spline approximation. Centroids for each of these slices were calculated using area weighted sums of triangle method (Zwillinger, 2003). The values of tangents to all the individual slices were also calculated by taking the first derivative of spline passing through the center points. Then the number of slices in between two adjacent contours were increased such that the average distance in between the slices would be equal to the distance in between two adjacent points in the same contour after down-sampling ie,720 points per contour be down sampled to 72 points per contour. This is important in order to obtain almost uniform gradient in all directions. This approach however does not completely yield in a uniform mesh because of tortuousness of the coronary. Hence, the number of equidistant contour needed in between adjacent contours was calculated. For each contour to be added, respective centers were calculated using linear

interpolations. On the other hand, the tangents to each new contours that were to be added were kept same as the tangent to the first contour in that slice. These centers and tangents to the new contours were calculated beforehand so that cubic spline of initial contours could be used to generate the new slices. First four splined slices were taken and all the 720 points per contour were axially resplined to generate some 3000 points per spline. These 3000 points per spline would then be used to find the points along the vessel wall for the new slices. A simple binary search algorithm was then used to determine which point out of the pool of newly generated points was closer to the desired plane. A calculation is performed to determine a vector passing through the desired centroid and a point to be checked. This is followed by the calculation of angle in between the calculated vector and the normal vector. Binary search is carried out to obtain a point oriented at either 90 or 270 degrees to the tangent vector keeping into consideration that the planes do not overlap. This procedure was followed for determining both the inner as well as the outer contours of the artery.

6.3.2 Down- Sampling

After determining the points on the vessel wall, the points in each contour were down sampled such that each adjacent point would be equally spaced. An average radius of all the radii lying in every 5 degrees was calculated, such that it covered 2.5 degrees in both clockwise and counterclockwise direction. It was necessary to down sample because of the limitation of the code to utilize a very fine mesh. In this way body fitted surface mesh of coronary artery was created with quadrilateral meshing.

Down sampling was done for both the surface meshes, i.e. for the mesh with reoriented contours as well as originally oriented contours.

6.3.3 End Caps

In order to apply boundary conditions like inlet velocity and outlet pressure, the openings/endcaps of the artery also need to meshed. Since we already have the points in the first and last cross section s as well as their centers, it was a matter of connecting these points such that a quadrilateral mesh is created. Though the cross sections are not completely circular, we know that these points were resampled at equal angular intervals. Hence these points in the first and last contours were further resampled to obtain 12 equally spaced points. The distance of these 12 points were calculated from the center of that contour. Each distance was divided into 5 equal parts, such that we joined the points after each division, we could create concentric circles. Now that we have our points, it was just a matter of connecting them to obtain a quadrilateral mesh. However, in the points that make the closest circle to the centre we only have 3 points. Since the goal was to make a quadrilateral mesh, it was necessary to create that fourth point. With this view, the distance in between the two points in the nearest concentric circle was halved and another point was created, as marked by red in Figure 6-1. Hence, even the closest concentric circle had four points which could be connected to produce a quadrilateral mesh.

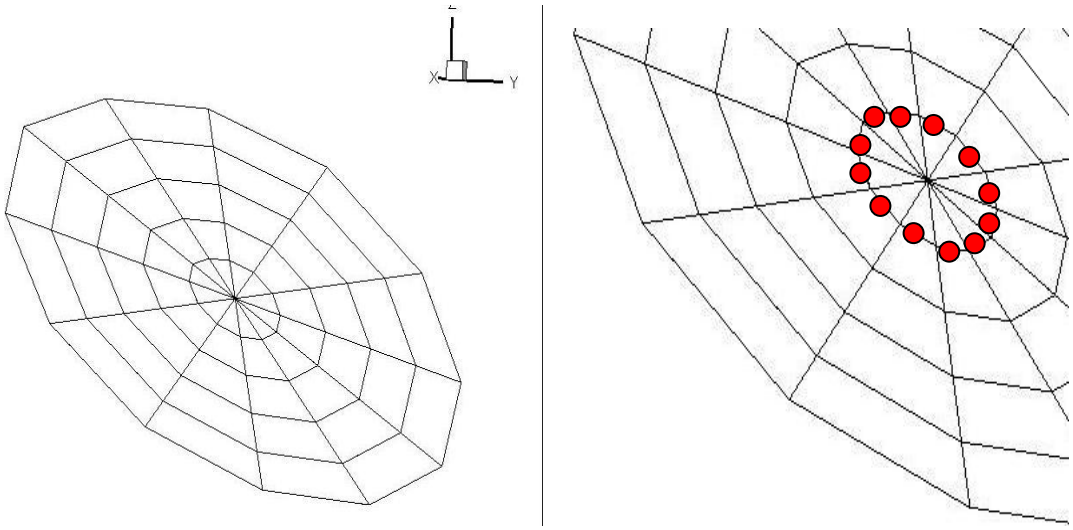

Figure 6-1 Schematic illustrations of the quadrilateral grid in end-cap

This is a figure illustrating the quadrilateral grid in end-cap. The other figure on the right is a zoomed view of the grid in end-cap where the locations of the midpoints calculated in between each and every points forming the innermost concentric circle has been shown.

6.3.4 Flow Solver

A three dimensional incompressible flow solver has been implemented in a computer code termed as ELAFINT3D (Eulerian Level-set-based Algorithm For Interfacial Transport in 3D). This code uses the representation of boundaries in terms of level-sets and employs second order accurate Cartesian grid based finite difference scheme for the discretization of the incompressible Navier Stokes equations. The code uses sharp interface treatment for the embedded boundaries.

Level sets can be defined as the signed distance functions. Use of level sets enables the representations of even the most complicated geometries (Sethian, 1999). A level set generating algorithm as such reads in the information regarding the surface and generates the level set field representing it. In our case, the input read for the level set generation was a quadrilateral surface mesh which was a file containing a number of points the surface and the information about their

connectivity. The points assigned with zero level set values were the determining points from where the distances of other points were calculated and connectivity aided in assigning the signs to each point.

Algorithm for generating level set field in near mesh region

1. The points of the surface mesh were read in along with connectivity information and they were offset and scaled as required.
2. Starting from the first point, for each and every point in the input mesh the South, West and Bottom neighboring points were determined from the array of Cartesian grid. In this way around each and every mesh point a box of Cartesian grid points is formed. These eight points forming the box will be provided level set values. In case the surface mesh is too coarse in compare to the grid, only few Cartesian grid points will be used while assigning initial level set values which will lead to loss in data because of the gaps created. In order to avoid this problem, all the points that were one mesh point away from the nearest points were also assigned level set values. These points were referred as near mesh points.
3. In order to determine the level set value for a point in Cartesian grid in 3D a surface closest to this point needs to be determined first. So as to find this surface it is necessary to determine the three closest points in the surface mesh which have connectivity. A single point is connected to several other points according to the type of mesh being used. Hence while determining the second and then third closest points we need to use connectivity information of the first selected point. In this way a plane surface is determined
4. The distance between this plane and the point is then calculated and is assigned as a level set value. Following equation is used to calculate the plane to point distance.

If $P1(x1, y1, z1)$, $P2(x2, y2, z2)$, and $P3(x3, y3, z3)$ be three points in a plane and P0(x0,y0,z0) be the point in Cartesian grid, the distance between surface and point P0 is calculated in following way.

Calculation of Normal to a plane:

$$N = P1P2 * P2P3 = a\hat{\imath} + b\hat{\jmath} + c\hat{k} \dots\dots (7)$$

Since the points in the plane are known, the equation of the plane is given by:

$$a(x_0 - x_1) + b(y_{0-}y_1) + c(z_0 - z_1) = 0 \dots\dots (8)$$

Or

$$ax + by + cz = ax_1 + by_1 + cz_1 = d \dots\dots (9)$$

Hence the signed distance is calculated as under. (Zwillinger, 2003).

$$D = \frac{N.P_1.P_0}{||N||} = \frac{ax_0 + by_0 + cz_0 + d}{\sqrt{[\![(a)]\!]^2 + b^2 + c^2)}} \dots\dots (10)$$

5. Though the method described above is simple and straight forward, it is quite time consuming as well. Hence in order to speed up the time taken to generate level sets Fast Marching Method was used. This method is devised to solve Eikonal equation (Sethain, 1996):

$$|\nabla\phi\,|F = 1 \dots\dots (11)$$

When upwind scheme is applied, the equation becomes:

$$\frac{1}{F_{ijk}} = [\max\left(D_{ijk}^{-x}\phi_{ijk}, -D_{ijk}^{-x}\phi_{ijk}, 0\right)^2 + \max\left(D_{ijk}^{-y}\phi_{ijk}, -D_{ijk}^{+y}\phi_{ijk}, 0\right)^2 + \max\left(D_{ijk}^{-z}\phi_{ijk}, -D_{ijk}^{+z}\phi_{ijk}, 0\right)^2\,]^{1/2} \dots\dots (12)$$

where ϕ is the LS value at current point.

$$D_{ijk}^{-x} = \frac{1}{\Delta x}\left(\phi_{i,j,k} - \phi_{i-1,j,k}\right) \dots\dots (13)$$

Since the values of the level set ϕ are known in the boundary, it is then a matter of propagating these values outwards or inwards in order to determine the corresponding level set.

In order to increase the efficiency of Fast Marching method, heapsort is also implemented. It is a method which sorts out data in an array in certain order like ascending or descending. Because the fast marching method works in Upwind fashion, min-hip is used such that it is convenient to find the points with lowest values of level set. (Sethian, 1999)

With the surface mesh now converted to a level set field, flow computations are straightforward and can be performed.

REFERENCES

Andrew, C., "Atherosclerosis- The Future Challenge for Europe‟s Health Economies" European Cardiology, 2010;5(2):86-8

Asakura, T. and Karino, T. (1990). "Flow patterns and spatial distribution of atherosclerotic lesions in human coronary arteries." Circ Res **66**(4): 1045-1066

Berne, R. M. and Levy, M.N. (2009). "Cardiovascular physiology"- Sixth Edition, St. Louis, MO, Mosby. WebMd (2009). Heart and coronary arteries. 2009.

Brinkman, A.M., Baker, P.B. et al. (1994) "Variability of Human Coronary Artery Geometry: An Angiographic Study of the Left Anterior Descending Arteries of 30 Autopsy Hearts"- Ann Biomed Eng

Bruschke, A.V., Wijers, T.S., Kolsters, W., Landmann, J. (1991),"The anatomic evolution of coronary artery disease demonstrated by coronary arteriography in 256 nonoperated patients. "- *Circulation* 1981;63:527-536

Caro, C.G., Fitz-Gerald J.M., Schroter R.C.(1971)," Atheroma and arterial wall shear: Observation, correlation and proposal of a shear dependent mass transfer mechanism for atherogenesis."-Proc R Soc Lond [Biol] 117: 109-159

Chandran, K. B., T. L. Yearwood, et al. (1979). "Experimental-Study of Pulsatile Flow in a Curved Tube." -Journal of Biomechanics 12(10): 793-805

Clarian.org (2010)

Cotran, R. S., Kumar, V., et al. (1999). "Robbins pathologic basis of disease."- Philadelphia, Saunders. Berger, S. A., L. Talbot, et al. (1983). "Flow in Curved Pipes." Annual Review of Fluid Mechanics"- **15**: 461-512.

Friedman, M.H., Deters, O.J., et al. (1983). "Arterial geometry affects hemodynamics. A potential risk factor for athersoclerosis." Atherosclerosis **46**(2): 225-231.

Gibson, C.M., Diaz, L., Kandarpa K., Sacks, F.M., Pasternak R.C., Sandor T., Feldman C.L., Stone P.H.. "Relation of vessel wall shear stress to atherosclerosis progression in human coronary arteries. Arteriosclerosis and Thrombosis." 1993;13(2):310–315

Gijsen, F.J.H., Wentzel, J.J., Thury, A., Lamers, B., Schuurbiers, J.C.H., Serruys, P.W., Steen, A.F. "A new imaging technique to study 3-D plaque and shear stress distribution in human coronary artery bifurcations in vivo". Journal of Biomechanics 40 (2007) 2349–2357

Gijsen, F.J.H., Wentzel, J. J., Thury, A., Mastik, F. and Schaar, J.A. *et al*., 2008. "Strain distribution over plaques in human coronary arteries relates to shear stress." Am. J. Physiol. Heart Circ. Physiol.,295: H1608-H1614. DOI: 10.1152/ajpheart.01081.2007

Goubergrits, L., Kertzscher, U., Scho¨neberg, B., Wellnhofer, E., Petz, C., Hege, H-C., (2008). "CFD analysis in an anatomically realistic coronary artery model based on non-invasive 3D imaging: comparison of magnetic resonance imaging with computed tomography", International Journal of Cardiovascular Imaging, 24: 411-421.

Greenspan, D. (1972). "Secondary flow in a curved tube." J. Fluid Mech. **57**(1): 167-176.

Grinberg, L., Karniadakis, G.E. (2008). "Outflow Boundary Conditions for Arterial networks with Multiple Outlets". Annals of Biomedical Engineering. Vol 36, No. 9, September 2008 pp 1496-1514

Hassan, T., Timofeev, E.V., Saito, T, Shimizu, H., Ezura, T., Tominaga, T., Takahashi, A., and Takayama, K., "Computational Replicas: AnatomicReconstructions of Cerebral Vessels as Volume Numerical Grids at Three-Dimensional Angiography". *AJNR Am J* Neuroradiol 25:1356–1365, September 2004

He, X., Ku, D.N., (1995) "Flow in T-bifurcations: effect of the sharpness of the flow divider." Biorheology, 1995 Jul-Aug;32(4):447-58

Heart Disease and Stroke Statistics 2010 update at a glance

Kirpalani, A., Park, H., Butany, J., Johnston, K.W., and Ojha, M., "Velocity and wall shear stress patterns in the human right coronary artery."- *J. Biomech.* 121:1–6, 1999.

Krams, R.,Cuhlmann, S., Foin, N., Evans, P., "Shear stress, inflammation and Atherosclerosis"- ElsevierArtery Research (2010) 4,41-46

Ku, D. N., Giddens, D.P., Zarins, C.K., and Glagov, S., "Pulsatile flow and atherosclerosis in human carotid bifurcation: Positive correlation between plaque location and low and oscillating shear stress."-*Arteriosclerosis* 5:293–302,1985.

Lee, B. K., Kwon, H.M., "Computed numerical analysis of the biomechanical effects on coronary atherogenesis using human hemodynamics and dimensional variables. "-*Yonsei Med. J.* 39:166–174, 1998

Lutz, R.J., Cannon, J.N., Bishoff, K.B., Dedrick, R.L., Stiles, R.K., Fry, D. L. "Wall Shear Stress Distribution in a Model Canine Artery during Steady Flow". *Circ. Res.* 1977; 41; 391-399

Lyne, W. H., "Unsteady viscous flow in a curved pipe." J. Fluid Mech. **45**(1): 13-31, 1970.

Mayers, J.G., Moore, J.A, Ojha, M., Johnston, K.W., Either, C.R, "Factors Influencing Blood Flow Patterns in the Human Right Coronary Artery", 2000.

Miller, A. B., "A symposium: coronary atherosclerosis: early detection and aggressive management strategies. Introduction." Am J Cardiol 88(10A): 1M, 2000.

Friedman, M.H., Ding, Z., "Relation between the structural asymmetry of coronary branch vessels and the angle at their origin", J Biomech, 1998 Mar, 31(3):273-8.

Murata, S., Y. M., Inaba, T., "Laminar Flow in a Curved Pipe with Varying Curvature." J. Fluid Mech, 1976, **73**(4): 735-725.

Pedersen, E.M., Oyre, S., Agerbaek, M., Kristensen, I.B., Ringgard, S., Boesiger, P., Paaske, W.P., "Distribution of early atherosclerotic lesions in the human abdominal aorta correlates with wall shear stress measured in vivo,"-Eur J Vasc Endovasc Surg, 1999,18(4): 328-33.

Qiu, Y, Tarbell, J.M., "Numerical simulation of pulsatile flow in a compliant curved tube model of a coronary artery", J Biomech Eng, 2000, 122, 77-85.

Richter, Y., Groothuis, A., Seifert, P., Edelman, E.R., " Dynamic flow alterations dictate leukocyte adhesion and response to endovascular interventions.", 2004 June.

Sabbah, H. N., Walburn, F.J., Stein, P.D., "Patterns of flow in the left coronary artery.",J Biomech Eng 1984 Aug; 106(3): 272-279.

Sabbah, H. N., Khaja, F., Brymer, J.F., Hawkins, E.T., Stein, P.D.,."Blood velocity in the right coronary artery:relation to the distribution of atherosclerotic lesions." Am J Cardiol Vol 53, Issue 8, 1 April 1984, Pages: 1008-1012

Santamarina, A., Weydahl, E., Siegel, J.M., Moore, J.E., "Computational analysis of flow in a curved tube model of the coronary arteries: Effects of time-varying curvature"- Ann Biomed Eng, Volume 26, pp. 944-954, 1998.

Sethian, J. A., "Level set methods and fast marching methods : evolving interfaces in computational geometry, fluid mechanics, computer vision, and materials science."- Cambridge, U.K. ; New York, Cambridge University Press.1999.

Shaaban, A.M., Duerinckx, A.J., "Wall Shear Stress and Early Atherosclerosis: A Review", AJR:174, June 2000.

Sonka, M., "Cardiovascular Image Analysis - Past, Present, and Future." Health Academy 02/2002: 15-24.

Vigmostad, S.C., "Hemodynamics and Wall Thickness in Relation to Localized Geometric Changes in Human Coronary Arteries", Masters Dissertation, The University of Iowa, Iowa City, Iowa, 2003.

Vignon-Clementel, I.E. , Figueroa, C.A. , Jansen, K. E., Taylor, C.A.." Outflow boundary conditions for three-dimensional finite element modeling of blood flow and pressure in arteries." Comput. Methods Appl.Mech. Engrg. 195 (2006)3776-3796.

Wahle, A., Prause, G.P.M., DeJon, S.C., Sonka, M., "Geometrically correct 3-D reconstruction of intravascular ultrasound images by fusion with biplane angiography--methods and validation." IEEE Trans Med Imaging 1999, **18**(8): 686-699.

Wahle, A., Lopez, J. J., Olszewski, M. E., Vigmostad, S.C., Chandran, K. B., Rossen, J. D., Sonka, M., "Plaque development, vessel curvature, and wall shear stress in coronary arteries assessed by X-ray angiography and intravascular ultrasound"-Med Image Anal,. 2006, Volume 10, Issue 4, Pages 615-631

Wentzel, J.J., Janssen, E., Vos, J., Schuurbiers, J.C.H., Krams, R., Serruys, P.W., Feyter, P.J., Slager, C.J., (2003) "Extension of Increased Atherosclerotic Wall Thickness Into High Shear Stress Regions Is Associated With Loss of Compensatory Remodeling"-Circulation 2003;108;17-23;

Wentzel, J. J., Whelan, D. M., Vander Giessen, W.J., Van Beusekom, H.M.M., Andhyiswara, I., Serruys, P.W., Slager, C.J., Krams, R., "Coronary stent implantation changes 3-D vessel geometry and 3-D shear stress distribution." -J Biomech, 2000, 33(10): 1287-1295.

White, C.R., and Frangos, J.A. (2007) "The shear stress of it all: the cell membrane and mechanochemical transduction"- Phil. Trans. R. Soc. B (2007) 362, 1459–1467

Williams, G.S., Hubbell, C.W. and Fenkell, G.H., "Experiments at Detroit. Mich. on the effect of curvature upon the flow of water in pipes" Trans. ASCE, 1902, v47. 1-196

Yutani, C., Imakitaa, M., Ishibashi-Ueda, Yamamoto, A., Takaichi, S., "Localization of lipids and cell population in atheromatous lesions in aorta its main arterial branches in patients with hypercholesterolemia. In: Role of Blood Flow in Atherogenesis,"- edited by Yoshida *et al.* Tokyo: Springer, 1988.

Zarins, C.K., Giddens, D.P., Bharadvaj, B.K., Sottiurai, V.S., Mabon, R.F., Glagov, S., "Carotid bifurcation atherosclerosis. Quantitative correlation of plaque localization with flow velocity profiles and wall shear stress."- Circ. Res. 1983; Vol. 53;502-514

Zhao, S.Z, Xu, X.Y., Collins, M.W., Stanton, A.V., Hughes, A.D., Thom, S.A., "Flow in carotid bifurcations: effect of the superior thyroid artery." Med Eng Phys. 1999 May, 21(4),207-14.

Zhou, Y., Kassab, G.S. and Molloi, S.," On the design of the coronary arterial tree: A generalization of Murray"s law.", Phys Med Biol,1999 Dec;44(12):2929-45.